transformation or to reaction between solids in this temperature range not involved with any weight change [7]. Finally, a significant drop in weight loss is also observed above 650 ^{o}C associated with the DTA peaks at the same temperature range. This may be attributed to full crystallization of PZT phase together with the PbO volatilization commonly found in the lead-based perovskites [5,6]. These data and literature [4] were used to assign the range of calcination temperatures for XRD investigation.

To further study the phase development with increasing calcination temperature, the powders were calcined for 1 h with heating/cooling rates of 10 ^{o}C/min at various temperatures followed by phase analysis using XRD. As shown in Fig. 2, for the uncalcined powder, only X-ray peaks of precursors $PbZrO_3$ (?), PbO (?) and TiO_2 (▼), which could be matched with JCPDS file numbers 77-1971, 35-0739 and 21-1272, respectively, are present, indicating that no reaction had yet been triggered during the milling process. It is seen that PZT crystallites (▽) were already found in the powders at a calcination temperature as low as 600 °C, accompanying with $PbZrO_3$ and $PbTiO_3$ as separated phases. This observation agrees well with those derived from the TG-DTA results. The occurrence of $PbTiO_3$ in this work can be attributed to the result of formation between PbO and TiO_2 precursors during firing process as proposed by Matsua and Sasaki [8].

As the temperature increased to 800 °C, the intensity of the PZT peaks was further enhanced and became the predominant phase. The optimum calcination temperature for the formation of a high purity PZT phase was found to be about 900 ^{o}C, i.e. slightly higher than the exothermic temperature in Fig. 1. In general, the strongest reflections apparent in the majority of the XRD patterns indicate the formation of two PZT phases. These can be matched with JCPDS file number 73-2022 and 33-0748 for the rhombohedral $Pb(Zr_{0.58}Ti_{0.42})O_3$ and tetragonal $Pb(Zr_{0.52}Ti_{0.48})O_3$ (Fig. 2), respectively. As is well known, the variation in composition may lead to a diffuse morphotropic phase boundary (MPB) between the tetragonal and rhombohedral PZT phases [1]. The most obvious difference between the patterns for tetragonal and rhombohedral PZT phases concerns the presence of a splitting of (002)/(200) peak at *2?* about 43^{o}-46^{o} for the former phase (inset shown in Fig. 2). It is seen that the rhombohedral PZT phase is always present in the product. This study also shows that minor amount of the intermediate phases of $PbZrO_3$ and $PbTiO_3$ tends to coexist along with the PZT phase, agreed with earlier work [9]. Upon calcination at 900 ^{o}C with heating/cooling rates of 10 or 30 ^{o}C/min, the phases of $PbZrO_3$ and $PbTiO_3$ have been found to completely disappear, and crystalline PZT of both tetragonal and rhombohedral is the only detectable phase in the powder. The finding condition is close to that

of Fernandes *et al*. [10] (900 ^{o}C for 1 h with heating/cooling rates of 5 ^{o}C/min) but with significantly faster heating/cooling rates. By increasing temperature up to 1000 ^{o}C, the yield of the tetragonal PZT phase seems to increase.

The experimental work carried out here suggests that the optimal calcination condition for single-phase PZT (with impurities undetected by XRD technique) is 900 ^{o}C for 1 h, with heating/cooling rates of 30 ^{o}C/min. The morphology of these PZT powders was also examined as illustrated in Fig. 3. In general, the particles are basically irregular in shape with substantial agglomerations. This observation is also similar to that of PZT powders synthesized by previous researchers [4,10] but with smaller particle sizes of about 74-725 nm (estimated from SEM micrographs).

4. CONCLUSIONS

Perovskite phase of PZT powders may be produced by employing a two-stage solid stage reaction process using $PbZrO_3$ as precursor. Evidence has been obtained for a pure PZT phase after calcined at 900 ^{o}C for 1 h with heating/cooling rates of 30 ^{o}C/min.

ACKNOWLEDGEMENTS

This work was supported by the nanoscience and nanotechnology center, Thailand Research Fund (TRF), Commission on Higher Education (CHE), the Faculty of Science and the Graduate School, Chiang Mai University.

REFERENCES

[1] A.J. Moulson and J.M. Herbert, Electroceramics (Wiley, Chichester, 2003).

[2] S. Mori, H. Mitsuda, K. Date, H. Hioki and T. Miyazawa, Natl. Tech. Rept. 10, 32 (1964).

[3] O. Babuhskin, T. Lindback, J.C. Lue and J.Y.M. Leblais, J. Eur. Ceram. Soc. 16, 1293 (1996).

[4] R. Tipakontitikul and S. Ananta, Mater. Lett. 58, 449 (2004).

[5] S. Ananta and N.W. Thomas, J. Eur. Ceram. Soc. 19, 155 (1999).

[6] W. Chaisan, O. Khamman, R. Yimnirun and S. Ananta, J. Mater. Sci. (2006) in press.

[7] R.N. Das, A. Pathak, S.K. Saha, S. Sannigrahi and P. Pramanik, Mat. Res. Bull. 36, 1539 (2001).

[8] Y. Matsuo and H. Sasaki, J. Am. Ceram. Soc. 48, 289 (1965).

[9] N. Chakrabarti and H.S. Maiti, Mater. Lett. 30, 169 (1997).

[10] J.C. Fernandes, D.A. Hall, M.R. Cockburn and G.N. Greaves, Nucl. Instrum. Meth. B 97, 137 (1995).

Figure Caption:

Figure 1 TG-DTA curves for the mixture of $PbZrO_3$-PbO-TiO_2 powders.

Figure 2 XRD patterns of PZT powders calcined at various conditions for 1 h (inset: enlarged XRD peaks for the tetragonal (T) and rhombohedral (R) phases as a function of calcination temperatures).

Figure 3 SEM micrograph of the PZT powders calcined at 900 ^{o}C for 1 h with heating/cooling rates of 30 ^{o}C/min.

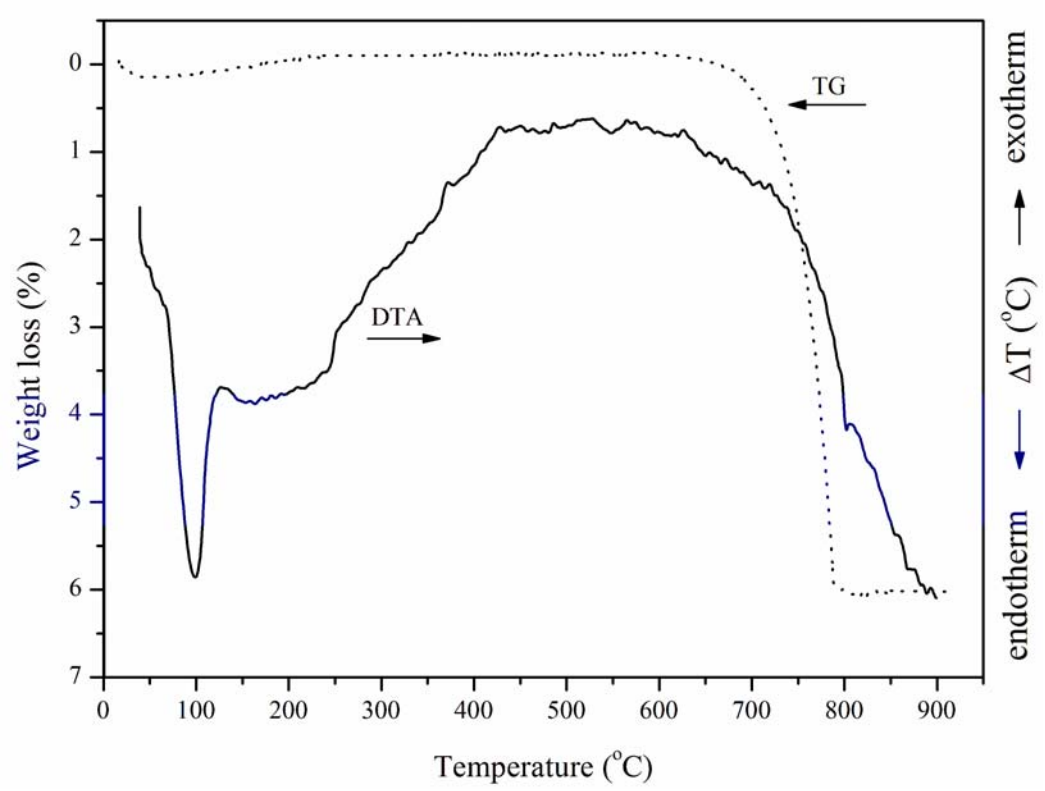
TG
DTA
Weight loss (%)
ΔT (°C)
exotherm
endotherm
Temperature (°C)
0
1
2
3
4
5
6
7
0
100
200
300
400
500
600
700
800
900

Fig. 1

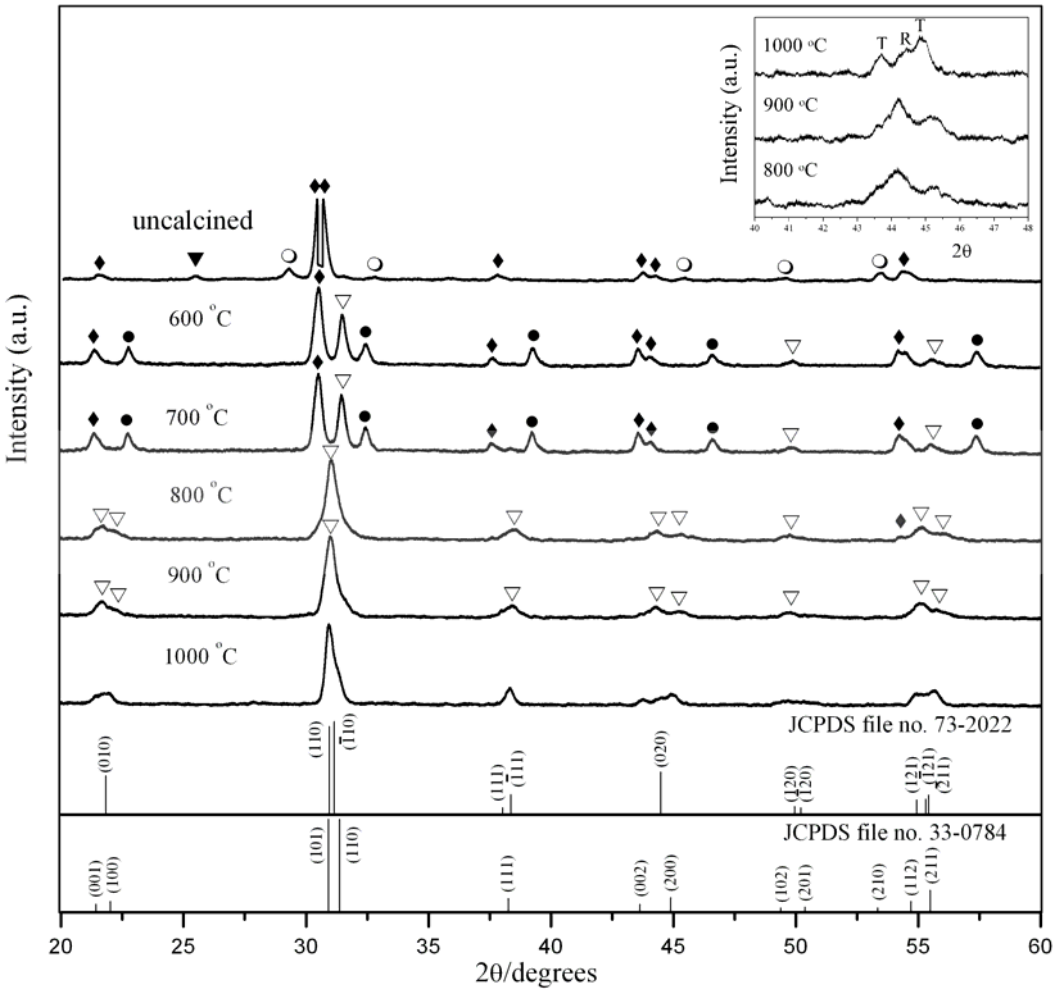
Intensity (a.u.)
uncalcined
600 °C
700 °C
800 °C
900 °C
1000 °C
JCPDS file no. 73-2022
JCPDS file no. 33-0784
2θ/degrees
1000 °C
900 °C
800 °C
T
R
T
2θ

Fig. 2

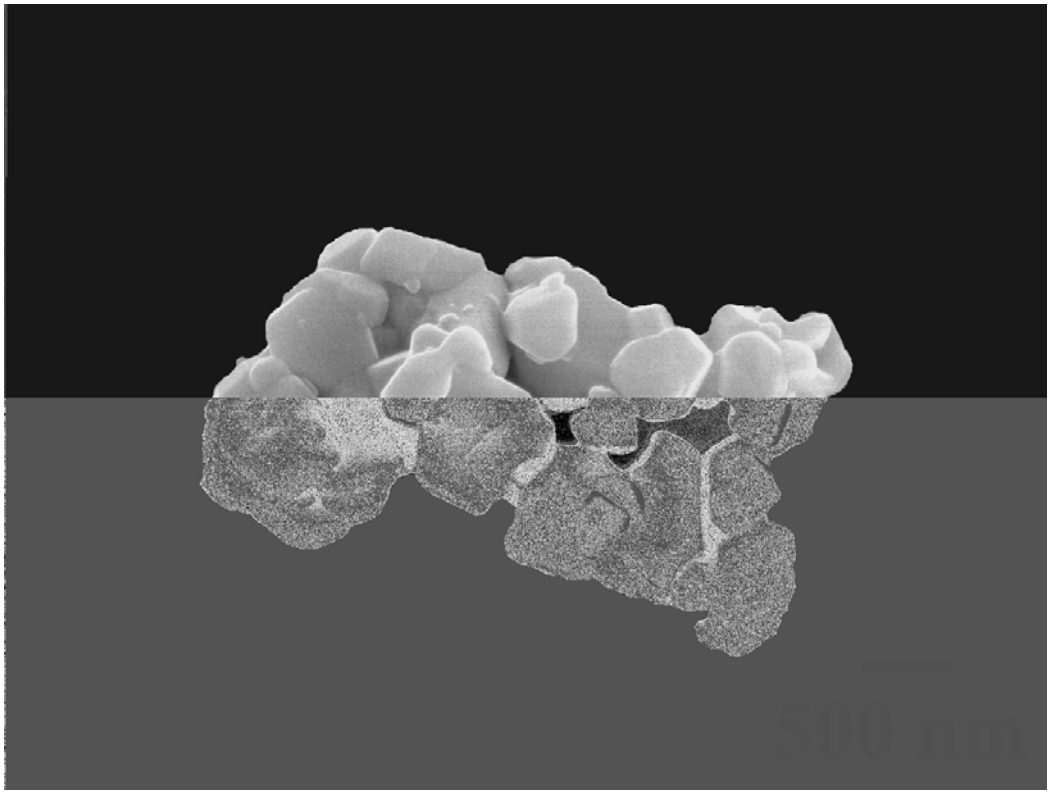

Fig. 3

Dielectric Properties of Lead Magnesium Niobate-Lead Titanate Ceramics Prepared by Mixed-Oxide Method

Rattikorn Yimnirun

Department of Physics, Faculty of Science, Chiang Mai University,

Chiang Mai 50200 Thailand

Author for correspondence, e-mail: rattikornyimnirun@yahoo.com

ABSTRACT

In this study, the (1-x)Pb($Mg_{1/3}Nb_{2/3}$)O_3–x$PbTiO_3$ (when x = 0.1, 0.3 and 0.5) ceramics were prepared from PMN and PT powders by a mixed-oxide method. The dielectric properties of the ceramics were measured as functions of both temperature (-150 - 400 °C) and frequency (100 Hz - 1 MHz). The results indicated that the dielectric properties of pseudo-cubic phase 0.9PMN-0.1PT and tetragonal phase 0.5PMN-0.5PT ceramics followed that of relaxor and normal ferroelectric behaviors, respectively, while the dielectric behaviors of a near MPB phase 0.7PMN-0.3PT ceramic showed a mixture of normal and relaxor ferroelectric behaviors. In addition, the Curie temperature (T_C) increased with increasing PT contents, while the diffusivity decreased. This confirmed a gradual transition from a relaxor ferroelectric behavior in 0.9PMN-0.1PT to a normal ferroelectric behavior in 0.5PMN-0.5PT. The difference in dielectric behaviors was attributed to the structural symmetry of the ceramics.

Key words : PMN-PT, Dielectric Properties

1. INTRODUCTION

Ceramics are one of many classes of electronic materials. The electronic industries are demanding smaller, higher packing density and higher frequency electronic devices [1]. Among those features, volume efficiency can be easily improved by reduction of the dimensions of devices and by increasing the dielectric constant of the materials used. This is particular the case for capacitor industry, in which uses of high dielectric constant ceramics are of great success. A family of materials which dominates the industry is lead-based ferroelectrics, especially lead magnesium niobate, $Pb(Mg_{1/3}Nb_{2/3})O_3$ or PMN, and its solid solution with lead titanate, $PbTiO_3$ or PT, the so-called PMN-PT compounds, which show dielectric constant in excess of 20,000, making them candidate materials for capacitors [2]. In addition, they exhibit electrostrictive behavior at temperatures above their transition temperatures. This particular feature leads to their uses in transducers and actuators [3,4].

Lead magnesium niobate (PMN) is generally established as a representative of relaxor ferroelectrics. Though the Curie temperature of PMN is well below room temperature [5], it can be easily shifted upward with PT addition, a normal ferroelectric compound which has a transition at 490 ^{o}C. A spontaneous phase transition is indicated in the solid solution PMN-PT as a result of a change in the degree of ordering induced by substitution of cationic sites. An addition of ~28% PT causes the material to revert to a normal ferroelectric tetragonal phase with $T_C \sim 130$ ^{o}C. The (1-x)PMN-(x)PT system also shows a morphotropic phase boundary (MPB) near $x \sim 0.4$, separating pseudo-cubic phase and tetragonal phases. As observed in other systems such as PZN-PT and PZT, anomalously large dielectric and piezoelectric properties are observed for compositions lying near the MPB [6]. This study is aimed

at investigating the dielectric properties, as functions of both temperature and frequency, of ceramics in PMN-PT system. In particular, three compositions, 0.9PMN-0.1PT, 0.7PMN-0.3PT, and 0.5PMN-0.5PT representing pseudo-cubic, near MPB, and tetragonal phases, respectively, are chosen for the study to examine the roles of MPB as well as to establish the structure-property relations for the PMN-PT system.

2. MATERIALS AND METHODS

The $Pb(Mg_{1/3}Nb_{2/3})O_3$-$PbTiO_3$ ceramics were prepared from PMN and PT powders by a mixed-oxide method. Perovskite-phase PMN powders were obtained via a well-known columbite method [7], while PT powders were prepared by a more conventional mixed-oxide method. For PMN powders, the magnesium niobate ($MgNb_2O_6$) powders were first prepared by mixing starting MgO (> 98%) (Fluka, Switzerland) and Nb_2O_5 (99.9%) (Aldrich, Germany) powders and then calcining the mixed powders at 1100 °C for 3 hours with the heating/cooling rates of 20 °C/min. This yielded a so-called columbite powder ($MgNb_2O_6$). The columbite powders were subsequently ball-milled with PbO (99%) for 24 hours. The mixed powders were calcined at 800 °C for 1 hour with the heating/cooling rates of 20 °C/min. X-ray diffraction analysis was employed to confirm the formation of perovskite-phase PMN. PT powders were prepared from reagent-grade PbO (99%) and TiO_2 (98.5%) starting powders (Fluka, Switzerland). These powders were ball-milled for 24 hours and then calcined at 600 °C for 1 hour with the heating/cooling rates of 20 °C/min. The (1-x)$Pb(Mg_{1/3}Nb_{2/3})O_3$-x$PbTiO_3$ powders (when x = 0.1, 0.3 and 0.5) were subsequently prepared from the precursor PMN and PT powders by a mixed-oxide technique. Initially, PMN and PT powders for a given composition were weighed and then ball-milled in ethanol for 24 hours. The mixed powders were calcined for 2 hours at 900,

800, and 750 °C for compositions with x = 0.1, 0.3, and 0.5, respectively, with the heating/cooling rates of 20 °C/min. To fabricate PMN-PT ceramics, the calcined powders were pressed hydraulically to form disc-shaped pellets 15 mm in diameter and 2 mm thick, with 5 wt.% polyvinyl alcohol (PVA) as a binder. The pellets were stacked in a covered alumina crucible. Finally, the sintering was carried out at a sintering temperature for 2 hours with 15 min/°C heating and cooling rates. The sintering temperature was optimized at 1240 °C for compositions with x = 0.1 and 0.3, and at 1220 °C for composition with x = 0.5. More details of the powder and ceramic preparation studies were described thoroughly in previous publication [8] and will not be included in this present context, which is focused on the dielectric properties of the successfully prepared ceramics.

The dielectric properties of the sintered ceramics were studied as functions of both temperature and frequency with an automated dielectric measurement system. The computer-controlled dielectric measurement system consisted of an LCR-meter (Hewlett-Packard Precision LCR-Meter HP 4284A), a temperature chamber (Delta Design 9023), and a computer system. The detailed description of this system was explained elsewhere [9]. For dielectric property characterizations, the sintered samples were lapped to obtain parallel faces, and the faces were then coated with silver paint as electrodes. The samples were heat-treated at 750 °C for 12 min to ensure the contact between the electrodes and the ceramic surfaces. The capacitance and the dielectric loss tangent were determined over the temperature of –150 and 400 °C with the frequency ranging from 100 Hz to 1 MHz. The measurements were carried out on cooling continuously. Before each cooling run, the samples were first heated up to 400 °C and then cooling run was performed at the rate of 4 °C/min. The dielectric constant was then calculated from $\varepsilon_r = Cd / \varepsilon_0 A$, where C is the capacitance of the

sample, d and A were the thickness and the area of the electrode, respectively, and ε_0 was the dielectric permittivity of vacuum (8.854 x 10^{-12} F/m).

3. RESULTS AND DISCUSSION

The experimental results on physical properties, the phase formation behavior, and microstructure features of all the sintered ceramics are presented and discussed thoroughly elsewhere [10]. Hence, these results will not be shown here. However, it should be stated here that the sintered ceramics are in perovskite phase with a pseudo-cubic crystal structure for 0.9PMN-0.1PT, and with a tetragonal crystal structure for 0.5PMN-0.5PT. It is of interest to see that 0.7PMN-0.3PT composition shows a mixed pseudo-cubic and tetragonal symmetry, which confirms that the MPB of the PMN-PT system lies between x =0.3 and 0.4 [6]. Table I includes the density and grain-size range for all ceramic compositions. It should be noted that a variation in these physical features could impose significant effects on dielectric properties. However, as seen in Table I, the density and the grain size range are not significantly different and are not expected to show marked effects on the dielectric properties of the ceramics. Therefore, in this case it is reasonable to assume that the dielectric properties of the ceramics are mainly influenced by their structural symmetry as will be discussed in the following context.

The dielectric properties, e.g. dielectric constant (ε_r) and tan δ, are measured as functions of both temperature and frequency, as shown in Fig. 1 (a-c). As listed in Table 1, the Curie temperature (T_C) (determined at measuring frequency of 1 kHz) increases from 38 °C in 0.9PMN-0.1PT to 250 °C in 0.5PMN-0.5PT. This is a direct result of PT addition to PMN (T_C ~ -8 °C) since PT itself has a Curie temperature of 490 °C [11]. The maximum dielectric constant for all the ceramics studied is in excess

of 20,000. This is clearly a reason for their potential applications in capacitors [1-4]. As shown in Fig. 1 (a), for 0.9PMN-0.1PT ceramic both dielectric constant (ε_r) and dielectric loss tangent (tan δ) exhibit strong temperature-frequency dependence below the transition temperature. This is a typical dielectric behavior of relaxor ferroelectrics [3], in which a strong temperature-frequency dependence is observed and the temperatures of maximum dielectric constant and dielectric loss tangent are shifted to higher temperature with increasing frequency. The maximum value of the dielectric constant decreases with increasing frequency, while that of the dielectric loss tangent increases. The dielectric properties then become frequency independence above the transition temperature [12-14]. PMN is a well-known relaxor ferroelectric material with diffused phase transition (DPT) as a result of a short-range ordered structure with a nanometer scale heterogeneity in composition [12]. Small addition of PT to PMN causes an increase in T_C, but the strong relaxor behavior still exists. In addition, since 0.9PMN-0.1PT ceramic has a pseudo-cubic symmetry it is therefore intrinsically electrostrictive (i.e. its electrically-induced strain is quadratically proportional to the applied electric field and is non-hysteretic) [4]. With its enhanced dielectric properties at room temperature, as listed in Table 1, it is widely employed in transducers and actuators [2-4].

Further increase in PT contents leads to more observable normal ferroelectric behavior because PT is intrinsically a normal ferroelectric [3,4]. The dielectric properties of 0.7PMN-0.3PT ceramic, as plotted in Fig. 1 (b), exhibit a mixture of both normal and relaxor characteristics, in which the transition temperature is not shifted as much as for relaxor 0.9PMN-0.1PT ceramic. Similar tendency has also been observed in several prior investigations [12-14]. It should be noted that 0.7PMN-0.3PT ceramic composition is close to MPB of the PMN-PT system. Therefore, its structural

symmetry is a mixture of pseudo-cubic and tetragonal, which in turn causes a mixture of normal and relaxor characteristics observed for dielectric properties. With a tetragonal symmetry, the 0.5PMN-0.5PT ceramic, on the other hand, exhibits a normal ferroelectric behavior with a very sharp phase transition. As plotted in Fig. 1 (c), the dielectric properties of 0.5PMN-0.5PT ceramic change significantly with temperature, but are nearly independent of frequency, except in the vicinity of the phase transformation temperature. This is a typical characteristic of normal ferroelectric ceramics with a long-range ordered structure [3,12]. It should also be noted here that the dielectric properties in all ceramics increase significantly at high temperature as a result of thermally activated space charge conduction [13,14].

When PT is added to form the binary system with PMN, the T_C increases monotonically, as shown in Table 1 and Fig. 2, and the dielectric behavior is shifted from relaxor ferroelectric towards normal ferroelectric. The degree of broadening or diffuseness is used to assess such behavior in the observed dielectric variation. This could be estimated with the diffusivity (γ) using the expression $\ln(1/\varepsilon_r - 1/\varepsilon_{max})$ vs $(T-T_{max})^{\gamma}$. The value of γ can vary from 1, for normal ferroelectrics with a normal Curie-Weiss behavior, to 2, for completely disordered relaxor ferroelectrics [13-16]. The plots in Fig. 3 show that the variation is very linear. The mean value of the diffusivity (γ) is extracted these plots by fitting a linear equation. The values of γ listed in Table 1 vary between 1.14 for 0.5PMN-0.5PT and 1.96 for 0.9PMN-0.1PT. These results confirm that diffuse phase transition occur in 0.9PMN-0.1PT ceramic ($\gamma = 1.96$) with a nearly complete disorder characteristic, while a strong normal ferroelectric behavior is observed for 0.5PMN-0.5PT ceramic with $\gamma = 1.14$. With the γ value of 1.63, 0.7PMN-0.3PT ceramic is expected to possess a mixed behavior, as is confirmed by the dielectric data plotted in Fig. 1 (b). In addition, it should also be noted that even if

it is established that the diffuseness could be caused by the decrease of grain size in a perovskite ferroelectric material [12], the observed difference of the degree of the diffuseness in this study is not a result of the grain size variation because of the uniformity of the grain size range of the ceramics studied.

4. CONCLUSIONS

The (1-x)$Pb(Mg_{1/3}Nb_{2/3})O_3$–x$PbTiO_3$ (when x = 0.1, 0.3 and 0.5) ceramics are prepared from PMN and PT powders by a mixed-oxide method. The dielectric properties of the ceramics are determined as functions of both temperature and frequency with an automated dielectric measurement system. The measurement takes place over the temperature range of -150 °C and 400 °C with measuring frequency between 100 Hz and 1 MHz. The results indicate that the dielectric properties of pseudo-cubic phase 0.9PMN-0.1PT and tetragonal phase 0.5PMN-0.5PT ceramics follow that of relaxor and normal ferroelectric behaviors, respectively, while the dielectric behaviors of a near MPB phase 0.7PMN-0.3PT ceramic show a mixture of normal and relaxor ferroelectric behavior. In contrast to an increase in T_C with increasing PT contents, the degree of broadening or diffuseness shows a decrease, which confirms a transition from a relaxor ferroelectric behavior in 0.9PMN-0.1PT to a normal ferroelectric behavior in 0.5PMN-0.5PT. The difference in dielectric behaviors is attributed to the structural symmetry of the ceramics.

ACKNOWLEDGEMENTS

The author expresses his gratitude for financial supports from the Thailand Research Fund (TRF). Helps with the sample preparation by Dr. A. Udomporn and with the dielectric measurements by Dr. Y. Somiya are gratefully acknowledged.

REFERENCES

[1] A.J. Moulson, J.M. Herbert. Electroceramics: Materials, Properties, Applications, 2nd Ed., John Wiley & Sons Ltd, New York, 2003.

[2] G.H. Haertling, J. Am. Ceram. Soc. 82(4) (1999) 797.

[3] L.E. Cross, Mater. Chem. Phys. 43 (1996) 108.

[4] S.E. Park, T.R. Shrout, Mater. Res. Innov. 1 (1997) 20.

[5] G.A. Smolenskii, A.I. Agranovskaya, Sov. Phys.-Solid State 1 (1960) 1429.

[6] S.W. Choi, J.M. Tang, A.S. Bhalla, Ferroelectrics. 189 (1996) 27.

[7] S.L. Swartz, T.R. Shrout, Mater. Res. Bull. 17 (1982) 1245.

[8] A. Udomporn ,S. Ananta, Mater. Lett. 58 (2004) 1154.

[9] Q. Jiang, Ph.D. Thesis, The Pennsylvania State University, University Park, 1992.

[10] A. Udomporn, Ph.D. Thesis, Chiang Mai University, Chiang Mai, 2004.

[11] B. Jaffe, W.R. Cook, H. Jeffe Piezoelectric Ceramics, Academic Press, New York, 1997.

[12] V. Koval, C. Alemany, J. Briancin, H. Brunckova, K. Saksl, J. Eur. Ceram. Soc., 23 (2003) 1157.

[13] R. Yimnirun, S. Ananta, P. Laoratanakul, Mater. Sci. Eng. B. 112 (2004) 79.

[14] R. Yimnirun, S. Ananta, P. Laoratanakul, J. Euro. Ceram. Soc. 25 (2005) 3225.

[15] E.F. Alberta, A.S. Bhalla, J. Phys. Chem. Solids 63 (2002) 1759.

[16] W. Chaisan, R. Yimnirun, S. Ananta, D.P. Cann, Mater. Lett. 59 (2005) 3732.

Table 1. Physical and dielectric properties of PMN-PT ceramics (at 1 kHz).

Ceramic	Density (g/cm^3)	Grain Size (μm)	T_C (°C)	Maximum Properties		Room Temp. Properties		Diffusivity (γ)
				ε_r	tan δ	ε_r	tan δ	
0.9PMN-0.1PT	7.98	0.42-3.66	38	25400	0.049	19400	0.087	1.96
0.7PMN-0.3PT	7.86	0.41-2.80	197	23500	0.011	2320	0.022	1.63
0.5PMN-0.5PT	7.78	0.48-3.76	250	23200	0.085	1010	0.025	1.14

List of Figure Captions

Fig. 1 (a). Temperature and frequency dependences of dielectric properties of 0.9PMN-0.1PT ceramic (open markers with dotted lines indicate data for the dielectric loss tangent (tan δ) at the same frequency).

Fig. 1 (b). Temperature and frequency dependences of dielectric properties of 0.7PMN-0.3PT ceramic (open markers with dotted lines indicate data for the dielectric loss tangent (tan δ) at the same frequency).

Fig. 1 (c). Temperature and frequency dependences of dielectric properties of 0.5PMN-0.5PT ceramic (open markers with dotted lines indicate data for the dielectric loss tangent (tan δ) at the same frequency).

Fig. 2. Temperature dependence of dielectric constant of PMN-PT ceramics (measured at 1 kHz).

Fig. 3. Variation of $\ln (1/\varepsilon_r - 1/\varepsilon_{max})$ vs $\ln (T-T_{max})$ of PMN-PT ceramics in the paraelectric region at 1 kHz.

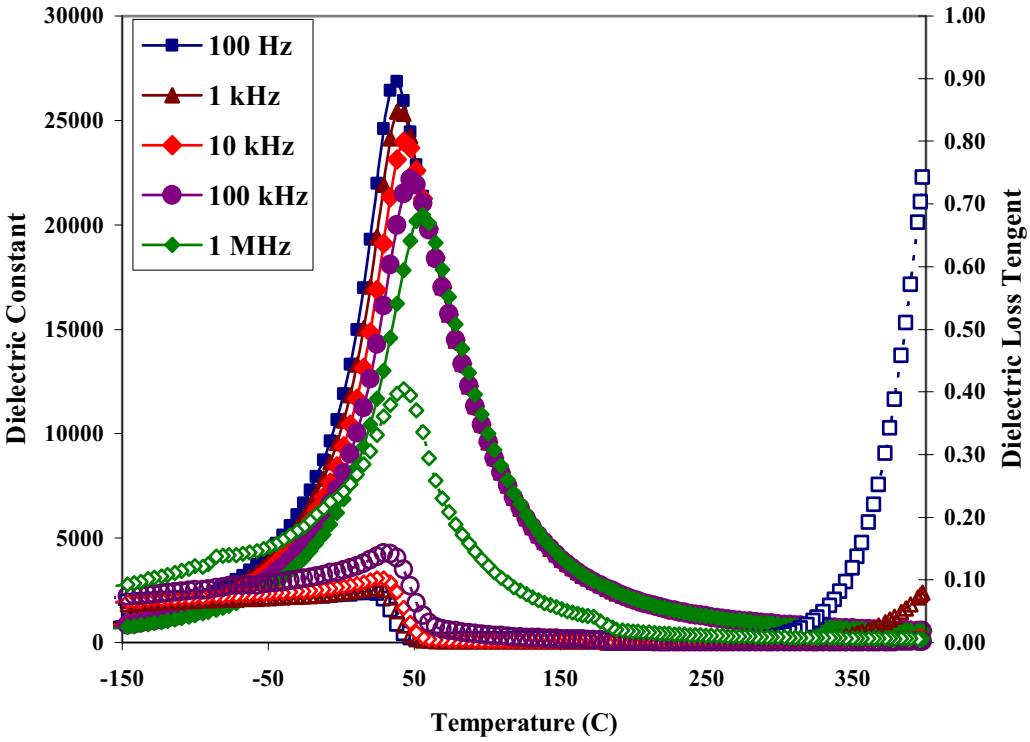

Fig. 1 (a) Temperature and frequency dependences of dielectric properties of 0.9PMN-0.1PT ceramic (open markers with dotted lines indicate data for the dielectric loss tangent (tan δ) at the same frequency)

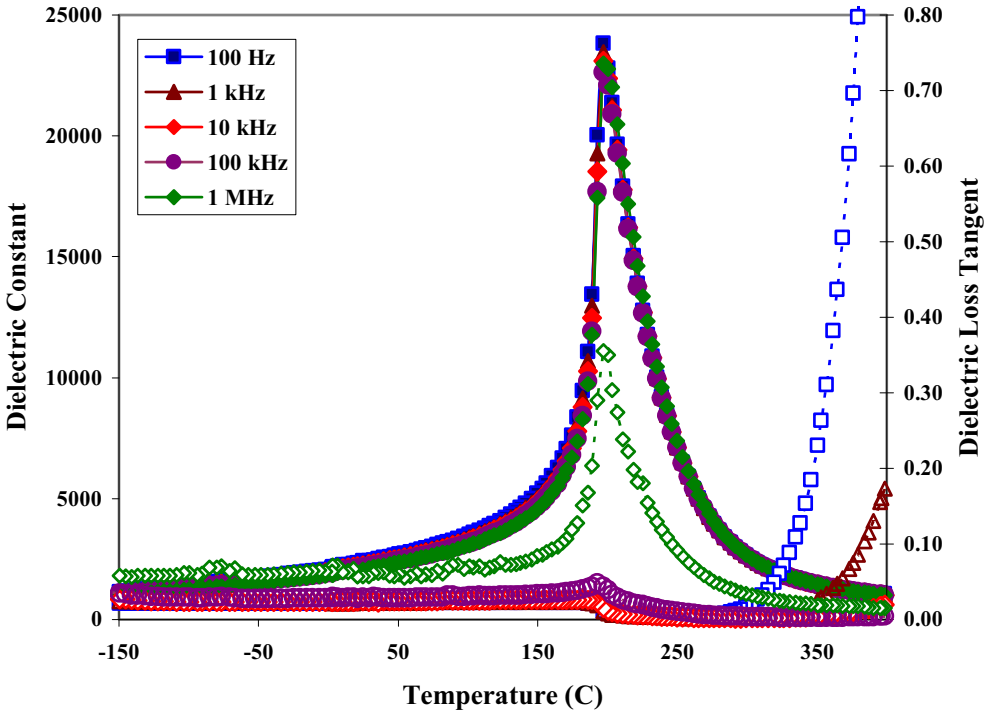

Fig. 1 (b) Temperature and frequency dependences of dielectric properties of 0.7PMN-0.3PT ceramic (open markers with dotted lines indicate data for the dielectric loss tangent (tan δ) at the same frequency)

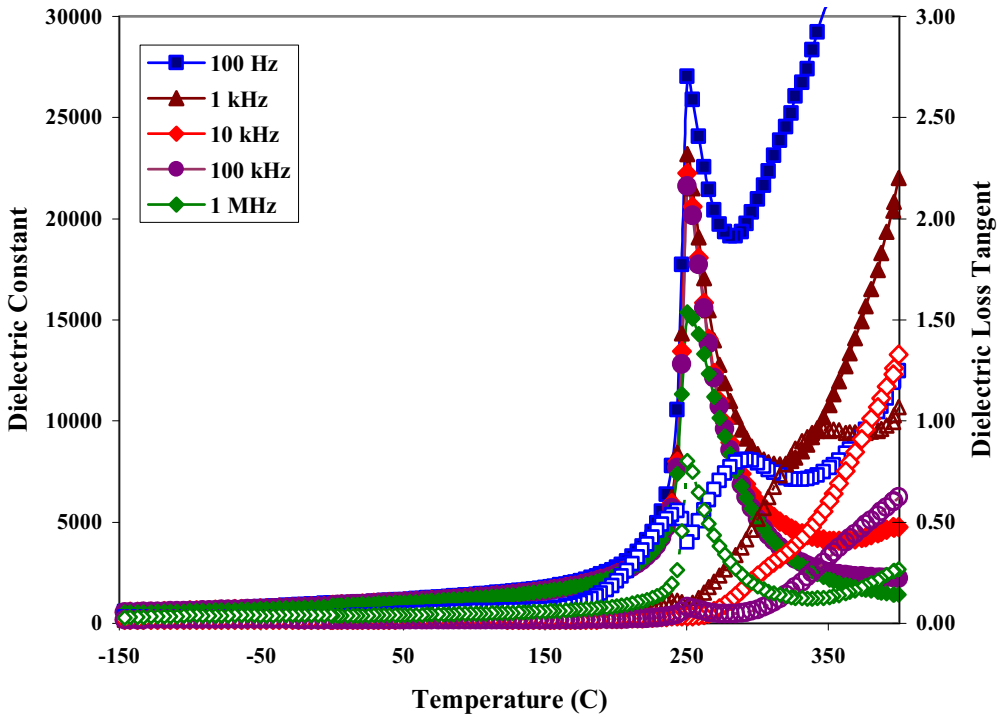

Fig. 1 (c) Temperature and frequency dependences of dielectric properties of 0.5PMN-0.5PT ceramic (open markers with dotted lines indicate data for the dielectric loss tangent (tan δ) at the same frequency)

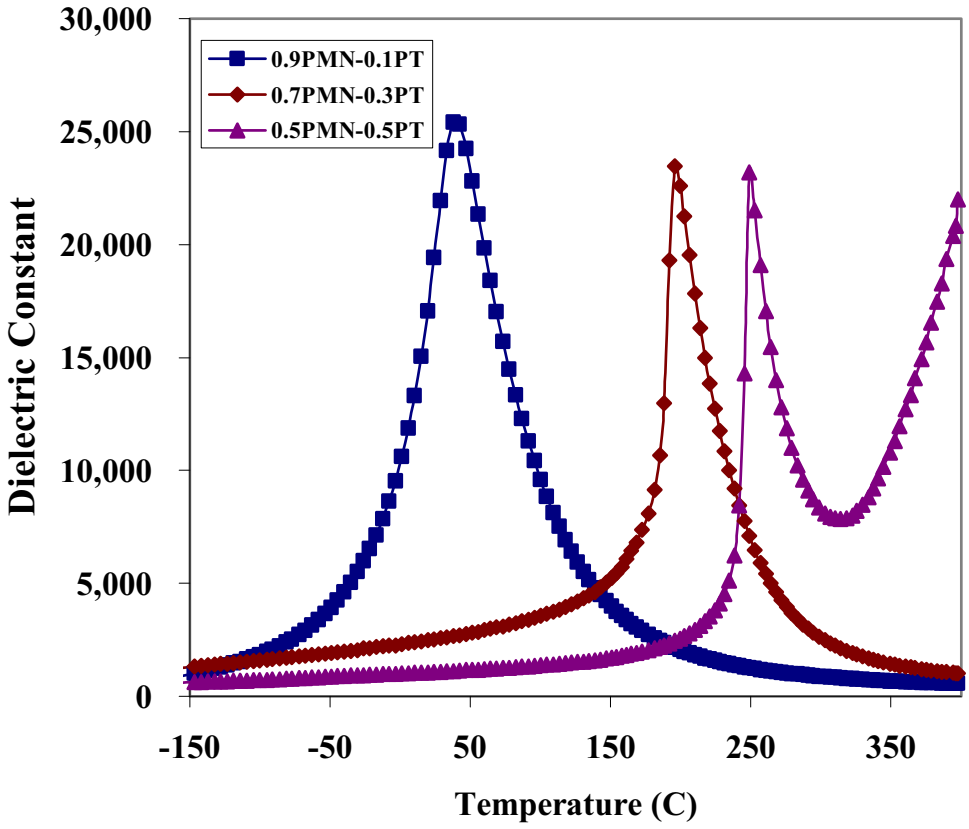

Fig. 2 Temperature dependence of dielectric constant of PMN-PT ceramics (measured at 1 kHz)

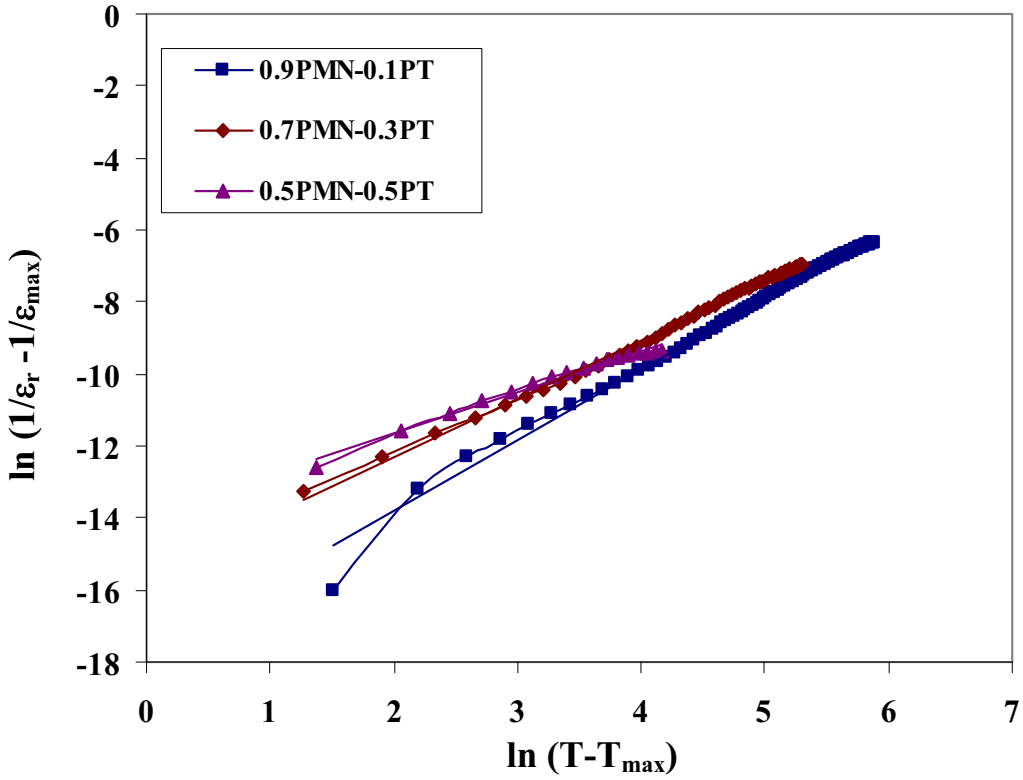

Fig. 3 Variation of ln $(1/\varepsilon_r - 1/\varepsilon_{max})$ vs ln $(T-T_{max})$ of PMN-PT ceramics in the paraelectric region at 1 kHz.

Effect of Sintering Temperature on Phase Formation, Dielectric, Piezoelectric, and Ferroelectric Properties of Nb-Doped $Pb(Zr_{0.52}Ti_{0.48})O_3$ Ceramics

PIYACHON KETSUWAN*, ATHIPONG NGAMJARUROJANA,YONGYUT LAOSIRITAWORN, SUPON ANANTA and RATTIKORN YIMNIRUN

Department of Physics, Faculty of Science, Chiang Mai University, Chiang Mai 50200, Thailand

The effects of sintering temperature on physical and electrical properties of the $Pb(Zr_{0.52}Ti_{0.48})O_3$ ceramics with addition of 1wt% Nb_2O_5 prepared by conventional mixed oxide technique were investigated. The samples were sintered over temperature rang 1200 -1300 ^oC. At lower sintering temperature, the dominant phase was rhombohedral while the tetragonal phase became dominant at higher temperature. The dielectric constant increased with increasing sintering temperature from 1200 to 1250 ^oC. Further increase in temperature resulted in a drop of the dielectric constant. Similar trend was also observed for the d_{33}-constant. For the ferroelectric properties, the electrical coercivity and remnant polarization decreased with increasing sintering temperature.

Keywords: PZT-Nb, Phase formation, Dielectric, Piezoelectric, Ferroelectric

1. INTRODUCTION

$Pb(Zr_{0.52}Ti_{0.48})O_3$ is a composition near the morphotropic phase boundary (MPB) of $Pb(Zr,Ti)O_3$, that separates rhombohedral and tetragonal ferroelectric forms with the coexistence of the 14 orientation states: 6-tetragonal and 8-rhombohedral. That is essential to allow the strong polarization for piezoelectricity. As the MPB is nearly vertical on the phase diagram, intrinsic property persists over a wide temperature range [1]. Almost all useful PZT ceramics are doped or modified to improve properties for specific applications [2]. Lead zirconate titanate solid solution modifications are controlled by aliovalent cation additions. The excess charge cation addition is called donor doped or soft PZTs, and the charge deficient cation is acceptor doped or hard PZTs. One approach of modification is off-valent donor doping, such as Nb^{5+} replacing Zr^{4+}. This makes domain wall move more easily and results in enhanced dielectric constant and coupling factor but reduced electric coercivity [3].

For PZT ceramics, a high temperature sintering process (>1200 ^oC) is normally employed to produce dense ceramics, which was the key factor for ensuring good physical and electrical properties. There have been many studies on effects of processing conditions on properties of lead-based perovskite ceramics [4-6]. Previous work on effect of sintering conditions on electric properties of PZT ceramics also showed interesting

results [7,8]. However, there have been only few reports on effect of sintering temperature of electrical properties of Nb-doped PZT ceramics prepared with conventional mixed-oxide method [9-11].

As an extension of earlier work, this study is therefore aimed at detailed and comprehensive investigation of influence of sintering temperature from 1200 to 1300 ^{o}C on phase formation, dielectric, piezoelectricc and ferroelectric properties of Nb-doped $Pb(Zr_{0.52}Ti_{0.48})O_3$ ceramics.

2. EXPERIMENTAL

The $Pb(Zr_{0.52}Ti_{0.48})O_3$ ceramics with addition of 1wt% Nb_2O_5 were prepared by conventional mixed oxide technique from PbO (Fluka 99.0%), ZrO_2 (Fluka 99.0%), TiO_2 (Fluka 99.9%) and Nb_2O_5 (Aldrich 99.9%) powders. After ball milling in ethanol for 24 h, the slurry was dried and calcined at 975 ^{o}C for 2 h [5]. Then, the calcined powder was pressed into discs (d =10 mm). The pellets were placed inside a closed alumina crucible covered with lead zirconate ($PbZrO_3$) powder to compensate the PbO volatilization and sintered at 1200-1300 ^{o}C for 2 h.

The x-ray diffraction (XRD) was used for structure and phase formation analysis. The microstructure was observed by scanning electron microscope (SEM). The bulk densities of sintered discs were measured by

the Archimedes method. The dielectric, piezoelectric and ferroelectric properties were determined by automated LCR-meter, d_{33}-meter and a Sawyer-Tower circuit, respectively. The specimens were poled under 30 kV/cm at 150 ^{o}C for 30 min in silicone oil [12,13].

3. RESULTS AND DISCUSSION

The x-ray diffraction pattern of $Pb(Zr_{0.52}Ti_{0.48})O_3$ +1wt% Nb_2O_5 ceramics with varying sintering temperature is shown in Figure 1(a). The peak intensity indicates the formation of perovskite phases, which could be matched with JCPDS file 73-2022 for rhombohedral phase of PZT and JCPDS file 33-0784 for tetragonal phase of PZT. At lower sintering temperature, the dominant phase was the rhombohedral phase which was characterized by a (020) peak between 43^{o} – 46^{o} (Figure 1(b)). The rhombohedral phase shift is also obvious for the specimens sintered at 1200 to 1250 ^{o}C for the peaks of (020). However, a distinct tetragonal splitting can be seen when sintered at 1275 ^{o}C, which was characterized by (020) and (200) peaks. Finally, the tetragonal phase became dominant at 1300 ^{o}C. The presence of rhombohedral phase is believed to be the effect of the over PbO volatilization in the lower sintering temperature from the covered lead zirconate ($PbZrO_3$) powder as the excess PbO has strong influence on the phase composition of PZT system near the MPB [14]. It

should be noticed that the ceramics sintered at 1250 ^{o}C show coexistence of tetragonal and rhombohedral phase (as shown in Figure 1(b)), which could explain enhanced properties [1], as will be discussed later.

The densification behavior of the specimens is shown in Figure 2. The density is seen to decrease with increasing temperature in the range of 1200 to1300 ^{o}C. Earlier reports also observed very similar trend [10,11]. The surface morphology of sintered ceramics was observed by using scanning electron microscope (SEM), as shown in Figure 3. The mean grain size of the ceramics was determined by using line intercept method. Also depicted in Figure 2, the mean grain size tends to increase with increasing sintering temperature. Similar observations have been reported in other systems [7,15,16]. However, the average grain size of $Pb(Zr_{0.52}Ti_{0.48})O_3$ with addition of 1 wt% Nb_2O_5 sintered at 1300 ^{o}C cannot be determined accurately due to the present of abnormal grain growth (Figure 3(e)) that is believed to be the result of the PbO loss at very high sintering temperature [17].

The maximum dielectric constant at Curie temperature(T_C) increased when the sintering temperature was increased from 1200 to 1250 ^{o}C (Figure 4(a)). Further increase in the sintering temperature resulted in a drop of the maximum dielectric constant. Similar trend is observed for the near room temperature dielectric constant (Figure 4(b)). The increased

dielectric properties with sintering temperature upto 1250 ^{o}C is belived to be a result of shifting of phase composition to near MPB, as supported by XRD in Figure 1(b). As shown in Figure 4(a) and listed in Table I, it should be noticed that over sintering temperature range of 1200 - 1250 ^{o}C the T_C is approximately 376 ^{o}C, while at higher sintering temperature (1275 ^{o}C and 1300 ^{o}C) T_C deceases to about 372 - 373 ^{o}C. Interestingly, the turning point at 1250 ^{o}C coincides with rhombohedral to tetragonal phase change identified by XRD. This observation is also observed in $Pb(Zr_{0.51}Ti_{0.49})O_3$ ceramics doped with 1 wt% MnO_2 as reported by Okazaki and Nagata [18]. The reason could be the composition shift or Pb-loss, especially at high sintering temperature, i.e. 1275 ^{o}C and 1300 ^{o}C.

In addition, as also listed in Table I, piezoelectric d_{33}-constant also increased with increasing sintering temperature from 1200 to 1250 ^{o}C, Though it is expected that the d_{33}-constant should further increase with increasing grain size [19], a drop of the d_{33}-constant was observed when the sintering temperature was further increased to 1300 ^{o}C with increasing grain size to 2 m. The explanation lies in the co-existence of two phases at 1250 ^{o}C, which results in the enhancement of d_{33}–value. Therefore, this is an evident of competing mechanism between grain size and sintering temperature in controlling the d_{33}–constant. In this case, the sintering temperature, which controls the phase formed, dominates [20].

As listed in Table I, it should be noticed that the optimum soft piezoelectric behavior with high $_r$, d_{33} and low E_c is observed in ceramics sintered at 1250 ^oC, in agreement with earlier reports [10,21,22], as also supported by the coexistence of tetragonal and rhombohedral phases discussed earlier.

The ferroelectric hysteresis behavior of $Pb(Zr_{0.52}Ti_{0.48})O_3$ with addition of 1 wt% Nb_2O_5 is shown in Figure 5. The electrical coercivity (E_c) and the remnant polarization (P_r) are seen to decrease with increasing sintering temperature. On the other hand, in the view of hysteresis behavior versus grain size, E_c is increased with decreasing grain size while the P_r decreased. These observations clearly indicate the soft piezoelectric behavior of Nb-doped PZT, as expected. Most importantly, this study shows that to achieve the optimum properties not only the starting chemical composition one also needs to obtain suitable sintering conditions.

4. CONCLUSION

The effects of sintering temperature on the physical and electrical properties of $Pb(Zr_{0.52}Ti_{0.48})O_3$ ceramics with addition of 1wt% Nb_2O_5

were investigated. The density decreased with increasing sintering temperature, while the grain size increased. The dielectric constant and d_{33}-constant reached maximum values at sintering temperature of 1250 ^{o}C. The electrical coercivity and remnant polarization decreased with increasing sintering temperature.

ACKNOWLEDGMENTS

This work was supported by the Thailand Research Fund (TRF), Graduate School and Faculty of Science, Chiang Mai University.

REFERENCES

[1] L. E. Cross, Mater. Chem. Phys., **43**, 108 (1996).

[2] G. H. Haertling, J. Am. Ceram. Soc., **82(4)**, 797 (1999).

[3] K. Okazaki, K. Nagata, J. Am. Ceram. Soc., **56**, 82 (1973).

[4] R. Wongmaneerung, R. Yimnirun and S. Ananta, Mater. Lett., **60**, 2666 (2006).

[5] W. Chaisan, R. Yimnirun, S. Ananta and D.P. Cann, Mater. Lett., **59(28)**, 3732 (2005).

[6] S. Wongsaenmai, Y. Laosiritaworn, S. Ananta and R. Yimnirun, Mater. Sci. Eng. B, **128(1-3)**, 83 (2006).

[7] R. Yimnirun, R. Tipakontitikul, S. Ananta, Inter. J. Mod. Phys. B, **20(17)**, 2415 (2006).

[8] D. A. Buckner and P. D. Wilcox, Am. Ceram. Soc. Bull., **51(3)**, 218 (1972).

[9] P. GR. Lucuta, Fl. Constantinecu, and D. Barb, J. Am. Ceram. Soc., **68(10),** 533 (1985).

[10] S.Y. Chu, T.Y. Chen, I. T.Tsai, Integra. Ferr., **58**, 1293 (2003).

[11] C. A. Randll, N. Kim, J. P. Kucera, W. Cao, T. R. Shrout, J. Am. Ceram. Soc., **81[3]**, 677 (1998).

[12] R. Yimnirun, S. Ananta and P. Laoratanakul, J. Eur. Ceram. Soc., **25(13)**, 3225 (2005).

[13] R. Yimnirun, Ferroelectrics, **331**, 9 (2006)

[14] K. Kakegawa, O. Matunaga, T. Kato, Y. Sasaki, J. Am. Ceram. Soc., **78(4)**, 1071 (1995).

[15] Y. S. Hong, H. B. Park and S. J. Kim, J. Eur. Ceram. Soc., **18**, 613 (1998).

[16] T. Y. Chen, S. Y. Chu and Y. D. Juang, Sensor. Actuat. A-Phys, **102**, 6 (2002).

[17] S. Chiang, N. Nasihoka, R.M. Fulrath and J.A. Pask, Am. Ceram. Soc. Bull., **60 (4)**, 484 (1981).

[18] K. Okazaki, K Nagata, J. Soc. Mater. Sci. Jpn. **4**, 404 (1972).

[19] K. Okazaki, K Nagata, J. Electron. Commun. Soc. Jpn. C, **53**, 815 (1970).

[20] Y. Xu, Ferroelectric Materials and Their Application (North-Holland, 1991).

[21] B. H. Chen, C. L. Huang and L. Wu, Solid. Electron., **48**, 2293 (2004).

[22] C. L. Huang, B. H. Chen and L. Wu, Solid. Commun., **130**, 19 (2004).

Table Caption

Table 1 Sintering temperature dependence of d_{33} , P_r , E_c , T_c and $_r$.

Figure Caption

Figure 1 (a) XRD pattern of $Pb(Zr_{0.52}Ti_{0.48})O_3$ +1wt% Nb_2O_5 ceramics sintered at various temperatures (b) magnification of XRD peaks near 45^o showing peaks evolution.

Figure 2 Dependence of density and grain size of $Pb(Zr_{0.52}Ti_{0.48})O_3$ +1wt% Nb_2O_5 ceramics on the sintering temperature.

Figure 3 SEM micrographs of $Pb(Zr_{0.52}Ti_{0.48})O_3$ +1wt% Nb_2O_5 ceramics sintered at (a) 1200 ^{o}C (b) 1225 ^{o}C (c) 1250 ^{o}C (d) 1275 ^{o}C and (e) 1300 ^{o}C.

Figure 4 Dielectric constant as a function of sintering temperature of $Pb(Zr_{0.52}Ti_{0.48})O_3$ +1wt% Nb_2O_5 ceramics measured at (a) Curie temperature (b) near room temperature (1kHz).

Figure 5 Sintering temperature dependence of P-E hysteresis loop of $Pb(Zr_{0.52}Ti_{0.48})O_3$ +1wt% Nb_2O_5 ceramics.

Figure 1 (a)

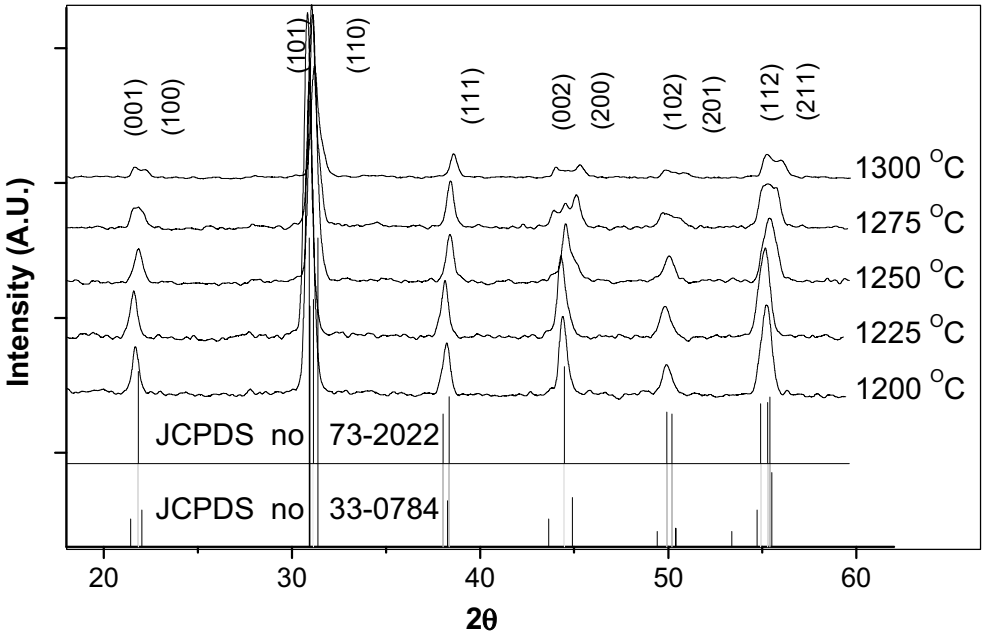
(001)
(100)
(101)
(110)
(111)
(002)
(200)
(102)
(201)
(112)
(211)
1300 °C
1275 °C
1250 °C
1225 °C
1200 °C
JCPDS no 73-2022
JCPDS no 33-0784
Intensity (A.U.)
20
30
40
50
60
2θ

Figure 1(b)

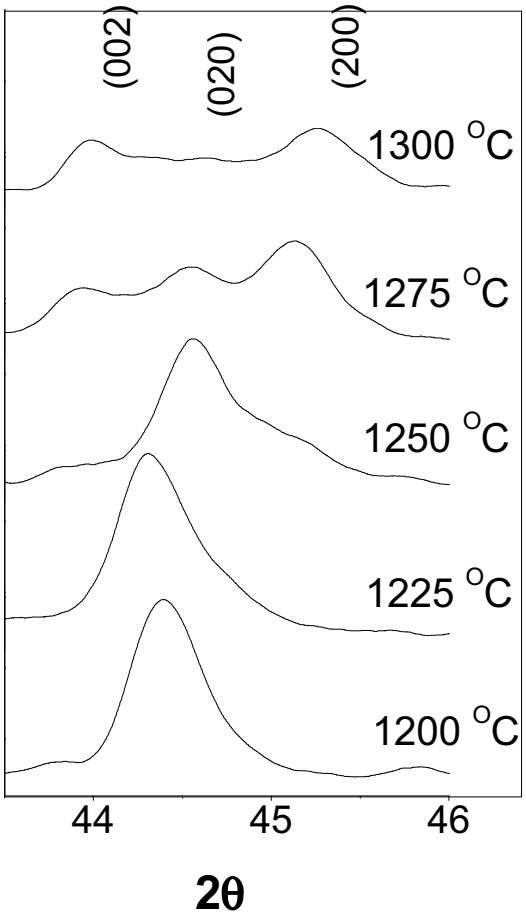

Figure 2

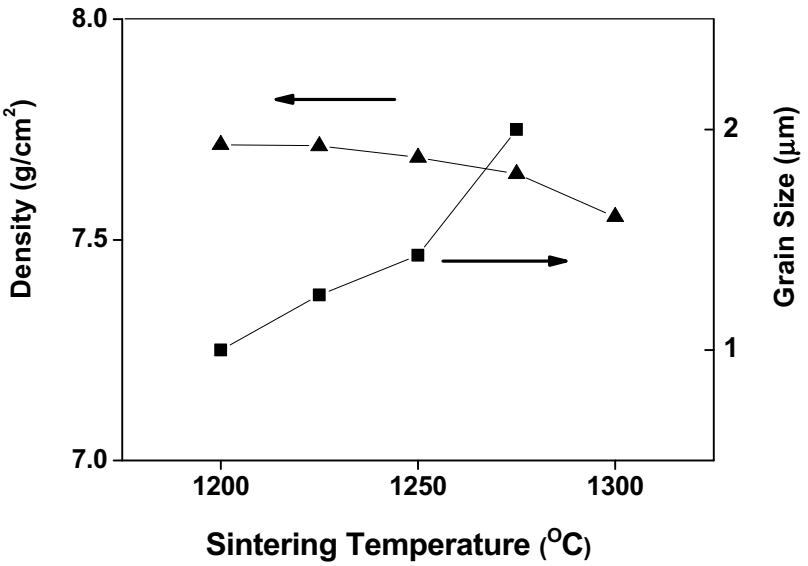
8.0
7.5
7.0
Density (g/cm^2)
2
1
Grain Size (μm)
1200
1250
1300
Sintering Temperature (^{O}C)

Figure 3

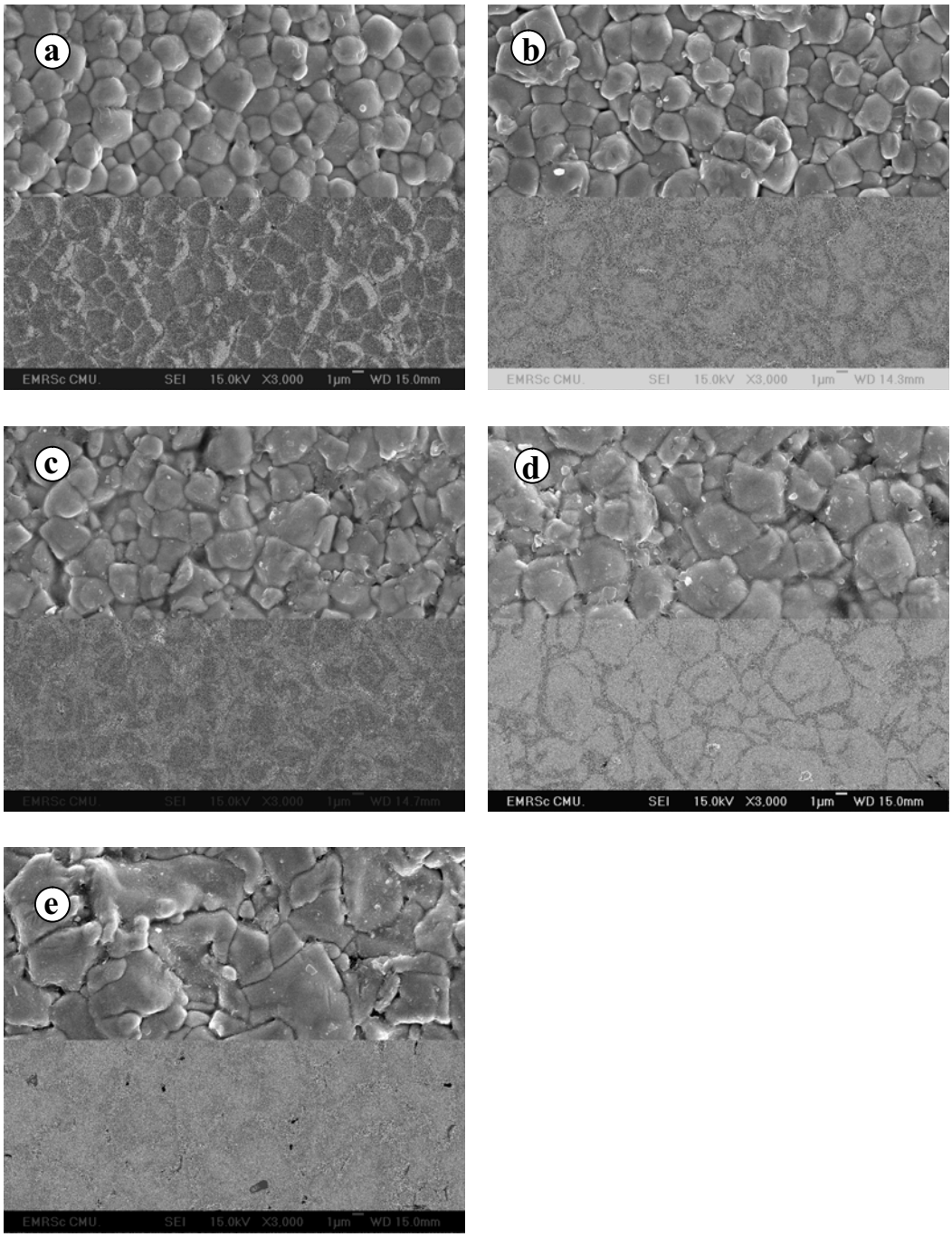
a
EMRSc CMU. SEI 15.0kV X3,000 1μm WD 15.0mm
b
EMRSc CMU. SEI 15.0kV X3,000 1μm WD 14.3mm
c
EMRSc CMU. SEI 15.0kV X3,000 1μm WD 14.7mm
d
EMRSc CMU. SEI 15.0kV X3,000 1μm WD 15.0mm
e
EMRSc CMU. SEI 15.0kV X3,000 1μm WD 15.0mm

Figure 4

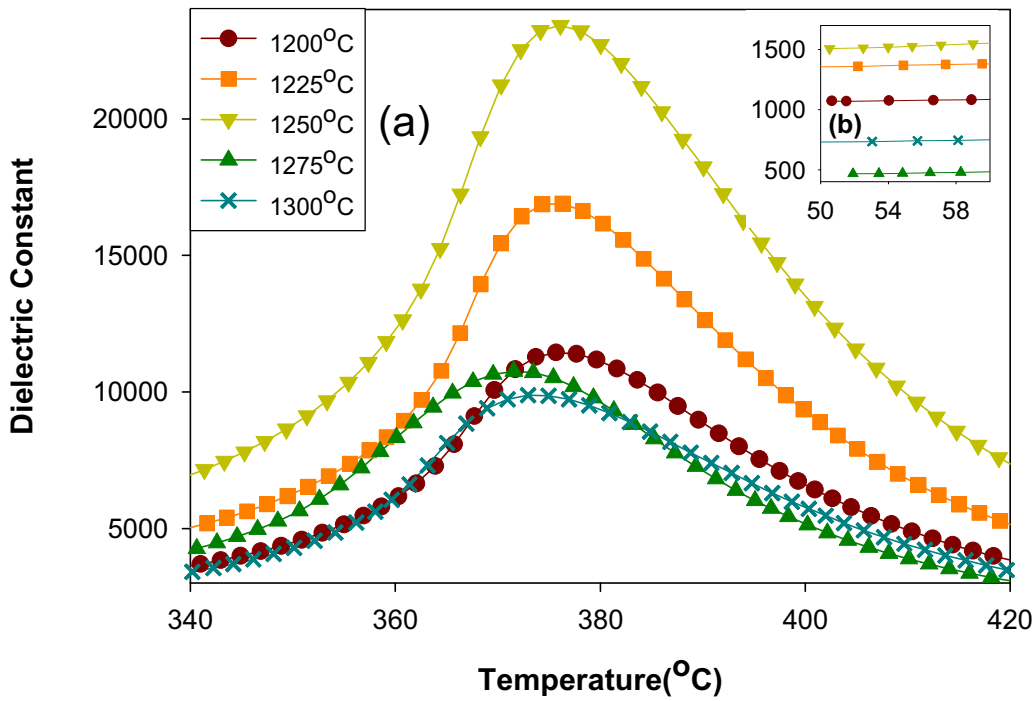
1200°C
1225°C
1250°C
1275°C
1300°C
(a)
(b)
Dielectric Constant
Temperature(°C)
20000
15000
10000
5000
340
360
380
400
420
1500
1000
500
50
54
58

Figure 5

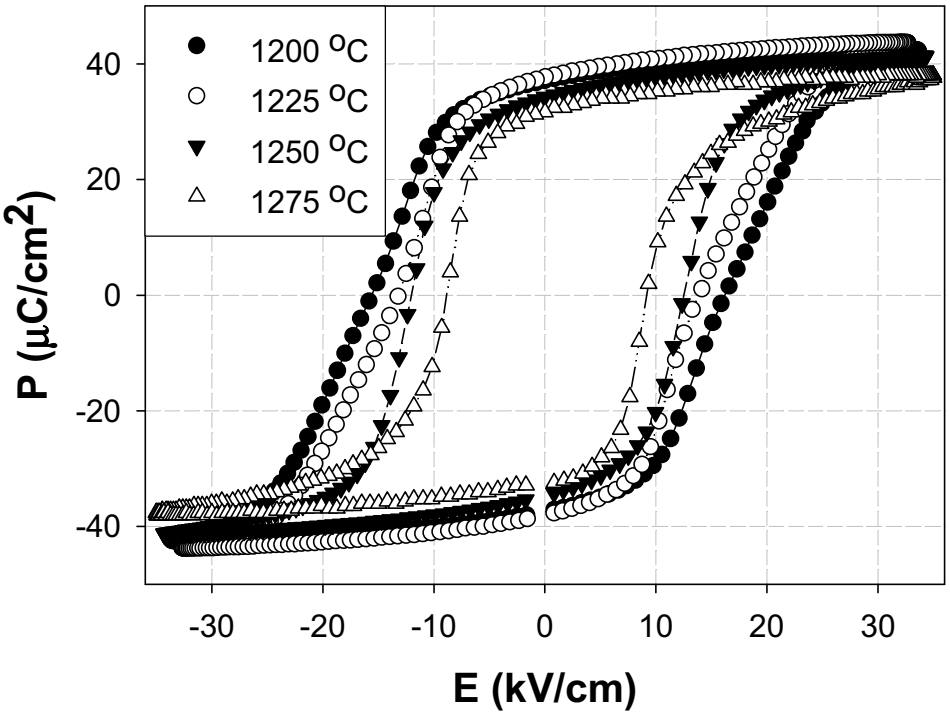
1200 °C
1225 °C
1250 °C
1275 °C
P (μC/cm2)
E (kV/cm)
40
20
0
-20
-40
-30
-20
-10
0
10
20
30

Table 1

Sintering temperature (^oC)	d_{33} (pC/N)	P_r ($\mu C/cm^2$)	E_c (kV/cm)	T_c (^oC)	ε_r(room)	ε_r(max)
1200	157	37.30	15.90	375.7	1073	11443
1225	221	37.90	13.52	376.3	1354	16895
1250	305	34.48	12.27	376.1	1508	23424
1275	206	32.23	9.00	371.6	466	10756
1300	109	-	-	373.0	730	9880

Scaling Behavior of Dynamic Ferroelectric Hysteresis in Soft PZT Ceramic: Stress Dependence

Rattikorn Yimnirun, Supon Ananta, Yongyut Laosiritaworn,

Athipong Ngamjarurojana and Supattra Wongsaenmai

Department of Physics, Faculty of Science, Chiang Mai University,

Chiang Mai, 50200 Thailand

Effects of electric field frequency, electric field amplitude, and mechanical stress on the hysteresis area were investigated on soft PZT ceramic. At stress-free condition, the investigation found the area scales with frequency and field amplitude in power law form, $A \quad f \quad E_0$; however, with different set of exponents in comparing to those in the investigation on thin films structure. On the other hand, with compressive stresses turning on, the same set of the exponents with the stress free condition is found to confirm universality. In addition, the scaling form of the area to triple parameters; i.e., frequency, field amplitude, and stress in a power law form, $\langle A \rangle \quad \langle A_{\sigma\ 0} \rangle \quad \langle A \quad A_{\sigma\ 0} \rangle \quad f^{\ 0.25} E_0 \sigma^{0.44}$, was obtained.

Keywords: Scaling, Stress, Hysteresis, soft PZT

Short Title: Stress Dependence Scaling of Soft PZT Ceramic

INTRODUCTION

In many sensor and actuator applications, as well as in more recently developed ferroelectric random access memories (Fe-RAMs), the dynamic hysteresis, i.e., hysteresis area <*A*> as a function of the field amplitude E_0 and frequency *f*, characteristics have become important consideration since they present a lot of information critical for the applications whose performance is related to the signal amplitude and frequency [1-3]. Theoretical studies have been carried out to understand the dynamic response of hysteresis curves in spin systems [4-6]. In particular, attention is focused on scaling law $A \quad f^{\alpha} E_0^{\beta}$ (where *a* and *ß* are exponents that depend on the dimensionality and symmetry of the system). The theoretical three-dimensional models $((F^2)^2$ and $(F^2)^3$ with O(N) symmetry (N? 8)) by Rao *et al.* and other investigators [4,6,7] proposed scaling relations applicable to the high-*f* limit as follows,

$$A \quad f^{\ 1} E_0 \quad \text{as} \quad f \qquad (1)$$

Apart from its theoretical importance, since reliable measurement of the hysteresis at ultra-high frequency is still a big challenge, it is technologically helpful to understand the scaling behavior so that the ultra-high frequency of the hysteresis can be predicted. Hence, there has been a great deal of interest in the

scaling behavior of the dynamic hysteresis in ferromagnetic and ferroelectric thin films [6-10]. Interestingly, some discrepancies between the theoretical predictions and the experimental results have already been reported for ferroelectric thin-films systems [9-12]. In contrast to the theoretically predicted scaling relation in Eq. (1), the experimental investigation on PZT thin films [11] has resulted in a different relation, i.e.,

$$A \quad f^{1/3} E_0 \quad \text{as} \quad f \tag{2}$$

Though bulk ferroelectric materials are useful and widely used in many applications [1-3], there has however been no report on the scaling behavior studies of ferroelectric hysteresis loops of bulk ferroelectric ceramics. It is therefore of great interest to investigate the form of this scaling relation for bulk systems. Hence, one of the aims of this present study is to investigate the scaling behavior of the dynamic hysteresis of the bulk ceramic.

More importantly, in many applications the ceramic specimens are often subjected to mechanical loading, either deliberately in the design of the device itself or because the device is used to change shapes as in many smart structure applications or the device is used under environmental stresses [1-3,13]. A prior knowledge of how the material properties change under different load conditions is inevitably crucial for proper design of a device and for suitable selection of materials for a specific application. It is therefore important to determine the

properties of these materials as a function of applied stress. Previous investigations on the stress-dependent electrical properties of many ceramic systems, such as undoped-PZT, PLZT, BT, PMN-PT, PZT-BT, PMN-PZT, and PZT and SBT thin films [14-20] have clearly emphasized the importance of the subject. This study will focus on very important bulk ceramic, i.e., donor-doped or soft lead zirconate titanate ($Pb(Zr_{1-x}Ti_x)O_3$ or PZT) ceramics. Because of the "soft" piezoelectric behaviors with higher dielectric and piezoelectric activities, soft PZT have been employed extensively in sensor and actuator applications, as well as smart systems [1-3]. Many investigations have already revealed interesting results on the electrical properties of the soft PZT ceramics under applied stress [14,17,20]. The ferroelectric properties of the soft PZT ceramics have been observed to change significantly with the applied stress [17,20]. However, it is interesting that there have been no report on the influence of the external stress on the scaling behavior of any materials. Therefore, the main aim of this study is to establish the scaling behavior of the dynamic hysteresis responses of the technically important and commercially available soft PZT bulk ceramics under the influence of the external stress.

EXPERIMENTS

The dynamic hysteresis (P E) loops of commercially available soft PZT ceramic (PKI-552, Piezo Kinetics Inc., USA) were characterized at room temperature (25 C) by using a computer controlled modified Sawyer-Tower circuit with f

covering from 2 to 100 Hz and E_0 from 0 to 18 kV/cm. The electric field was applied to a sample by a high voltage AC amplifier (Trek, model 610D) with the input sinusoidal signal from a signal generator (Goodwill, model GAG-809). The detailed descriptions of this system are explained elsewhere [18,20]. Effects of the external stress on the dynamic hysteresis were investigated with the compressometer, which was developed for simultaneous applications of the mechanical stress and the electric field [20]. Measurements were performed as a function of mechanical stress applied discretely between 0 and 24 MPa. During the measurements, a desired stress was first applied to the sample and then the electric field with varying frequency was applied. The dynamic hysteresis (P E) loop was then recorded for each applied field and frequency. The measurements reported were for the samples during their first mechanical stress cycle. It should also be noted that the reported ferroelectric parameters were obtained after a total of 10 cycles of the electric field were applied to the sample at each constant stress.

RESULTS AND DISCUSSION

The hysteresis profiles for various frequencies f, field amplitude E_0, and stress σ are obtained. Figs. 1(a) and 1(b) show examples of the hysteresis loops at different f but fixed E_0 (18 kV/cm), and at different E_0 but fixed f (100 Hz), respectively, under a stress-free condition. From Fig. 1(a), where E_0 is fixed, one sees the evolution of the pattern at different f. It is very interesting to observe

that as the frequency increases the hysteresis changes from an unsaturated loop with near square shape and rounded at the tips at low frequency (2 Hz) to well saturated loops at higher frequencies. The loop area $<A>$, remanent polarization (P_r), and coercive field (E_c) decrease with an increase of frequency. The observation that the $<A>$ decreases with increasing frequency in this high-f region is ascribed to the delayed response of the spin reversal to the varying external field [9,10]. Figure 1(b) shows the dependence of the hysteresis loop on the amplitude of the electric field. For small fields, the loop does not saturate and appears as an ellipse inclined at an angle to the E axis. An increase in the amplitude of the field E_0 makes the loop larger and increases its angle of inclination. For a given frequency of 100 Hz, as shown in Fig. 1(b), loop area $<A>$, remanent polarization (P_r), and coercive field (E_c) increase with an increase of E_0 until well saturated loop is achieved. Figure 1(c) displays the hysteresis loops of the soft PZT ceramics under different compressive stress during loading at fixed f of 100 Hz and fixed E_0 of 18 kV/cm. It should first be noticed that the area of the P E loops decreases steadily with increasing the stress. The P E loop area indicates the polarization dissipation energy of a ferroelectric material subjected to one full cycle of electric field application [18,20]. This amount of the energy loss is directly related to volume involved in the switching process during the application of electric field [17].When the mechanical stress is applied, more and more ferroelectric domains are constrained by the applied stress and cannot be re-oriented by the electric field

so as to participate in the polarization reversal. Consequently, both the saturation and remanent polarizations become lower with increasing the compressive stress [17,20]. The polarization dissipation energy is consequently found to decrease with increasing the applied stress, indicating that the sample volume contributing to polarization reversal decreases with the increasing stress. Similar observation has also been found in other investigations [17-20].

To investigate the scaling behavior under stress-free condition, we first followed the previous theoretical predictions on the loop–area by plotting the data of <*A*> against $f\ E_0$. This bases on an assumption that Eq. (1) is applicable, and the frequency range used in this study can be considered as the high frequency region since the loop–area decreases with increasing frequencies. The data are shown in Fig. 2(a) and the dotted line represents a fitting in terms of $A\quad f^{1}E_0$. Clearly, the theoretically proposed scaling relation in Eq. (1) cannot be directly applied to the data obtained in this study.

On the other hand, earlier experimental work by Liu *et al.* [11] on the scaling behavior of PZT thin films also showed different relation, as shown in Eq. (2). In that study, the scaling takes the form of $A\quad f\quad E_0$. To check the validity of the relation on the bulk system, i.e., soft PZT ceramic, we plot the data of <*A*> against $f\quad E_0$. The data are shown in Fig. 2(b) and the dotted line represents a fitting in terms of $A\quad f\quad E_0$. Large deviation is also observed in this case. Therefore, this implies that the scaling relations from both the

theoretical prediction and the experimental investigation are not applicable for the soft PZT bulk ceramic in this present study.

To obtain the suitable scaling relation, one can fit the data with $A \quad f^m E_0^n$ where m and n are exponents to be determined directly from the experimental data. By plotting $\langle A \rangle$ against f at fixed E_0, one obtains the exponent m. On the other hand, the exponent n can be obtained from plotting $\langle A \rangle$ against E_0 at fixed f. It should also be noted that there is more deviation from the minor loops without saturation at small field amplitudes, and these data were excluded from the fitting reported. It can be seen in Fig. 2(c) that the suitable exponent m for the frequency component has the value of –0.25 (within the limit of experimental errors), while the hysteresis area $\langle A \rangle$ is found to increase linearly with the applied field amplitude E_0, hence the exponent n should take the value of 1. Therefore, it is revealed that the data obtained under stress-free condition can be much better fitted (with R^2 = 0.97), within the measured uncertainty, by

$$A \quad f \quad E_0 \tag{3}$$

Therefore, Eq. (3) is identified as the suitable scaling relation for the soft PZT bulk ceramic under the stress-free condition.

Moreover, as evident in Fig. 1(c), at any given frequencies the hysteresis area $\langle A \rangle$ is found to decrease steadily with increasing the applied

stress. Therefore, instead of including only the field amplitude E_0 and the frequency term *f*, the scaling relation should also include the stress (σ) term, i.e.

$$A \quad f^m E_0^n \sigma^p \tag{4}$$

However, due to increasing number of exponents, to simplify the problem, we assume the validity of the scaling form $A \quad \sigma \quad f^{0.25} E_0$ for all applied stresses. Consequently, the area $\langle A \rangle$ for each stress is plotted against $f^{0.25} E_0$, as shown in Fig. 3(a). As can be seen form the least square linear fits, reasonably good linear relations can be found. As a result, the condition of universality having $m = -0.25$ and $n = 1$ in soft PZT bulk ceramic systems is confirmed whereas the proportional constant in Eq. (4) may still be a function of σ. Therefore, by discarding minor loops which usually occur at very low E_0, it is found that

$$\langle A \rangle \quad \langle A_{\sigma\ 0} \rangle \quad \langle A \quad A_{\sigma\ 0} \rangle \quad f^{0.25} E_0 \sigma^{0.44}, \tag{5}$$

where $\langle A_{s=0} \rangle$ refers to stress free hysteresis area which will be a dominant term for zero stress. Note that from the appearance of stress s, $\langle A - A_{s=0} \rangle$, referring to the difference in energy dissipation between under stress and stress free condition, increases with increasing stress suggesting a decay of $\langle A \rangle$ with s at a rate of $s^{0.44}$ as observed in experiments. As a result, from our studies, it may be concluded that in bulk ceramics, the difference of the

hysteresis area between under–stress and stress–free condition scales with frequency, field–amplitude and stress via exponents m = –0.25, n = 1, and p = 0.44. However, at a particular fixed stress, Eq. (5) yields Eq. (3) which is the original form for how the area scales with the frequency and the field–amplitude.

CONCLUSIONS

In this study, we investigated the hysteresis properties of the soft PZT bulk ceramics under the effect of mechanical stress at various frequencies and field amplitudes of the external applied electric field. Considering the scaling law for the loop area, at zero stress, the investigation found the area scales with frequency and the field amplitude in a power law function. However, the exponents to the scaling in this bulk ceramic system do not match with previous investigation on thin films structure. On the other hand, with inserting the uniaxial stress, the same set of exponents to frequency and field amplitude in stress free condition is found which confirms the condition of universality in bulk system. Furthermore, the difference of the energy dissipation between the under stress and stress free condition is found to scale with $f^{-0.25}E_0 s^{0.44}$.

ACKNOWLEDGMENTS

Financial supports from the Commission on Higher Education (CHE), Thailand Research Fund (TRF), and Faculty of Science and Graduate School of Chiang

Mai University are gratefully acknowledged.

REFERENCES

[1] K. Uchino, Ferroelectric Devices (Marcel Dekker, New York, 2000).

[2] B. Jaffe, W. R. Cook, and H. Jaffe, Piezoelectric Ceramics (Academic Press, New York, 1971).

[3] J.F. Scott, Ferroelectr. Rev. **1**, 1 (1998).

[4] M. Rao, H.R. Krishnamurthy, and R. Pandit, Phys. Rev. B **42**, 856 (1990).

[5] M. Acharyya and B.K. Chakrabarti, Phys. Rev. B **52**, 6560 (1995).

[6] J.-M. Liu, H.L.W. Chan, C.L. Choy, and C.K. Ong, Phys. Rev. B **65**, 014416 (2001).

[7] M. Rao and R. Pandit, Phys. Rev. B **43**, 3373 (1991).

[8] Q. Jiang, H.N. Yang, and G.C. Wang, Phys. Rev. B **52**, 14911 (1995).

[9] B. Pan, H. Yu, D. Wu, X.H. Zhou, and J.-M. Liu, Appl. Phys. Lett. **83**, 1406 (2003).

[10] J.-M. Liu, H.L.W. Chan, C.L. Choy, Y.Y. Zhu, S.N. Zhu, Z.G. Liu, and N.B. Ming, Appl. Phys. Lett. **79**, 236 (2001).

[11] J.-M. Liu, H.P. Li, C.K. Ong, and L.C. Lim, J. Appl.Phys. **86**, 5198 (1999).

[12] J.-M. Liu, H. Yu, B. Pan, and X.Y. Chen, Mater. Sci. Eng. **B118**, 2 (2005).

[13] L.E. Cross, Mater. Chem. Phys. **43**, 108 (1996).

[14] Q.M. Zhang, K. Uchino, and J. Zheng, J. Mater. Res. **12**, 226 (1997).

[15] D. Viehland and J. Powers, J. Appl. Phys. **89**, 1820 (2001).

[16] R. Yimnirun, Ferroelectrics **331**, 9 (2006).

[17] D.Zhou, M. Kamlah, and D. Munz, J. Euro. Ceram. Soc. **25**, 425 (2005).

[18] R. Yimnirun, S. Ananta, A. Ngamjarurojana, and S. Wongsaenmai, Appl. Phys. A-Mater. **81**, 1227 (2005).

[19] T. Kumazawa, Y. Kumagai, H. Miura, M. Kitano, and K. Kushida, Appl. Phys. Lett. **72**, 608 (1998).

[20] R. Yimnirun, M. Unruan, Y. Laosiritaworn, and S. Ananta, J. Phys. D: Appl. Phys. **39**, 3097 (2006).

List of Figure Captions

Fig. 1 Hysteresis loops for soft PZT ceramic (a) at various f (E_0 = 18 kV/cm and σ = 0 MPa), (b) at various E_0 (f = 100 Hz and σ = 0 MPa), and (c) at various σ (f = 100 Hz and E_0 = 18 kV/cm).

Fig. 2 Scaling of hysteresis area <A> against (a) f E_0 (b) f E_0 and (c) f E_0 for soft PZT ceramic under stress-free condition.

Fig. 3 Scaling of hysteresis area <A> against (a) f E_0 at various compressive stresses, and (b) collapse of the scaling area against f E_0 under the effect of compressive stress s for soft PZT ceramics.

Fig. 1(a)

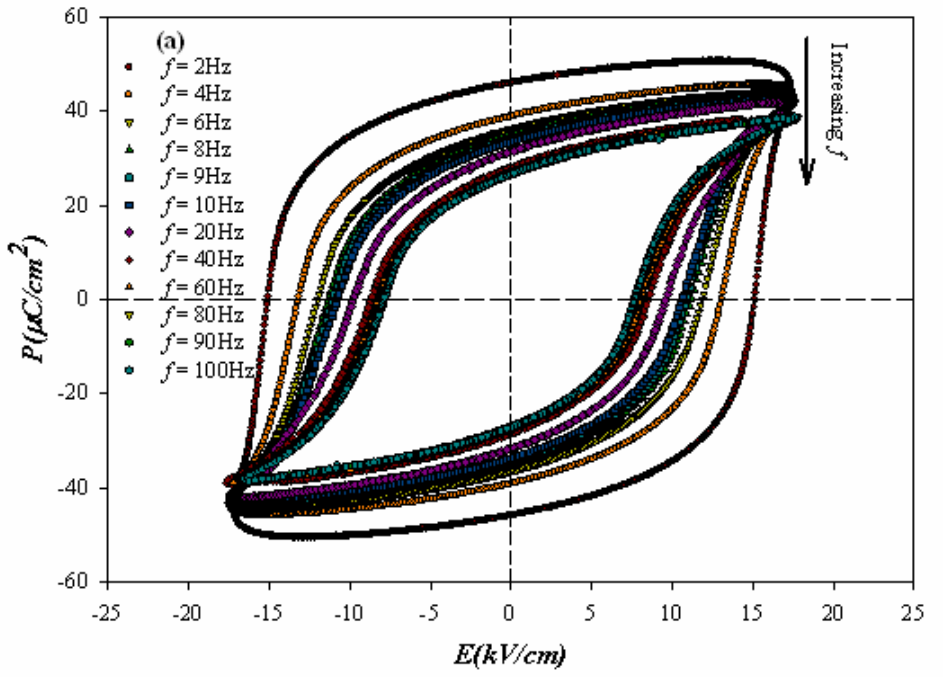
(a)
f = 2Hz
f = 4Hz
f = 6Hz
f = 8Hz
f = 9Hz
f = 10Hz
f = 20Hz
f = 40Hz
f = 60Hz
f = 80Hz
f = 90Hz
f = 100Hz
Increasing f
P(μC/cm²)
E(kV/cm)
60
40
20
0
-20
-40
-60
-25
-20
-15
-10
-5
0
5
10
15
20
25

Fig. 1(b)

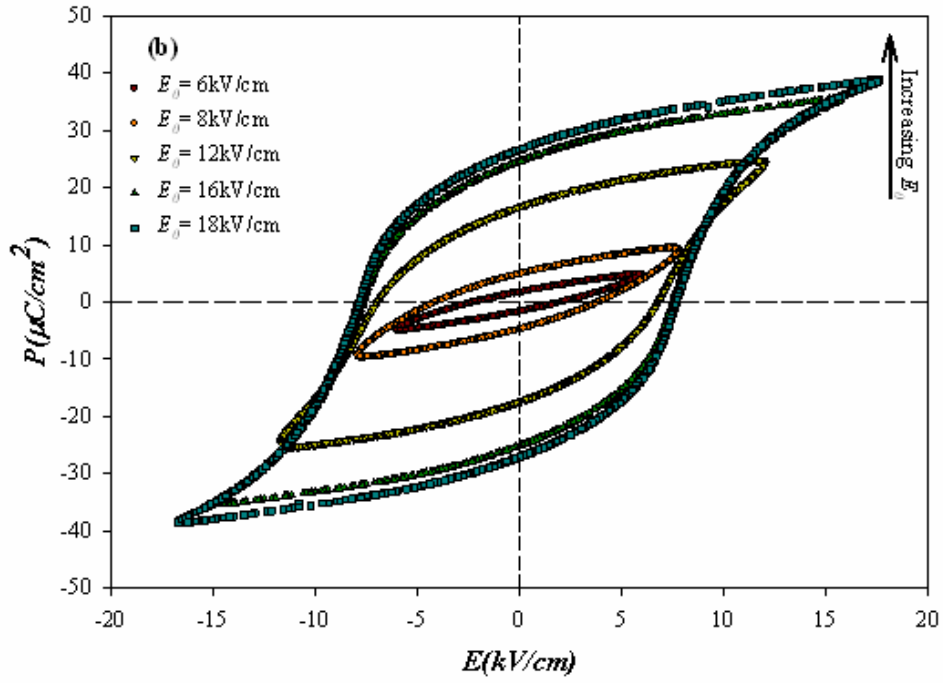
(b)
E_0 = 6kV/cm
E_0 = 8kV/cm
E_0 = 12kV/cm
E_0 = 16kV/cm
E_0 = 18kV/cm
Increasing E_0
P(μC/cm²)
E(kV/cm)
50
40
30
20
10
0
-10
-20
-30
-40
-50
-20
-15
-10
-5
0
5
10
15
20

Fig. 1(c)

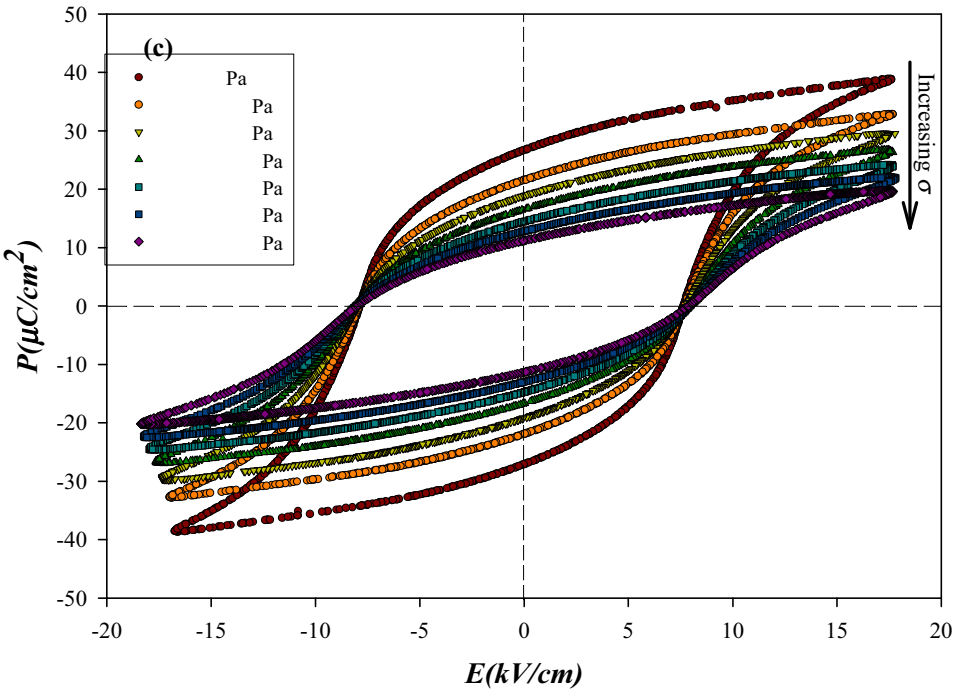
(c)
Pa
Pa
Pa
Pa
Pa
Pa
Pa
Increasing σ
P(μC/cm²)
E(kV/cm)
50
40
30
20
10
0
-10
-20
-30
-40
-50
-20
-15
-10
-5
0
5
10
15
20

Fig. 2(a)

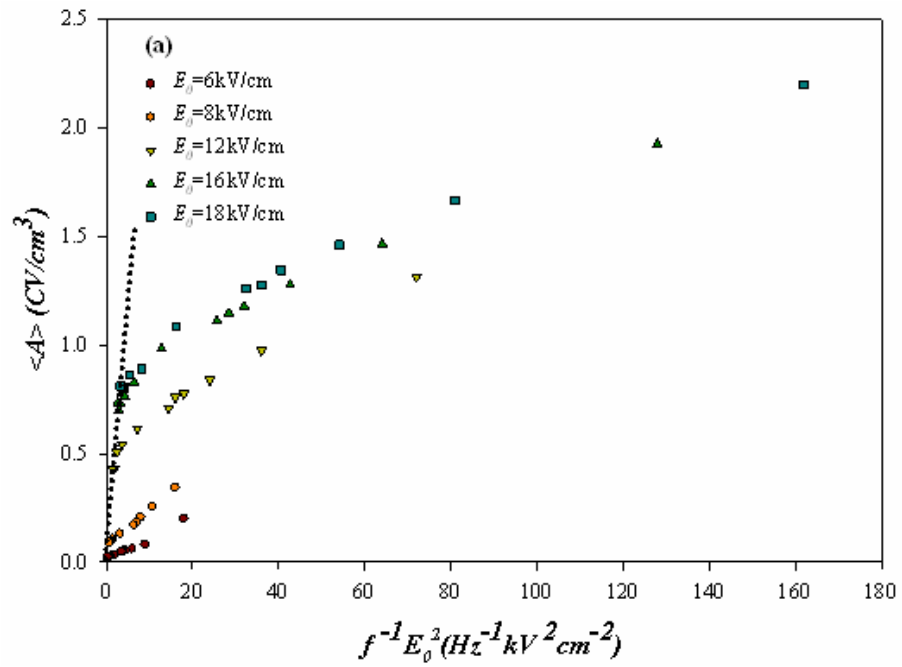
(a)
E_0=6kV/cm
E_0=8kV/cm
E_0=12kV/cm
E_0=16kV/cm
E_0=18kV/cm
<A> (CV/cm^3)
$f^{-1}E_0^2$(Hz^{-1}kV^{2}cm^{-2})
0.0
0.5
1.0
1.5
2.0
2.5
0
20
40
60
80
100
120
140
160
180

Fig. 2(b)

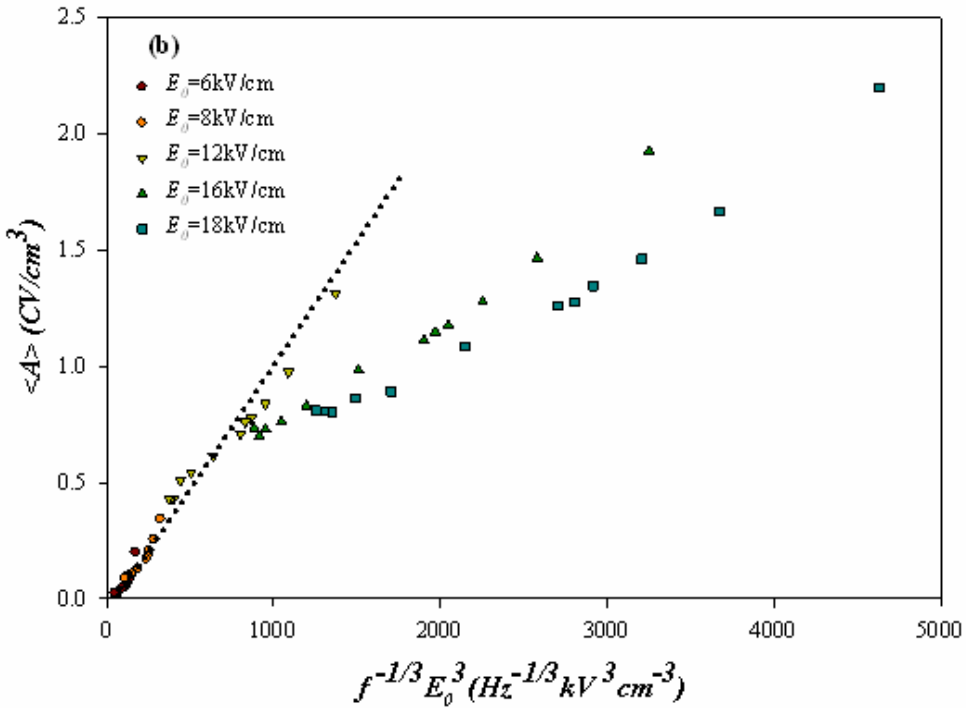
(b)
E_0=6kV/cm
E_0=8kV/cm
E_0=12kV/cm
E_0=16kV/cm
E_0=18kV/cm
<A> (CV/cm^3)
$f^{-1/3}E_0^3$ (Hz$^{-1/3}$kV^{3}cm^{-3})
0.0
0.5
1.0
1.5
2.0
2.5
0
1000
2000
3000
4000
5000

Fig. 2(c)

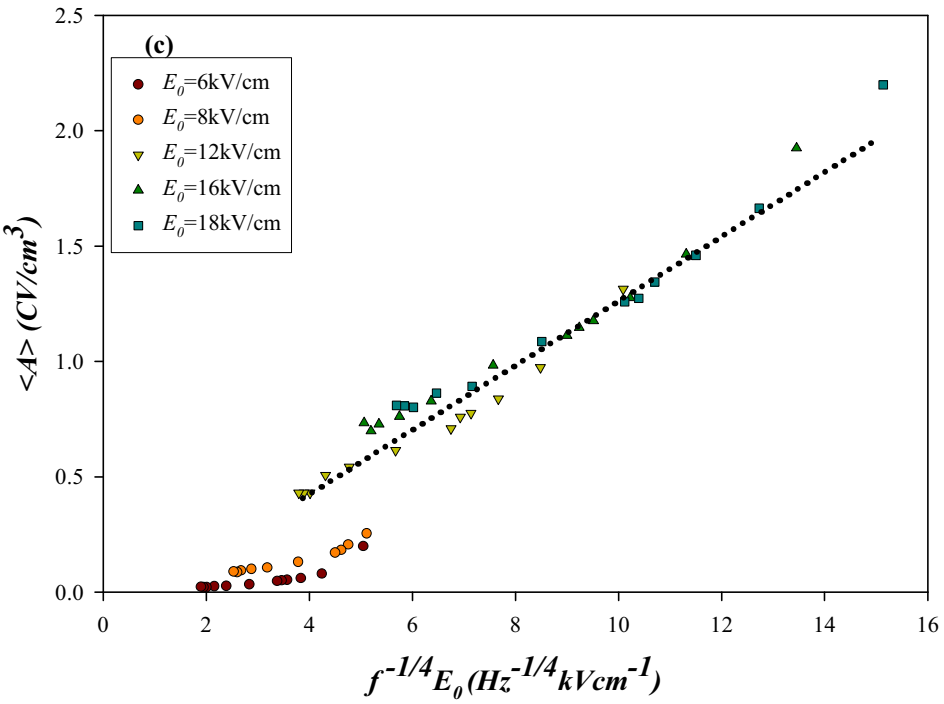
(c)
E_0=6kV/cm
E_0=8kV/cm
E_0=12kV/cm
E_0=16kV/cm
E_0=18kV/cm
<A> (CV/cm^3)
$f^{-1/4}E_0$ (Hz$^{-1/4}$kVcm^{-1})
0.0
0.5
1.0
1.5
2.0
2.5
0
2
4
6
8
10
12
14
16

Fig. 3(a)

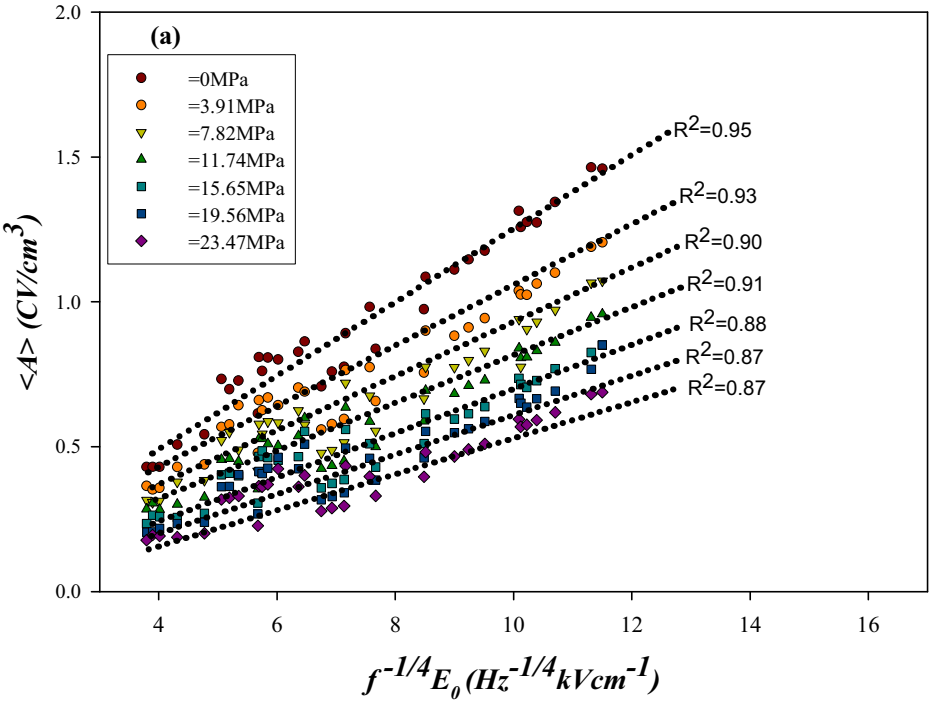
(a)
=0MPa
=3.91MPa
=7.82MPa
=11.74MPa
=15.65MPa
=19.56MPa
=23.47MPa
R2=0.95
R2=0.93
R2=0.90
R2=0.91
R2=0.88
R2=0.87
R2=0.87
<A> (CV/cm3)
f-1/4E0 (Hz-1/4kVcm-1)
0.0
0.5
1.0
1.5
2.0
4
6
8
10
12
14
16

Fig. 3(b)

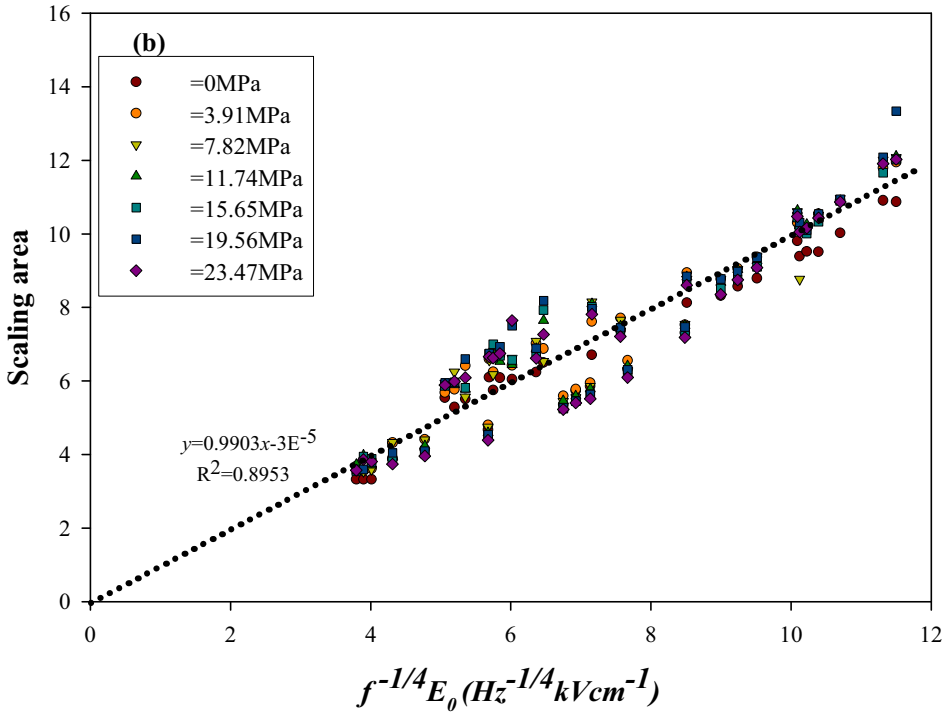
(b)
=0MPa
=3.91MPa
=7.82MPa
=11.74MPa
=15.65MPa
=19.56MPa
=23.47MPa
y=0.9903x-3E-5
R2=0.8953
Scaling area
f-1/4E0 (Hz-1/4kVcm-1)
0
2
4
6
8
10
12
14
16

Effect of Addition of BT on Relaxor Behavior of PIN-PT Ceramics

Supattra Wongsaenmai*[1], Rattikorn Yimnirun[1], Supon Ananta[1], Ruyan Guo[2] and Amar S. Bhalla[2]
[1]Department of Physics, Faculty of Science, Chiang Mai University, Chiang Mai 50200, Thailand
Tel: (6653)-943445, e-mail: wongsaenmai@yahoo.com
[2]Materials Research Laboratory, The Pennsylvania State University, University Park, PA 16802, USA
Tel: (1814)-8659232, e-mail: asb2@psu.edu

ABSTRACT: Ferroelectric ceramics with chemical formula $(1-x)Pb(In_{0.5}Nb_{0.5})O_3$-$(x)PbTiO_3$ and $(1-x)Pb(In_{0.5}Nb_{0.5})O_3$-$(x)PbTiO_3$ with 20 %mol of BT (x = 0.0, 0.1, 0.2 and 0.3) were prepared via the wolframite method. The relaxor behavior was analyzed from the dielectric properties and thermal expansion measurements. The dielectric properties were measured at frequencies between 100 Hz and 100 kHz whereas the thermal expansion was measured in the temperature range between -145°C and 500°C. It is found that the addition of BT effects the relaxor behavior of PIN-PT system. The broad and diffused dielectric constant maxima and essentially no change in Burns temperature were measured and thus suggesting the glassy polarization and relaxor behavior in the PIN-PT-BT compositions.

Keywords: PIN-PT, PIN-PT-BT, Relaxor ferroelectric, Thermal expansion, Dielectric properties

INTRODUCTION

The relaxor ferroelectric ceramics, which have the $Pb(B'B'')O_3$ complex perovskite structure, show broad dielectric transition maxima, high dielectric constant over a wide temperature range and frequency dispersion of dielectric properties [1-4]. Several models have been proposed to explain the relaxor behavior. However these models explain some features of the relaxor behavior but none can fully explain all the interesting properties observed in this class of materials. The glassy polarization behavior of relaxor ferroelectric, has been considered by Burns and Dacol's and supported by the measurements of the optic index of refraction, n(T), dependence on the temperature [5-8]. The deviation from the linear n(T) was observed starting at Burns temperature (T_d) which is much higher than the dielectric transition temperature maxima (T_m). This behavior was interpreted in term of the local polar regions of dynamic polarization (P_d), randomly orientated, small sizes with small number of unit cells, which grow with the reducing temperature. The local polarization exists above the transition temperature while disappear or become unmeasurable above Burns temperature [9]. The other techniques like Raman scattering [9], neutron powder diffraction [10] and neutron elastic scattering [11], dynamic light scattering [12], dielectric measurements [13–15], including thermal expansion technique [16] have been used to measure Burns temperature and explain the relaxor glassy behavior. There are reports on the relaxor behavior analysis by using the thermal expansion measurement in other classic relaxor ferroelectric such as PMN-PT, PMN, PZN, PLZT and tungsten bronze structure family [6, 8, 17-20], but no reported data on the glass-like behavior of order-disorder relaxor ferroelectric like PIN-based system.

PIN is of interest for the study of chemical ordering in relaxor systems. It is a member of relaxor family with a 1:1 stoichiometric B-site ordering which can be brought from disordered state into ordered state by a thermal treatment [21]. The disordered state of PIN exhibits a typical relaxor behavior which shows a broad dielectric maximum near 66 ºC [22, 23]. In contrast, the ordered state shows an antiferroelectric behavior with a sharp change in dielectric constant vs. temperature measurements at 168 ºC [23, 24]. The solid solution of relaxor ferroelectric and normal ferroelectric PT has excellent piezoelectric and electrostrictive properties [25, 26]. It is reported that the addition of BT to PMN- and PZN-based systems helps

decrease T_m of the systems and at the same time stabilizes the perovskite structure [27, 28]. Interestingly, there has been no report for the PIN-PT-BT system.

In this paper, the relaxor behavior of PIN-PT and the PIN-PT systems with addition of BT were studied for their dielectric properties and thermal expansion behavior. The broad maxima at the phase transition of dielectric constant vs. temperature were analyzed. Thermal expansion behavior of both the systems was studied and it showed deviation from the linear relationship below the Burns temperature. The local polarization (glassy behavior) was calculated from the collected thermal strain data. Both the dielectric and thermal expansion measurements suggest that the addition of PT lead to the normal ferroelectric while the addition of BT leads to the more relaxor ferroelectric like behavior.

EXPERIMENTAL

The powders of $(1-x)Pb(In_{0.5}Nb_{0.5})O_3$-$(x)PbTiO_3$ and $(0.8-x)Pb(In_{0.5}Nb_{0.5})O_3$-$(x)PbTiO_3$-$0.2BaTiO_3$ (x = 0.0, 0.1, 0.2 and 0.3, abbreviated as PIN-PT and PIN-PT-BT, respectively) were synthesized by a two-step solid solution reaction method [29]. The wolframite $InNbO_4$ was first prepared from oxide powder of In_2O_3 and Nb_2O_5 [30]. Mixed powders were milled and calcined at temperature 1100ºC for 2 hours to obtain the intermediate precursor $InNbO_4$ [31]. The wolframite precursor was then mixed with reagent grade powder of PbO, TiO_2 for PIN-PT system and PbO, $BaCO_3$, TiO_2 for PIN-PT-BT system. Excess amount of PbO (2%) and In_2O_3 (2%) were added at this stage. The mixtures were milled again following the intermediate precursor stage. After drying, the mixtures were calcined at temperature between 800ºC and 1000ºC, 1050ºC and 1250ºC with soaking time of 2 hours for PIN-PT and PIN-PT-BT, respectively [32]. Pellets were pressed with the addition of 1% PVA. The pressed pellets were sintered with the soaking time of 2 hours in a double crucible configuration at temperature from 1100ºC to 1125ºC for PIN-PT system and 1250 to 1300ºC for PIN-PT-BT system. To prevent PbO loss, the pellets were buried in protective powders.

The temperature dependence of the dielectric properties was measured with an LCR meter (HP-4284A, Hewlett-Packard, Santa Clara, CA) in conjunction with an environmental chamber (9023, Delta Design, Poway, CA). A heating rate of 2ºC/min and frequencies of 100, 1k, 10k and 100k Hz were used during measurement.

For the thermal expansion measurement, first the ceramics were cut to rectangular bars with dimensions 5mm×1mm×1mm. The temperature dependent sample expansion (strain) was measured with a linear voltage-differential transformer (LVDT) dilatometer (Series 6500, theta industries, Inc., NY). A heating rate of 2ºC/min and temperature range between -145°C and 500°C, were used for the measurements.

RESULTS AND DISCUSSION

The temperature dependence of dielectric properties, at different frequencies of PIN-PT and PIN-PT-BT systems is shown in Fig.1. The plots show the broad and diffuse phase transition temperature maxima at various frequencies. The transition temperature maxima, (T_m), shift to higher side with increasing frequency whereas the maximum of dielectric loss does the contrary. For the PIN-PT system, the dielectric constant plots show the broad peak at composition x = 0.0 and x = 0.1, then gradually change to a sharper peak with increasing PT concentration. On the other hand, the system which has 20 %mol of BT, the dielectric constant plot is broader than that of PIN-PT with the same PT content. However, the changing to the sharper maxima was

also observed with increasing PT concentration. The frequency dispersion of the dielectric properties can also be viewed as the measure of relaxor behavior. Since $T_m = T_{m,\,100kHz} - T_{m,\,100Hz}$ can be used as a rough indication of the relaxor behavior, the various T_m are calculated for the compositions and are listed in Table I. It is clear that addition of PT results in smaller T_m and thus indicates the decreasing trend of relaxor behavior and increasing fine disorder at B-site with increasing PT content [33] while with the addition of BT, T_m increases and hence the relaxor behavior. These results are in line obtained for the PT and BT additions to the PZN-based system [27].

The temperature dependences of thermal strain of PIN-PT and PIN-PT-BT ceramics are shown in Fig. 2 and 3. The plots show the nonlinear behavior at low temperature and then follow a linear relationship above Burns temperature. There is no clear correlating anomaly of the thermal expansion with the dielectric transition temperature. This behavior differs from that of normal ferroelectric which shows an abrupt discontinuity at the transition temperature and then follows linear behavior above the transition temperature in the paraelectric region. The deviation from the linear relationship below Burns temperature was observed for all the compositions. The values of Burns temperatures between 380°C to 435°C depending on the PT concentration were determine from the plots and are listed in Table II. It shows that in most cases Burns temperature is much higher than the dielectric transition maxima temperature, T_m, as observed in other relaxor ferroelectrics [7]. Also it shows that the differential between transition temperature and Burns temperature decreases with increasing PT content. For the normal ferroelectric the deviation from the straight line appears at the transition temperature for the measurements like refractive index vs. temperature and thermal strain vs. temperature [34]. The increase in Burns temperature and T_m due to the addition of PT was attributed to the higher T_c of PT [35] but; the increase of PT concentration leads to the closeness of the two transition temperatures i.e. T_m and T_d as we approach the morphotropic phase boundary (MPB) composition in PIN-PT. This result leads to the conclusion that relaxor ferroelectric nature in PIN ceramics reduces with increasing PT concentration. The PIN-PT-BT compositions show lower Burns temperature compared to the same PT concentration. From these results, it is noticed that PIN-PT-BT system is of more relaxor in nature than the PIN-PT system. From the dielectric and thermal strain results, it is suggested that addition of PT leads the behavior towards a normal ferroelectric while addition of BT leading to an enhancement in relaxor behavior.

At high temperature above Burns temperature the strain and temperature shows a linear relation. The thermal expansion coefficient ( ) defined as $\alpha_T \quad dx_T / dT$ [34], were calculated at above and below T_d and are listed in Table II. These results show small thermal expansion coefficient values and compare well with reports on other relaxor ferroelectrics [11]. The plots of thermal expansion coefficient vs. temperature, as obtained from the measurements are shown in Fig 4. The nearly linear relation between thermal expansion coefficient and temperature above Burn temperature, which decreases rapidly below Burns temperature, is evident. At composition x = 0.3, PIN-PT twice the change in slope below the Burn temperature is noticed. It is possibly due to the morphotropic phase boundary transitions in this composition which is supposed to have shown a MPB transitions. On the other hand, such abrupt change has not been observed in case of PIN-PT-BT system. It is possibly due to the addition of BT and as a result shifting of the morphotropic phase boundary of PIN-PT.

The deviations from the straight line at Burns temperature was due to the slow down of the glassy polarization effect which occur from charge differences of

ions on the B-site which are highly disordered and dynamic leading to the strongly breaking of the translational symmetry above the T_d [7]. The glassy polarization phase with local polarization (P_d) slowed down substantially below Burns temperature. Due to the dynamic nature, there is no resultant local polarization (P=0) above transition temperature, T_m, but there is a finite value as non zero square of polarization ($\overline{P}^2$?0). The dynamic local polarizations above transition temperature can be calculated through the relation of thermal expansion with the local polarization as shown below:

$$x_{11} \quad \alpha(T \quad T_0) \quad (Q_{11} \quad 2Q_{12})P^2 \tag{1}$$

Where α is the thermal expansion coefficient, T_0 is the reference temperature and Q_{11} and Q_{12} are the electrostrictive coefficients [35]. For the calculations, the electrostrictive coefficients of $PbTiO_3$ were used [36] as the electrostrictive coefficients in general are small and are almost of the same order in most perovskite structures.

The calculated values of the local polarization, P_d, of PIN-PT and PIN-PT-BT ceramics are shown along with the temperature dependence of the reversible spontaneous polarization obtained from the hysteresis measurement, in Fig. 5. The local polarization shows slowly decreasing pattern to zero at Burns temperature while the reversible polarization becomes almost zero at the dielectric transition temperature. This behavior of reversible polarization shows some gradual decrease near transition temperature where the micro clusters undergoes the higher dynamic state and redistribution of the polar nano-regions. The local polarization derived from the $\overline{P}^2$ values slows a decrease with the temperature and finally leads to zero at the Burns temperature. From the figure, the local polarization of PIN-PT-BT is higher than that of PIN-PT implies that the addition of BT strongly breaks the translation symmetry leading to a more glassy polarization phase than in the PIN-PT system. These results suggest that the addition BT to PIN-PT system leads to the enhanced relaxor behavior.

CONCLUSION

Ferroelectric ceramics with chemical formula $(1-x)Pb(In_{0.5}Nb_{0.5})O_3$-$(x)PbTiO_3$ and $(0.8-x)Pb(In_{0.5}Nb_{0.5})O_3$-$(x)PbTiO_3$-0.2BT (x = 0.0, 0.1, 0.2 and 0.3) were prepared via the wolframite method. The relaxor behavior in the two systems was analyzed from the dielectric properties and thermal expansion measurement. The dielectric properties were measured at frequencies between 100 Hz and 100 kHz whereas the thermal expansion data was collected in the temperature range between -145°C and 500°C. The broad and diffuse dielectric constant maximum show that both systems are relaxor ferroelectrics and the glassy polarization behavior differs in two systems. The glassy polarization as calculated from the thermal expansion measurements suggest that there is an enhanced relaxor behavior in the PIN-PT-BT system as a result of the addition of BT in PIN-PT.

ACKNOWLEDGEMENTS

This work was supported by the Thailand Research Fund (TRF), Commission on Higher Education (CHE), Graduate School of Chiang Mai University and Ministry of

University Affairs in Thailand. The authors are also thankful for the support from NSF/DMR through the relaxor and metamaterials grants.

REFFERENCES

1. R. E. Newnham and S. Trolier-Mckinstry, *Ceramic Transcations, 32, J. Amer. Ceram. Soc.,* **32**, 1 (1993).
2. T. R. Shrout and A. Halliyal, *Am. Ceram. Soc. Bull*., **66(4)**, 704 (1987).
3. Y. Yoshikawa, *J. Eur. Ceram. Soc.,* **21**, 2041 (2001).
4. K. Nomura, T. Shingai, S-I. Ishino, H. Terauchi, N. Yasuda and H. Ohawa, *J. Phys. Soc. Jpn.*, **68(1)**, 39 (1999).
5. G. Burns and F. H. Dacol, *Solid. State. Commun.,* **42[1]**, 9 (1982).
6. G. Burns and F. H. Dacol, *Phys. Rev.B,* **28[5]**, 2527 (1983).
7. G. Burns and F. H. Dacol, *Solid. State. Commun.,* **48[10]**, 853 (1983).
8. G. Burns and F. H. Dacol, *Ferroelectrics,* **52**, 103 (1983).
9. G. Burns, F. H. Dacol, *Solid State Commun*., **58**, 567 (1986).
10. J. Zhao, A. E. Glazounov, Q. M. Zhang, B. Toby, *Appl. Phys. Lett*., **72**, 1048 (1998).
11. D. La-Orauttapong, J. Toulouse, Z.-G. Ye, W. Chen, R. Erwin, J. L. Robertson, *Phys. Rev. B,* **67**, 134110 (2003).
12. W. Kleemann, P. Licinio, T. Woike, R. Pankrath, *Phys. Rev. Lett.,* **86**, 6014 (2001).
13. D. Viehland, S. J. Jang, L. E. Cross, M. Wuttig, *Phys. Rev. B* ,**46**, 8003 (1992).
14. V. Bovtun, J. Petzelt, V. Porokhonskyy, S. Kamba, Y. Yakimenko, *J. Eur. Ceram. Soc*., **21**, 1307 (2001).
15. J. Dec, W. Kleemann, V. Bobnar, Z. Kutnjak, A. Levstik, R. Pirc, R. Pankrath, *Europhys. Lett*., **55**, 781 (2001).
16. A. S. Bhalla, R. Guo, L. E. Cross, G. Burns, F. H. Dacol and R. R. Neurgaonkar, *Ferroelectrics*, **106**, 161 (1990).
17. A. S. Bhalla, R. Guo, L. E. Cross, G. Burns, F. H. Dacol and R. R. Neurgaonkar, *Phys. Rev. B*, **36(4)**, 2030 (1987).
18. H. Arndt and G. Schmidt, *Ferroelectrics,* **79**, 149 (1988).
19. G. Burns and F. H. Dacol, *Ferroelectrics,* **104**, 25 (1990).
20. M. V. Gorev, I. N. Flerov, P. H. Sciau, V. S. Bondarev and A. G. LehMann, *Ferroelectrics,* **307**, 127 (2004).
21. C. A. Randall and A. S. Bhalla, *Jpn. J. Appl. Phys*., **29[2]**, 327 (1990).
22. E. F. Alberta and A. S. Bhalla, *Mater.Lett*., **29**, 127 (1996).
23. E. F. Alberta and A. S. Bhalla, *J. Phys. Chem. Solids*., **63**, 1759 (2002).
24. M. Iwata, S. Katagiri, H. Orihara, M. Maeda, I. Zusuki, H. Ohwa, N. Yasuda and Y. Ishibashi, *Ferroelectrics*., **301**, 179 (2004).
25. S-E. Park, T.R. Shrout, *IEEE Trans. Ultrason. Ferroelectri. Freq. Control*., **44**, 1298 (1997).
26. S-E. Park, T.R. Shrout, *Mater. Res. Innovat*., **1**, 20 (1997).
27. A. Halliyal, U. Kumar, R.E. Newnham and L.E. Cross, *J. Am. Ceram. Soc*., **70[2]**, 119 (1987).
28. Y. S. Cho, S. M. Pilgrim, H. Giesche and K. Bridger, *J. Am. Ceram. Soc*., **10**, 2473 (2000).
29. S. Wongsaenmai, S. Ananta and R. Yimnirun, *J. Mater. Sci.*, (2006) accepted.
30. S. Wongsaenmai, S. Ananta and R. Yimnirun, *Mater. Letter.,* (2006) inpress.
31. S. Wongsaenmai, O. Khamman, S. Ananta. and R. Yimnirun, *J. Electroceram*., (2006) accepted.
32. N. Yasuda and M. Fujie, *Jnp. J. Appl. Phys*., **31**, 3128 (1992).
33. C. Lei, K. Chen, X. Zhang and J. Wang, *Solid. State. Commun*., **123**, 445 (2002).

34. G. Burns, *Phase Transition*, **5**, 261 (1985).
35. V. Mueller, L. Läger, H. Beige, H-P. Abicht and Thomas Müller, *Solid. State. Commun.,* **129**, 757 (2004).
36. L. E. Cross, S. J. Jang. R. E. Newhnam, S. Nomura and K. Uchino, *Ferroelectrics*, **23**, 187 (1980).

Table I Dielectric properties of PIN-PT and PIN-PT-BT systems.

Composition	$_m$ at 1 kHz	T_m (°C) at 1 kHz	T_m (°C)
(1-x)PIN-(x)PT:			
x = 0.0	4308	70	26
x = 0.1	6823	144	14
x = 0.2	12752	208	6
x = 0.3	15963	279	1
(0.8-x)PIN-(x)PT-0.2BT:			
x = 0.0	7591	26	30
x = 0.1	8093	85	19
x = 0.2	17366	130	15
x = 0.3	18541	155	8

Table II Thermal expansion P_d, P_s, T_d and T_m of various compositions PIN-PT PT and PIN-PT-BT systems

Composition	T_d (°C)	T_m (°C)	$T_d - T_m$ (°C)	Properties at room temperature		
				$\times 10^{-6}$ ($°C^{-1}$)	P_s C/cm^2)	P_d C/cm^2)
(1-x)PIN-(x)PT:						
x = 0.0	380	70	310	2.2	7.6	16.0
x = 0.1	391	144	247	2.9	15.2	17.7
x = 0.2	420	208	212	3.4	18.7	19.9
x = 0.3	435	279	156	4.0	23.3	24.1
(0.8-x)PIN-(x)PT-0.2BT:						
x = 0.0	360	26	334	1.1	6.1	18.0
x = 0.1	383	85	298	1.3	13.4	21.1
x = 0.2	400	130	270	1.6	23.5	24.5
x = 0.3	416	155	261	1.8	27.9	28.2

List of Figure Captions

Fig.1 Temperature dependence of the dielectric constant and dielectric loss of (a) PIN, (b) 0.8PIN-0.2PT, (c) 0.8PIN-0.2BT and (d) 0.6PIN-0.2PT-0.2BT.

Fig.2 Temperature dependence of thermal expansion and T_d for PIN-PT system.

Fig.3 Temperature dependence of thermal expansion and T_d for PIN-PT-BT system.

Fig.4 Temperature dependence of thermal expansion coefficient (for PIN-PT system (a) x = 0.0, (b) x = 0.3 and PINPT-BT which (c) x = 0.0 and (d) x = 0.3.

Fig.5 The comparison of P_d and P_s of both PIN-PT and PIN-PT-BT systems which (a) x = 0.0, (b) x = 0.1, (c) x = 0.2 and (d) x = 0.3.

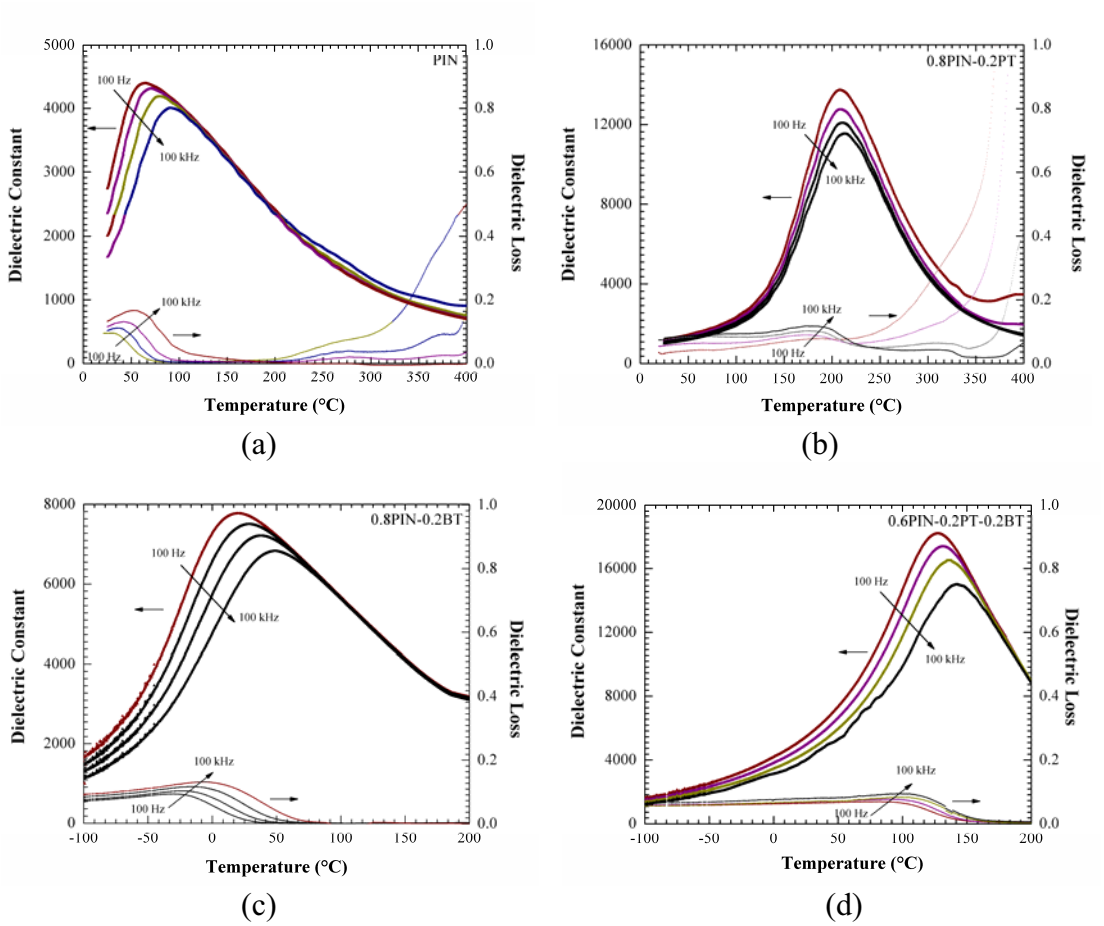
PIN
0.8PIN-0.2PT
0.8PIN-0.2BT
0.6PIN-0.2PT-0.2BT
Dielectric Constant
Dielectric Loss
Temperature (°C)
100 Hz
100 kHz
(a)
(b)
(c)
(d)

Fig.1

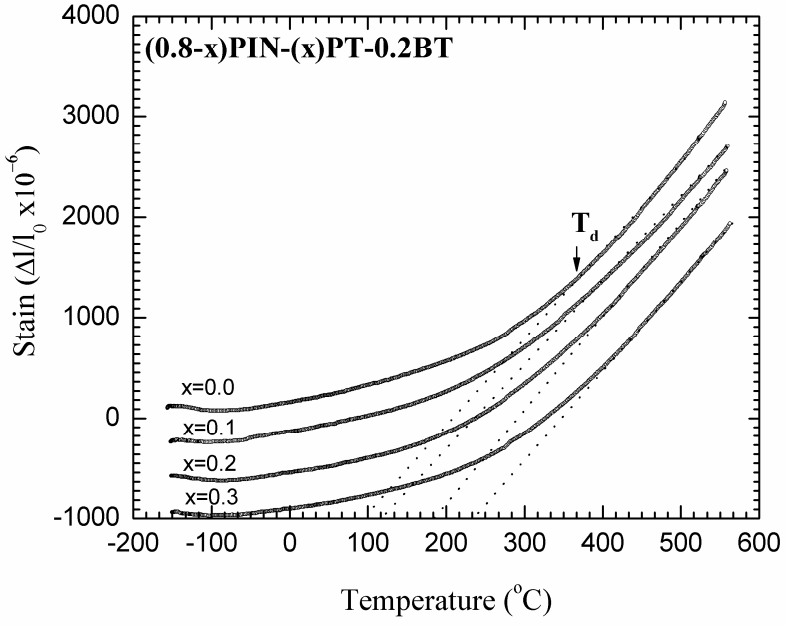
(0.8-x)PIN-(x)PT-0.2BT
Stain ($\Delta l/l_0$ x10^{-6})
Temperature (^{o}C)
T_d
x=0.0
x=0.1
x=0.2
x=0.3
4000
3000
2000
1000
0
-1000
-200
-100
0
100
200
300
400
500
600

Fig.2

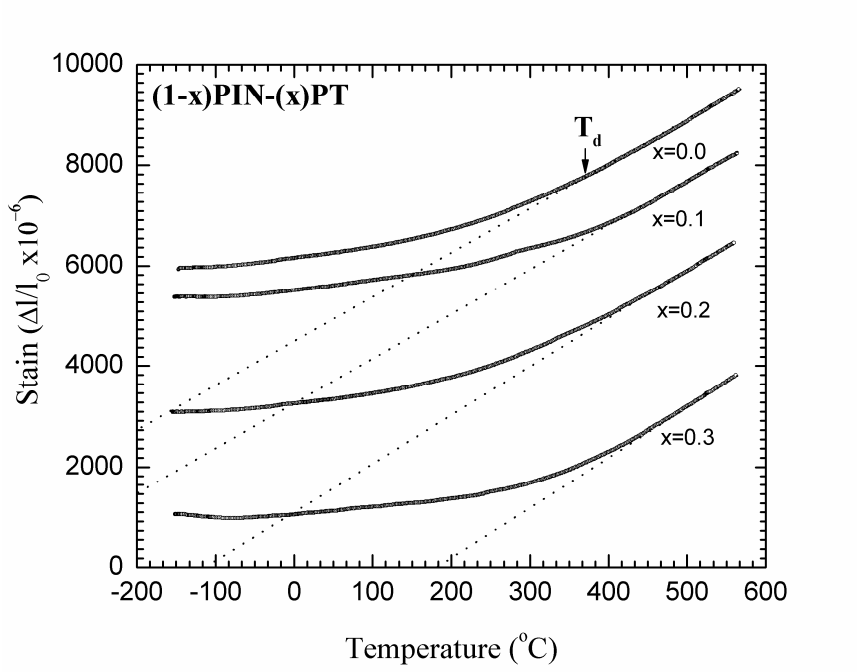
(1-x)PIN-(x)PT
T_d
x=0.0
x=0.1
x=0.2
x=0.3
Stain (Δl/l_0 x10^-6)
Temperature (°C)
10000
8000
6000
4000
2000
0
-200
-100
0
100
200
300
400
500
600

Fig. 3

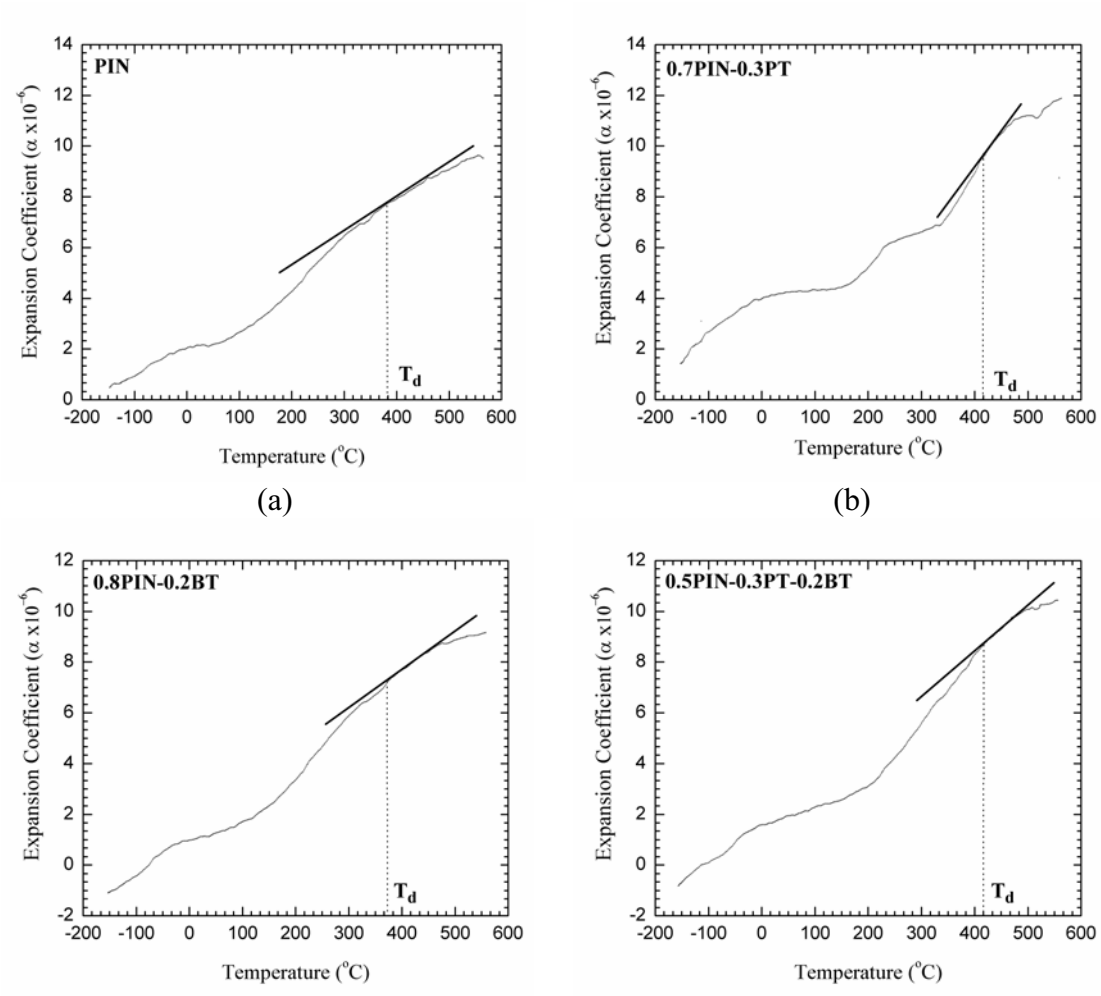
PIN
0.7PIN-0.3PT
0.8PIN-0.2BT
0.5PIN-0.3PT-0.2BT
Expansion Coefficient (α x10⁻⁶)
Temperature (°C)
T_d
(a)
(b)
(c)
(d)

Fig.4

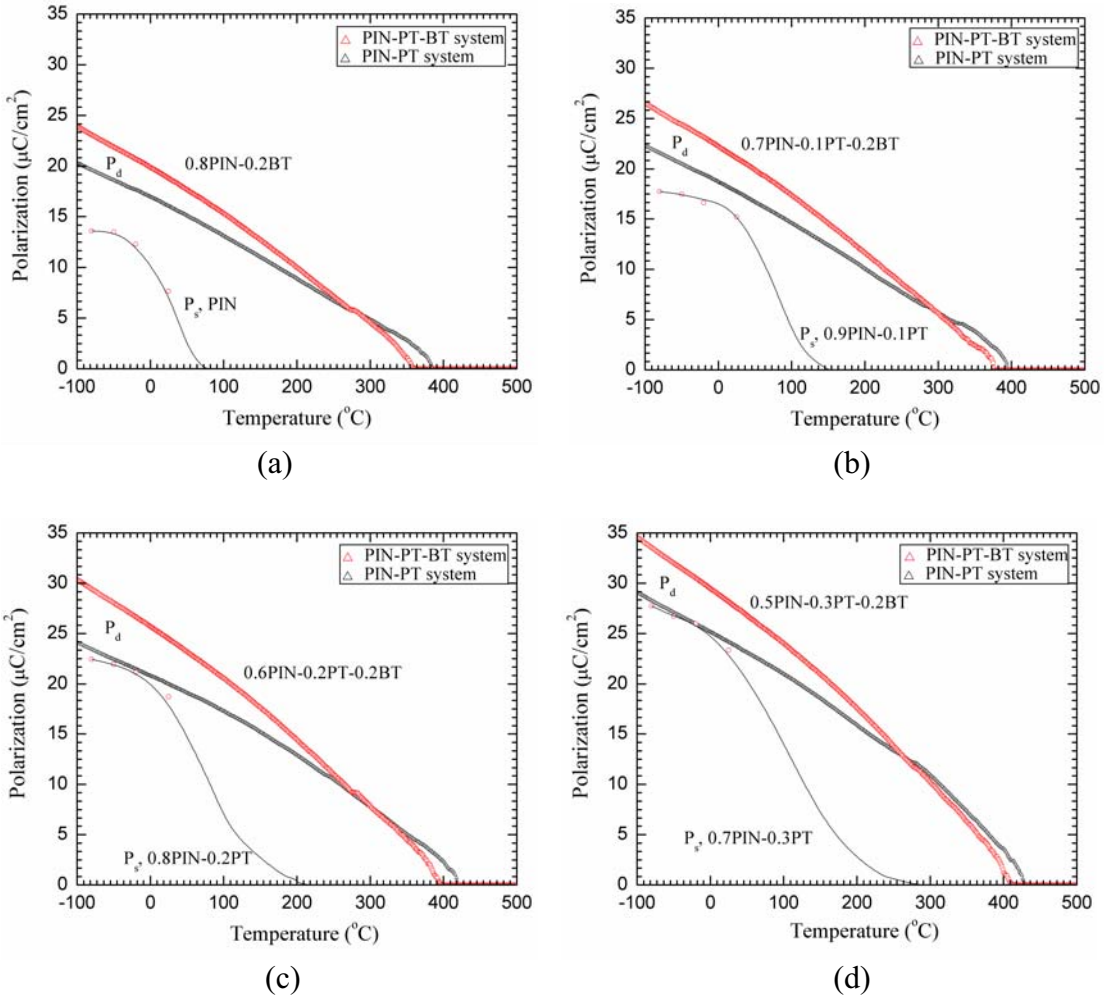
PIN-PT-BT system
PIN-PT system
Polarization (μC/cm²)
Temperature (°C)
P_d
0.8PIN-0.2BT
P_s, PIN
(a)
0.7PIN-0.1PT-0.2BT
P_s, 0.9PIN-0.1PT
(b)
0.6PIN-0.2PT-0.2BT
P_s, 0.8PIN-0.2PT
(c)
0.5PIN-0.3PT-0.2BT
P_s, 0.7PIN-0.3PT
(d)

Fig.5

Dielectric Properties and Relaxor Behavior of PIN Based System

Supattra Wongsaenmai*[1], Supon Ananta[1], Rattikorn Yimnirun[1], Ruyan Guo[2]and Amar S. Bhalla[2]
[1]Department of Physics, Faculty of Science, Chiang Mai University, Chiang Mai 50200, Thailand
Tel: (6653)-943367, e-mail: wongsaenmai@yahoo.com
[2]Materials Research Laboratory, The Pennsylvania State University, University Park, PA 16802, USA
Tel: (1814)-8659232, e-mail: asb2@psu.edu

ABSTRACT: Several compositions in the two PIN based systems (1-x)$Pb(In_{0.5}Nb_{0.5})O_3$-(x)$PbTiO_3$ and (0.8-x)$Pb(In_{0.5}Nb_{0.5})O_3$-(x)$PbTiO_3$-0.2$BaTiO_3$ (x = 0.0, 0.1, 0.2 and 0.3) were synthesized via the wolframite method. Dielectric properties were measured in the frequency range between 100 Hz and 100 kHz and were analyzed for understanding relaxor behavior in the system. The temperature dependence of the dielectric properties was analyzed by studying the deviation from the Curie-Weiss law while the frequency dependence of the dielectric properties was analyzed by the Vogel-Fulcher relation. The results showed that the addition of BT increased the dielectric constant and decreased the shift of the maximum dielectric constant temperature (T_m) of (1-x)PIN-(x)PT compositions. Finally, the analysis also confirmed that, when added to PIN, PT decreased and BT increased the relaxor behavior of the PIN-based ceramics.

Keywords: PIN-PT, PIN-PT-BT, Dielectric Properties, Curie Weiss Law, Vogel-Fulcher Relation

INTRODUCTION

The relaxor ferroelectric ceramics, which have the $Pb(B'B'')O_3$ complex perovskite structure, show broad ($_r$ vs. T) transitions, high dielectric constant frequency dispersion of dielectric properties [1-4] over a wide temperature range. These excellent properties persuaded various researchers to investigate these behaviors for high performance applications. Several models have been proposed to explain these relaxor behaviors. The composition fluctuation model proposed by Smolenskii [5] suggests that the different local Curie temperatures lead to broad diffuse phase transition. Cross proposed the polarization mechanism analogous to the superparamagnetic clusters in magnetic materials [6]. This model considered no interaction between each polar nano-regions or clusters. The clusters have two states of polarization orientation separated by energy barrier. The thermal energy affects the flipping of polarization reorientation; therefore frequency of flipping can be explained by an Arrhenius equation:

$$\varpi \quad \varpi_0 \exp \frac{E_a}{kT} \tag{1}$$

where E_a is the activation energy for flipping, ϖ_0 is the Debye frequency and T is the absolute temperature. The broad distribution and frequency dispersion of dielectric properties originate from slowing down of polarization reorientation in each cluster. The interaction between clusters can be analogous with magnetic spin glass model [7]. The freezing temperature was defined as the macroscopic polarization emergence. The relation of this was fitted with Vogel-Fulcher equation:

$$\varpi \quad f_0 \exp \frac{E_a}{k(T_m \quad T_f)} \tag{2}$$

where f_0, E_a and T_f are the Debye frequency, the activation energy and the static freezing temperature, respectively [7]. Though these models attempted to explain the relaxor behavior, none can completely explain their interesting properties.

PIN is of interest for its chemical ordering study. It is a member of relaxor family with a 1:1 stoichiometric of B-site ordering which can be brought from disordered state into ordered state by thermal treatment [8]. The disordered state of PIN exhibits relaxor behavior which shows broad dielectric maximum near 66 ºC [9, 10]. In contrast, the ordered state shows antiferroelectric behavior with a sharp peak in dielectric constant vs. temperature curve observed at 168 ºC [10, 11]. The solid solution of relaxor ferroelectric and normal ferroelectric PT has excellent piezoelectric and electrostrictive properties [12, 13]. The electrostrictive property with no hysteresis and low mechanical loss above the temperature of maximum dielectric constant (T_m) of ceramics has been considered for high performance application devices such as electostrictive transducer and actuator. It has been reported that the PIN-PT system has high temperature performance of electromechanical coupling factor at temperatures up to 200 ºC [14]. However, the most applications have generally been at near room temperature, thus it is also important to look for the new systems which have T_m near room temperature and at the same time maintain their low hysteresis behavior. From the published literature, it was noticed that the addition of BT to PMN- and PZN-based systems helps decrease T_m of the systems and at the same time stabilizes the perovskite structure [15, 16]. There have been no details or reports for the characteristic of PIN-PT-BT system.

In this paper, the relaxor behaviors of PIN-based system have been reported. The dielectric properties have been measured in PIN-PT and PIN-PT-BT complex systems. It was anticipated that an addition of PT would increase the dielectric properties whereas added BT could shift T_m closer to room temperature and increase disorder phase leading to extended relaxor behavior.

EXPERIMENTAL

The powders of $(1-x)Pb(In_{0.5}Nb_{0.5})O_3$-$(x)PbTiO_3$ and $(0.8-x)Pb(In_{0.5}Nb_{0.5})O_3$-$(x)PbTiO_3]$-$0.2BaTiO_3$ (x = 0.0, 0.1, 0.2 and 0.3, abbreviated as PIN-PT and PIN-PT-BT, respectively) were synthesized by a two-step solid solution reaction method [17]. The wolframite $InNbO_4$ was first prepared from oxide powder of In_2O_3 and Nb_2O_5 [18]. Mixed powder was milled and calcined at temperature 1100ºC for 2 hours to obtain the intermediate precursor $InNbO_4$ [19]. The wolframite precursor was then mixed with reagent powder of PbO, TiO_2 for PIN-PT system and PbO, $BaCO_3$, TiO_2 for PIN-PT-BT system. Excess amount of PbO (2%) and In_2O_3 (2%) were added at this stage. The mixtures were milled again following the intermediate precursor stage. After drying, the mixtures were calcined at temperature between 800ºC and 1000ºC, 1050ºC and 1250ºC with soaking time of 2 hours for PIN-PT and PIN-PT-BT, respectively [20]. Pellets were pressed with 1% PVA. The pressed pellets were sintered with the soaking time of 2 hours in a double crucible configuration at temperature from 1100ºC to 1125ºC for PIN-PT system and 1250 to 1300ºC for PIN-PT-BT system. To prevent PbO loss, the pellets were buried in protective powders.

The temperature dependence of dielectric properties was measured with an LCR meter (HP-4284A, Hewlett-Packard, Santa Clara, CA) in conjunction with an environmental chamber (9023, Delta Design, Poway, CA). A heating rate of 2ºC/min and frequencies of 100, 1k, 10k and 100k Hz were used during measurement.

RESULTS AND DISCUSSION

The temperature dependences of dielectric constant at frequencies of 100 Hz to 100 kHz are shown in Figs. 1 and 2 for PIN-PT and PIN-PT-BT systems, respectively. The broad dielectric curves are observed for compositions x = 0.0 and 0.1, then changing slightly to sharper peak with further increase in PT contents. In addition, the frequency dispersion in their dielectric properties was also considered. Since $T_m = T_{m,100kHz}-T_{m,\ 100Hz}$ can be used as a rough estimate for more relaxor behavior with higher T_m, as listed in Table I, addition of PT results in smaller T_m. These results indicate the decreasing of relaxor behavior with increasing PT content [21]. Moreover, as shown in Fig, 2, the dielectric behavior of PIN-PT-BT system shows a stronger frequency dispersion and broader dielectric maximum than observed in PIN-PT system. This implies that addition of BT promotes the distribution of polar nano-regions and then leads to relaxor behavior while the addition of PT leads to normal ferroelectric. The parameters of dielectric properties are summarized in Table I, show that with the same PT content the dielectric constant of PIN-PT-BT ceramic is higher than that of PIN-PT ceramic. The addition of BT also decreases the maximum dielectric constant temperature (T_m), as clearly evident from a comparison between 0.8PIN-0.2PT and 0.8PIN-0.2BT with T_m of 208 ºC and 26 ºC, respectively. Similar effect of PT and BT additions on the dielectric properties of PZN-based system has been reported earlier [15].

It is known that in the normal ferroelectric ceramics the dielectric constant follows the Curie-Weiss law above temperature of maximum dielectric constant (T_m) whereas the relaxor ferroelectrics could follow the modified Curie Weiss behavior up to the temperature much higher than T_m [22]. The deviation from Curie-Weiss law can be shown to follow the Curie-Weiss square law [23] as

$$\frac{1}{\varepsilon} \quad \frac{1}{\varepsilon_m} \quad \frac{T \quad T_m}{C}^{\gamma} \tag{3}$$

where and C' are constants. With = 1 for normal ferroelectric, the equation (3) reduces to the normal Curie-Weiss law, while = 2 leads to the quadratic law for relaxor behavior. The plotting of ln(1/ -1/ $_m$) vs. ln(T-T_m) of both systems are shown in Figs.3 and 4. By fitting these graphs with equation (3), the parameter which indicates degree of relaxor behavior, is obtained from slopes of these plots, The empirical parameter of all compositions is listed in Table I showing the maximum values of = 1.89 and 1.98 at x = 0.0 and minimum value of = 1.66 and 1.82 at x = 0.3 for PIN-PT and PIN-PT-BT system, respectively. Decreasing trend of value with increasing of PT content observed in both systems agrees with the previous study [24]. However, PIN-PT-BT system shows higher value than that of PIN-PT system. This provides support for the observation in the early discussion that the addition of BT leads to increasing relaxor behavior.

The dependence of temperature of maximum dielectric constant (T_m) on frequency of PIN-PT and PIN-PT-BT systems was also fitted with Vogel-Fulcher equation. An example of the fitting curve is shown in Fig.5 with solid line indicating plotting of equation (2) and solid circles indicating the experimental data. This plot shows that the experimental data can be fitted with the Vogel-Fulcher equation which suggests that the relaxor behavior of PIN-PT and PIN-PT-BT systems follow the glass-like behavior. The Debye frequency, the activation energy and the static freezing temperature obtained by fitting the experimental data with equation (2) are

listed in Table II. Similar observation has also been reported in the case of other relaxor-based systems [25]. From equation (2), it is known that the activated energy is an internal energy (minus sign) of the cluster, which concerns with an anisotropy energy, K_{anis} and the cluster volume, V [23]. The fitting results show that the activation energy increases with increasing PT content for both systems, indicating that PT induces the increase of the anisotropic energy and influence the cluster volume. It can be implied that size of isolated cluster or ordering change with increasing PT contents. For relaxor ferroelectrics, the value of Debye frequency relate with size of polar nano-region and interaction between polar nano-regions. In general, the stronger interaction and larger size show the smaller of the Debye frequency value. However, the addition of BT shows larger Debye frequency and smaller activation energy, as compared to the PIN-PT system, indication of smaller ordering or existence of distribution of ordering. From the experimental result and fitting of Vogel-Fulcher relation, it can be implied that the increasing PT content shows marked effect in decreasing relaxor behavior by increasing interaction between polar nano-regions. Meanwhile, the addition of BT tends to increase the relaxor behavior in PIN-based system, in good agreement with the observations discussed earlier.

CONCLUSION

The (1-x)$Pb(In_{0.5}Nb_{0.5})O_3$-(x)$PbTiO_3$ and (0.8-x)$Pb(In_{0.5}Nb_{0.5})O_3$-(x)$PbTiO_3$-0.2$BaTiO_3$ (x = 0.0, 0.1, 0.2 and 0.3) ceramics were prepared via the wolframite method. The dielectric properties of the ceramics were investigated as functions of both temperature and frequency. The dielectric properties were measured at frequency between 100 Hz and 100 kHz and used for relaxor behavior analysis. The temperature dependence of the dielectric properties was analyzed by the deviation from the Curie-Weiss law while the frequency dependence of the dielectric properties was analyzed by the Vogel-Fulcher relation. The results showed broaden phase transition at x = 0.0 and 0.1 for both systems. From the Curie-Weiss square law fitting plots, the maximum values of of 1.89 and 1.98 were observed for PIN-PT and PIN-PT-BT systems, respectively, and the value decreases with increasing PT content. Moreover the addition of BT leads to an increase of the value. These observations implied that in PIN-based system the addition of BT leads to the relaxor behavior while the addition of PT leads to the normal ferroelectric. Moreover, the Vogel-Fulcher relation analysis showed that PIN-PT and PIN-PT-BT systems are relaxor ferroelectrics with glass-like behavior.

ACKNOWLEDGEMENTS

This work was supported by the Thailand Research Fund (TRF), Commission on Higher Education (CHE), Graduate School of Chiang Mai University, Ministry of University Affairs in Thailand, and NSF/DMR relaxor and metamaterials grants at MRI, Penn State USA.

REFFERENCES

1. R. E. Newnham and S. Trolier-Mckinstry, *Ceramic Transcations, 32, J. Amer. Ceram. Soc.,* **32**, 1 (1993).
2. T. R. Shrout and A. Halliyal, *Am. Ceram. Soc. Bull*., **66(4)**, 704 (1987).
3. Y. Yoshikawa, *J. Eur. Ceram. Soc.,* **21**, 2041 (2001).
4. K. Nomura, T. Shingai, S-I. Ishino, H. Terauchi, N. Yasuda and H. Ohawa, *J. Phys. Soc. Jpn.*, **68(1)** 39 (1999).
5. G. A. Smolenskii, *Jpn. J. Appl. Phys*., **28**, 1970 (1970).
6. L. E. Cross, *Ferroelectrics*, **76**, 246 (1987).
7. D. Viehland, S-J. Jang and L. E.Cross, *J. Appl. Phys*., **68[6]**, 2916 (1990).
8. C. A. Randall and A. S. Bhalla, *Jpn. J. Appl. Phys*., **29[2]**, 327 (1990).
9. E. F. Alberta and A. S. Bhalla, *Mater.Lett*., **29**, 127 (1996).
10. E. F. Alberta and A. S. Bhalla, *J. Phys. Chem. Solids*., **63**, 1759 (2002).
11. M. Iwata, S. Katagiri, H. Orihara, M. Maeda, I. Zusuki, H. Ohwa, N. Yasuda and Y. Ishibashi, *Ferroelectrics*, **301**, 179 (2004).
12. S-E. Park, T. R. Shrout, *IEEE Trans. Ultrason. Ferroelectri. Freq. Control*., **44**, 1298 (1997).
13. S-E. Park, T. R. Shrout, *Mater. Res. Innovat*., **1**, 20 (1997).
14. N. Yasuda, H. Ohwa, M. Kume and Y. Yamashita, *Jpn. J. Appl. Phys*., **39**, 5586 (2000).
15. A. Halliyal, U. Kumar, R. E. Newnham and L. E. Cross, *J. Am. Ceram. Soc*. **70[2]**, 119 (1987).
16. Y. S. Cho, S. M. Pilgrim, H. Giesche and K. Bridger, *J. Am. Ceram. Soc*. **10**, 2473 (2000).
17. S. Wongsaenmai, S. Ananta and R. Yimnirun, *J. Mater. Sci.*, (2006) accepted.
18. S. Wongsaenmai, S. Ananta and R. Yimnirun, *Mater. Letter.,* (2006) inpress.
19. S. Wongsaenmai, O. Khamman, S. Ananta. and R. Yimnirun, *J. Electroceram*., (2006) accepted.
20. N. Yasuda and M. Fujie, *Jnp. J. Appl. Phys*., **31**, 3128 (1992).
21. C. Lei, K. Chen, X. Zhang and J. Wang, *Solid. State. Commun*., **123**, 445 (2002).
22. K. Uchino and S. Nomura*, Ferroelectric Lett.*, **44**, 55 (1982).
23. D. Viehland, S-J. Jang, L. E.Cross and M. Wutting*, Phys. Rev.B*, **46[13]**, 8003 (1992).
24. M. Kuwabara, S. Takahashi, K. Goda, K. Oshima and K. Watanabe, *Jpn. J. Appl. Phys.*, **31**, 3241 (1992).
25. G. Singh, V. S. Triwari and V. K. Wadhawan, *Solid. State. Commun.,* **129**, 665 (2004).

Table I The dielectric properties and calculated parameters for PIN-PT and PIN-PT-BT systems.

Composition	$_m$ at 1 kHz	T_m (K) at 1 kHz	T_m (K)		C
(1-x)PIN-(x)PT:					
x = 0.0	4308	343	26	1.89	1.9×10^5
x = 0.1	6823	417	14	1.86	1.7×10^5
x = 0.2	12752	481	6	1.71	2.4×10^5
x = 0.3	15963	552	1	1.66	4.2×10^5
(0.8-x)PIN-(x)PT-0.2BT:					
x = 0.0	7591	299	30	1.98	5.6×10^5
x = 0.1	8093	358	19	1.90	10.4×10^5
x = 0.2	17366	403	15	1.87	12.6×10^5
x = 0.3	18541	428	8	1.82	16.1×10^5

$T_m = T_m(100Hz)-T_m(100kHz)$, C = calculated Curie constant value

Table II The parameters obtained from fitting Vogel-Fulcher equation for PIN-PT and PIN-PT-BT systems.

Composition	T_m (K) at 1 kHz	T_f (K)	T_m-T_f	f_0 (Hz)	$_a$ (eV)
(1-x)PIN-(x)PT:					
x = 0.0	343	268	75	4.4×10^{10}	0.051
x = 0.1	417	389	28	3.1×10^{10}	0.036
x = 0.2	481	467	14	2.7×10^{10}	0.024
x = 0.3	552	548	4	1.2×10^{10}	0.005
(0.8-x)PIN-(x)PT-0.2BT:					
x = 0.0	299	248	51	6.2×10^{10}	0.068
x = 0.1	358	316	42	4.7×10^{10}	0.057
x = 0.2	403	379	24	3.9×10^{10}	0.035
x = 0.3	428	414	14	2.6×10^{10}	0.020

List of Figure Captions

Fig.1 Temperature dependence of dielectric constant for (1-x)PIN-(x)PT system with (a) x = 0.0, (b) x = 0.1, (c) x = 0.2 and (d) x = 0.3.

Fig.2 Temperature dependence of dielectric constant at for (0.8-x)PIN-(x)PT-0.2BT system with (a) x = 0.0, (b) x = 0.1, (c) x = 0.2 and (d) x = 0.3.

Fig.3 Plots of ln(1/ -1/ $_m$) vs. ln(T-T_m) on (1-x)PIN-(x)PT system.

Fig.4 Plots of ln(1/ -1/ $_m$) vs. ln(T-T_m) on (0.8-x)PIN-(x)PT-0.2BT system.

Fig.5 Temperature of maximum dielectric as a function of frequency for 0.8PIN-0.2BT ceramic.

PIN-PT system

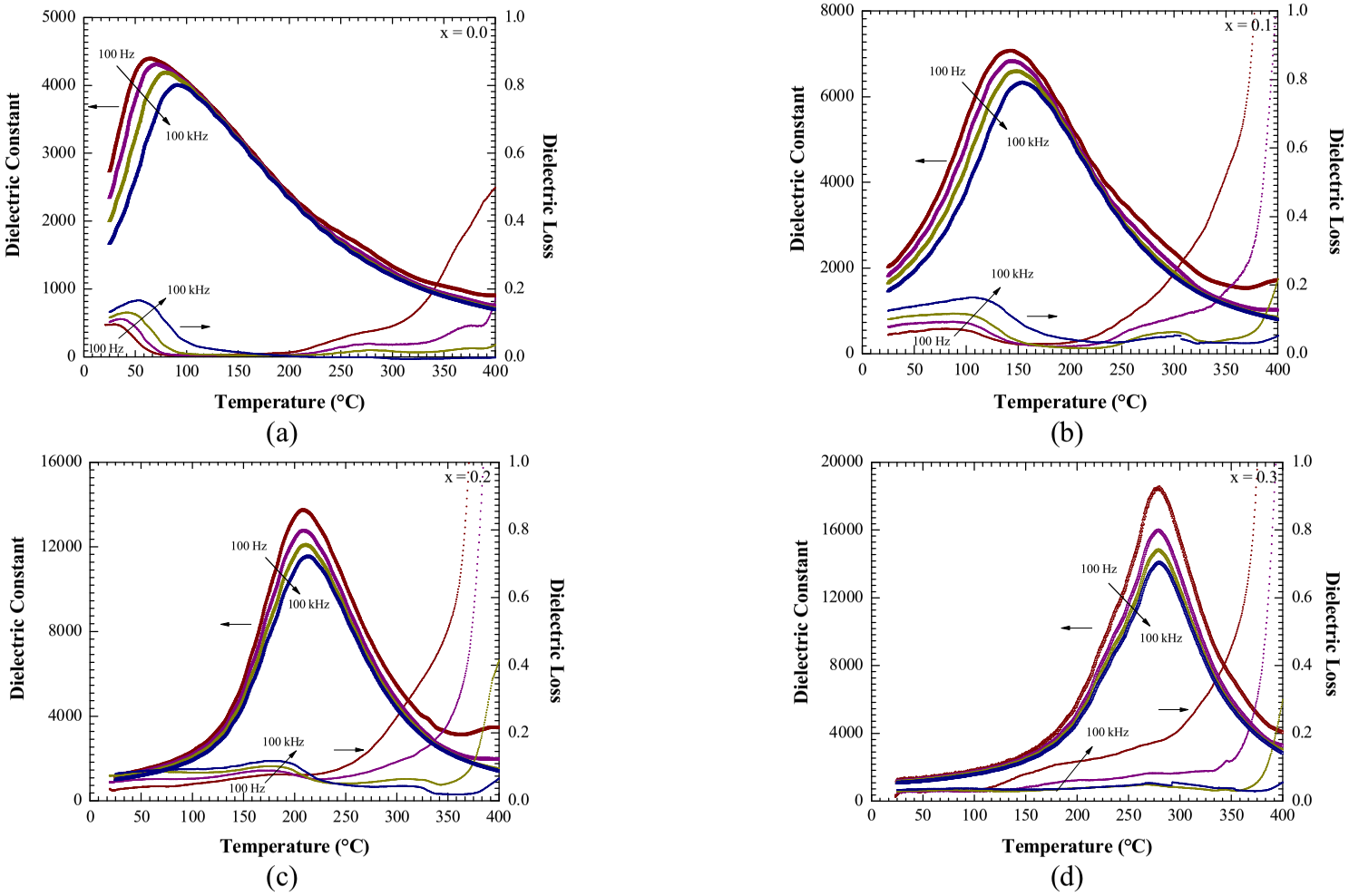

Fig. 1

PIN-PT-BT system

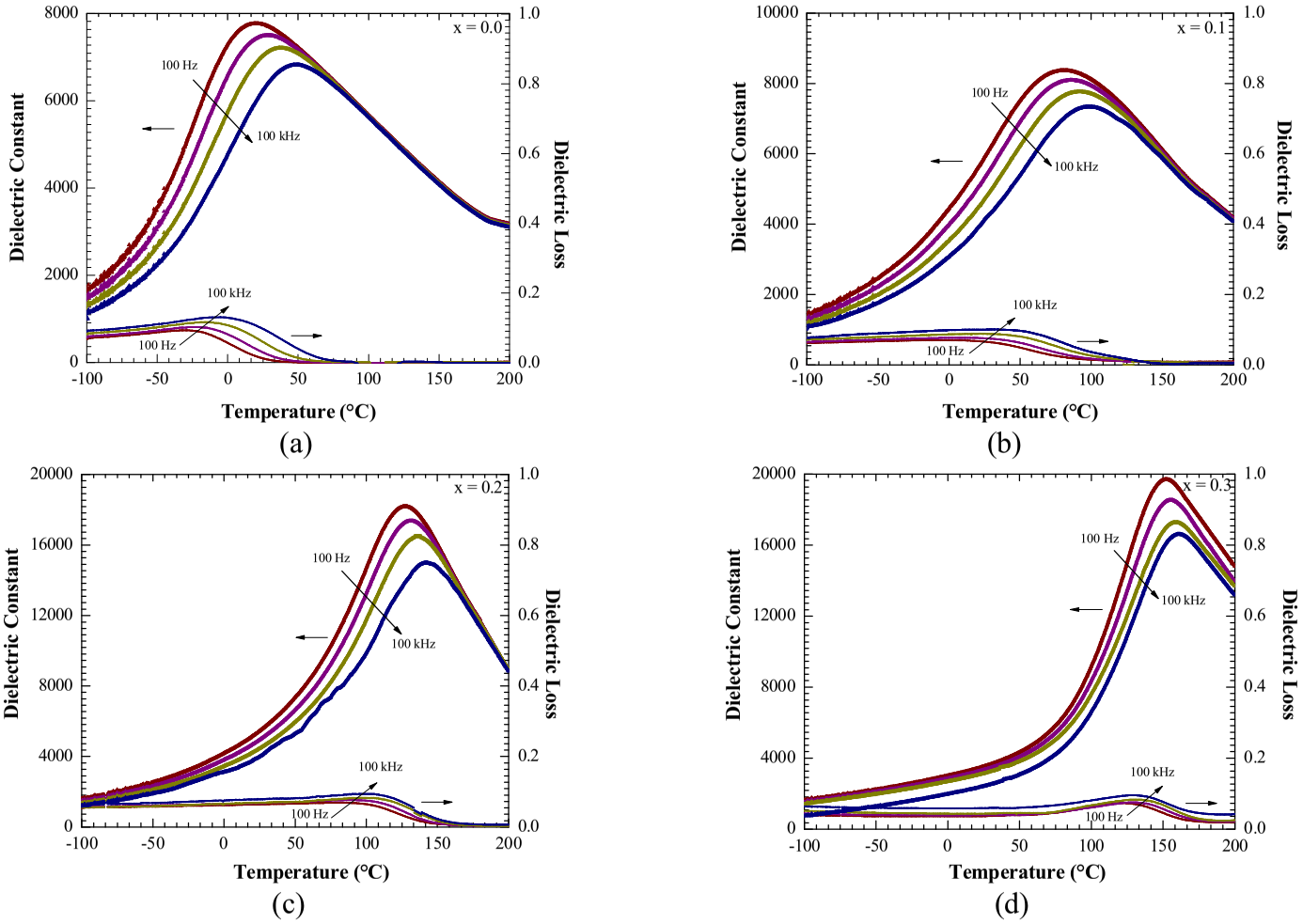

Fig.2

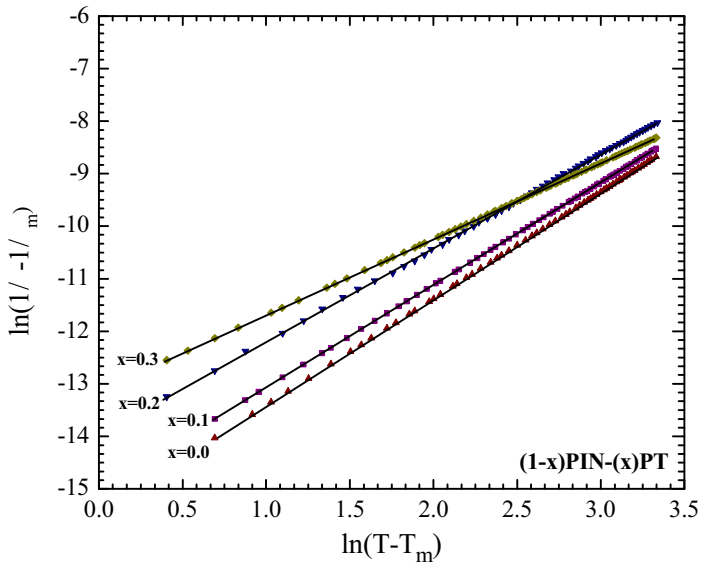
ln(1/ -1/ m)
ln(T-Tm)
x=0.3
x=0.2
x=0.1
x=0.0
(1-x)PIN-(x)PT

Fig.3

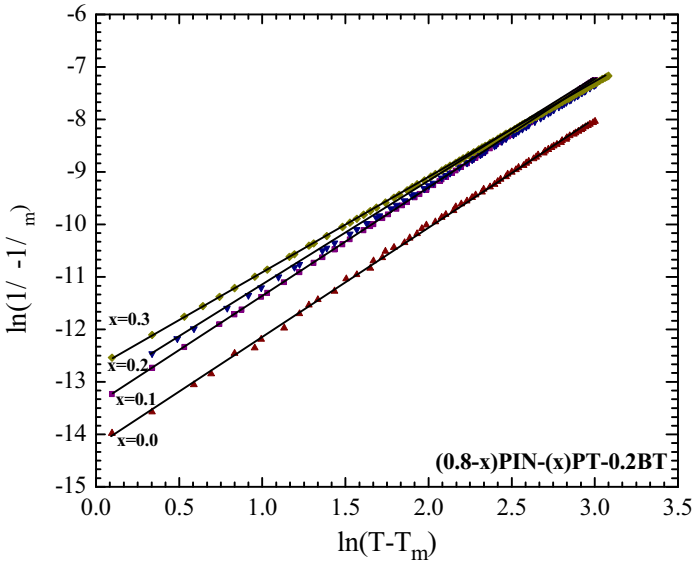
ln(1/ -1/ m)
ln(T-Tm)
x=0.3
x=0.2
x=0.1
x=0.0
(0.8-x)PIN-(x)PT-0.2BT

Fig.4

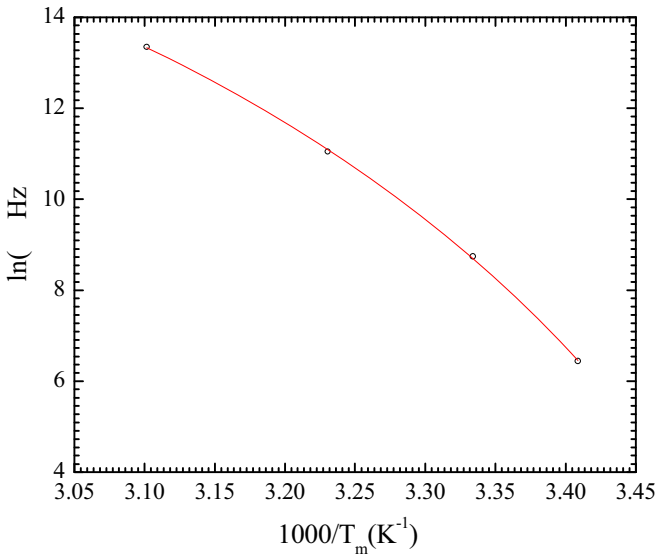

Fig.5

Editorial Manager(tm) for Journal of Materials Science
Manuscript Draft

Manuscript Number: JMSC5763R1

Title: Effects of Milling Time and Calcination Condition on Phase Formation and Particle Size of Lead Zirconate Nanopowders Prepared by Vibro-milling

Article Type: Manuscript

Section/Category:

Keywords: Lead zirconate; Perovskite; Nanopowders; Calcination; Phase formation

Corresponding Author: Dr. S. Ananta, PhD

Corresponding Author's Institution:

First Author: S. Ananta, PhD

Order of Authors: S. Ananta, PhD; O. Khamman; T. Sarakonsri; T. Sarakonsri; A. Rujiwatra; Y. Laosiritaworn; Rattikorn Yimnirun, PhD

Manuscript Region of Origin:

Abstract: Effect of calcination conditions on phase formation and particle size of lead zirconate ($PbZrO_3$) powders synthesized by a solid-state reaction with different vibro-milling times was investigated. A combination of the milling time and calcination conditions was found to have a pronounced effect on both the phase formation and particle size of the calcined $PbZrO_3$ powders. The calcination temperature for the formation of single-phase perovskite lead zirconate was lower when longer milling times were applied. More importantly, by employing an appropriate choice of the milling time and calcination conditions, single-phase $PbZrO_3$ nanopowders have been successfully prepared with a simple solid-state reaction method.

*** Response to Reviewer Comments**

Supon Ananta, Ph.D.
Associate Professor of Materials Science

Department of Physics, Faculty of Science
Chiang Mai University
Chiang Mai 50200 THAILAND

Telephone: (6653) 943-376
Fax: (6653) 357-512
E-mail:
suponananta@yahoo.com

February 1, 2007

Dear Editor;

Enclosed please find a *revised* manuscript being re-submitted for publication in **Journal of Materials Science**.

Based on very kind and useful comments from the reviewers on our submission, considerable changes have been incorporated into the revised manuscript (Marked in Red). The following points are responses (in bold) to the reviewer's comments;

COMMENTS FOR THE AUTHOR:

Reviewer #1: The authors report on the formation of PbZrO3 nanoparticles using Vibro-milling, and study the time-temperature range in which single phase PZ nanoparticles can be obtained. This peer reviewer find the data obtained in the said study useful as it delineates a commercially feasible way of preparing PZ nanoparticles. However, some improvements on the manuscript are called for. It is a well-established fact that ferroic nanoparticles undergo what is called a finite-size effect. Namely, at a certain particle size called the critical size, the high-temperature paraelectric phase is stabilized at room temperature. Prior reaching that size, the lattice paramaters as well as the paraelectric-ferroic phase transition temperature changes. Given these facts, the authors should do the following so as to enhance the interpretation of their data:

1) Plot lattice paramaters as a function of particle size for single phase powder and show systematic variation of the same with particle size

Fig.9 has been added to show these plots with discussions (in Pages 10-11).

2) Attempt to extrapolate from the smallest paricle size lattice parameter data so as to estimate a critical crystallite size.

The crystallite size is estimated from the plots in Fig. 9, as suggested (Pages 10-11).

3) If would also be desirable to show the variation of unit cell volume with decreasing particle size.

Fig.9 has been added to show these plots with discussions (in Pages 10-11).

4) Mention size effect phenomena that is already in the literature in relation to the work presented therein.

More discussions have been added to address this issue in Pages 10-11 with new references [21-29].

5) Clearly discuss that the nanoparticles are indeed polycrystalline and not single domain single crystalline as in the case of PbTiO3 nanoparticles reported in the literature. The comparison of X-ray crystallite size with SEM apparent crystalite size shows that the nanoparticles have imperfections (polycrystalline). Hence, comment on the possibility of introducing excess crystalline defects through milling.

More discussions have been added to address this issue in Pages 8-9.

6) Is it possible tha Vibro-milling causes local melting? For instance the 25 hrs sample in Fig 5 seems to show "necking" which is known to be thermally induced. The authors should clarify this point. Is there a hidden thermal history due to milling? If so, what is its extend?

More discussions have been added to address this issue in Page 9.

7) The abstract should also convey the important numerical results as well. Please do insert your most important results.

The abstract has been modified to include numerical results and important findings.

The authors should address these points, revise their manuscripts and then resubmit it for a second round of peer review.

All the issues have been addressed with proper references.

Reviewer #2: This paper reports a study on the effects of vibro milling (time) on the phase formation and particle characteristics of lead zirconate upon calcination at different temperatures. In the study, authors established a correlation between particle size and milling/calcination conditions. Although lead titanate has been widely investigated, the authors studied the correlations between processing conditions and the resulting particle characteristics in a rather systematic manner, which are of interest to the community working on electroceramic materials. I therefore recommend that the manuscript be published subject to minor improvement, as detailed as follows:

(1) Properly index all the main peaks for oxides and lead zirconate in figures 1-3, where some of the peaks are very close to each other;

Figs 1-3 have been properly modified, as suggested.

(2) The conclusion section is too short. Author shall list some details in the conclusion.

The abstract has been modified to include numerical results and important findings.

(3) Formation of pervoskite phase from mixed oxides by mechanical activation has been reported, for example, by S.E. Lee, et al, Acta Materialia, 47 (1999) 2633; and J.M. Xue, et al, Journal of the American Ceramic Society, 82 (1999) 1687, which shall be included in the introduction section, for a complete picture of the subject area.

This has been added in Introduction (refs. [9,10]).

Thank you very much for your valuable time and very kind consideration. Should you have any questions regarding the revised manuscript, please feel free to contact me. I am looking forward to hearing from you very soon.

Sincerely yours,

Supon Ananta
Department of Physics, Faculty of Science,
Chiang Mai University, Chiang Mai 50200
THAILAND
E-mail: suponananta@yahoo.com

*Corresponding author:
Dr. S. Ananta
Department of Physics,
Faculty of Science
Chiang Mai University
Chiang Mai 50200 Thailand
Tel: (00) 53 943367; fax: (00) 53 943445
E-mail: *suponananta@yahoo.com*

Effects of Milling Time and Calcination Condition on Phase Formation and Particle Size of Lead Zirconate Nanopowders Prepared by Vibro-milling

O. Khamman[a], T. Sarakonsri[b], A. Rujiwatra[b], Y. Laosiritaworn[a], R. Yimnirun[a] and S. Ananta[a*]

[a]*Department of Physics, Faculty of Science, Chiang Mai University, Chiang Mai 50200, Thailand*
[b]*Department of Chemistry, Faculty of Science, Chiang Mai University, Chiang Mai 50200, Thailand*

Abstract

Effect of calcination conditions on phase formation and particle size of lead zirconate ($PbZrO_3$) powders synthesized by a solid-state reaction with different vibro-milling times was investigated. A combination of the milling time and calcination conditions was found to have a pronounced effect on both the phase formation and particle size of the calcined $PbZrO_3$ powders. The calcination temperature for the formation of single-phase perovskite lead zirconate was lower when longer milling times were applied. The optimal combination of the milling time and calcination condition for the production of the smallest nanosized (~28 nm) high purity $PbZrO_3$ powders is 35 h and 750 °C for 4 h with heating/cooling rates of 30 °C/min, respectively.

Keywords: Lead zirconate; Perovskite; Nanopowders; Calcination; Phase formation

1. Introduction

Lead zirconate, $PbZrO_3$ or PZ, is one of the widely investigated antiferroelectric materials with a perovskite structure. The unique properties such as high transition temperature (~ 230 °C), free of remanant polarization and double hysteresis behaviour make it an interesting candidate for many applications especially for energy storage, low-loss linear capacitors, microelectronics and actuators [1,2]. There has been a great deal of interest in the preparation of single-phase PZ powders as well as in the sintering and electrical properties of PZ-based ceramics [2,3]. To fabricate them, a fine powder of perovskite phase with the minimized degree of particle agglomeration is needed as starting material in order to achieve a dense and uniform microstructure at the sintering temperature [1-3]. Some typical processes to synthesize perovskite lead-based powders are the microemulsion [4], the sol-gel technique [5], the co-precipitation [6], the hydrothermal reaction [7], mechanical activation [8,9], and the solid-state reaction or mixed oxides [10].

Recently, ultrafine powders (< 100 nm in diameter) are promising starting materials in the fabrication of advanced nanoceramics [2,3]. However, the evolution of a method to produce nano-sized powders of precise stoichiometry and desired properties is complex, depending on a number of variables such as starting materials, processing history, temperature, etc. The advantage of using a solid-state reaction method via mechanical milling for preparation of nano-sized powders lies in its ability to produce mass quantities of powder in the solid state using simple equipment and low cost starting precursors [11,12]. Although our earlier work has been done in the

preparation of PZ powders via a vibro-milling technique [13], a detailed study considering the role of both milling times and firing conditions on the preparation of PZ nanopowders has not been reported yet.

Therefore, the present work has been undertaken to investigate the effects of vibro-milling time together with calcination conditions on phase formation and particle size of lead zirconate powders synthesized by solid-state reaction method. The powder characteristics of the vibro-milling derived $PbZrO_3$ have also been thoroughly investigated.

2. Experimental procedure

The raw materials used were commercially available lead oxide, PbO (JCPDS file number 77-1971) and zirconium oxide, ZrO_2 (JCPDS file number 37-1484) (Fluka, > 99% purity). The two oxide powders exhibited an average particle size in the range of 3.0 to 5.0 μm. $PbZrO_3$ powder was synthesized by the solid-state reaction of these raw materials, in analogous with other similar lead-based perovskites as described in our previous works [12,14]. A McCrone vibro-milling technique [11,12] was employed for preparing the stoichiometric $PbZrO_3$ powders. In order to improve the reactivity of the constituents, the milling process was carried out for various milling times ranging from 15 to 35 h (instead of 30 min [13]) with corundum media in isopropanol. After drying at 120 °C for 2 h, various calcination conditions, i.e. temperature ranging from 550 to 800 °C, dwell times ranging from 1 to 6 h and heating/cooling rates ranging from 10 to 30 °C/min, were applied (the

powders were calcined in air inside a closed alumina crucible) in order to investigate the formation of $PbZrO_3$ [13].

All powders were subsequently examined by room temperature X-ray diffraction (XRD; Siemens-D500 diffractometer) using Ni-filtered CuK_α radiation, to identify the phases formed, optimum milling time and firing conditions for the production of single-phase $PbZrO_3$ powders. The crystalline lattice constants and average particle size were also estimated from the diffraction peak (240) of the perovskite pattern using Scherrer equation [15]. The particle size distributions of the powders were determined by laser diffraction technique (DIAS 1640 laser diffraction spectrometer) with the particle sizes and morphologies of the powders observed by scanning electron microscopy (JEOL JSM-840A SEM). The structures and chemical compositions of the phases formed were elucidated by transmission electron microscopy (CM 20 TEM/STEM operated at 200 keV) and an energy-dispersive X-ray (EDX) analyzer with an ultra-thin window. EDX spectra were quantified with the virtual standard peaks supplied with the Oxford Instrument eXL software. Powder samples were dispersed in solvent and deposited by pipette on to 3 mm holey copper grids for observation by TEM. In addition, attempt was made to evaluate the crystal structures of the observed compositions/phases by correcting the XRD and TEM diffraction data.

3. Results and discussion

Powder XRD patterns of the calcined samples after different milling times are given in Figs. 1-3, with the corresponding JCPDS patterns. As

shown in Fig. 1, for the uncalcined powder subjected to 15 h of vibro-milling and the powders calcined at 550 °C, only X-ray peaks of precursors PbO (•) and ZrO_2 (○) are present, indicating that no reaction was yet triggered during the vibro-milling or low firing processes, in agreement with literatures [13,16]. However, it is seen that crystalline phase of the perovskite $PbZrO_3$ (▼) was found as separated phase in the powders calcined at 600 °C, and became the predominant phase in the powders calcined at 700 °C. Further calcination at 800 °C with dwell time of 1 h does not result in very much increase in the amount of $PbZrO_3$ whereas the traces of unreacted PbO could not be completely eliminated. This could be attributed to the poor reactivity of lead and zirconium species [10,13]. However, it should be noted that after calcination at 800 °C for 2 h (Fig. 1 (f)), the single phase of perovskite $PbZrO_3$ (yield of 100% within the limitations of the XRD technique) was obtained. In general, the strongest reflections apparent in the majority of these XRD patterns indicate the formation of $PbZrO_3$. These can be matched with JCPDS file number 35-0739 for the orthorhombic phase, in space group *P2cb* (no. 32) with cell parameters *a* = 823.1 pm *b* = 1177 pm, and *c* = 588.1 pm [17], consistent with other works [7,13,16]. For 15 h of milling, the optimum calcination temperature for the formation of a high purity $PbZrO_3$ phase was found to be about 800 °C.

To further study the phase development with increasing milling times, an attempt was also made to calcine mixed powders milled at 25 h and 35 h under various conditions as shown in Figs. 2 and 3, respectively. In this connection, it is seen that by varying the calcination temperatures and dwell

times, the minimum firing temperature or dwell time for the single perovskite phase formation of each milling batch is decreased with increasing milling time (Figs. 1-3), in good agreement with other perovskite systems [12,14,18]. The main reason for this behavior is that a complete solid-state reaction probably takes place more easily when the particle size is milled down by accelerating an atomic diffusion mechanism to meet the suitable level of homogeneity mixing. It is thought that the reduction in the particle sizes significantly reduces heat diffusion limitations. It is therefore believed that the solid-state reaction to form perovskite $PbZrO_3$ phase occurs at lower temperatures or shorter dwell times with decreasing the particle size of the oxide powders [11,12].

As expected, there is evidence that, even for a wide range of calcination conditions, single-phase $PbZrO_3$ cannot easily be produced, in agreement with literatures [13,16]. In the work reported here, evidence for the minor phase of PbO which coexists with the parent phase of $PbZrO_3$ is found after calcination at temperature 600-750 °C, in agreement with literature [13,16]. This second phase has an orthorhombic structure with cell parameters a = 589.3 pm, b = 549.0 pm and c = 475.2 pm (JCPDS file number 77-1971) [19]. This observation could be attributed mainly to the poor reactivity of lead and zirconium species [13] and also the limited mixing capability of the mechanical method [11,12]. A noticeable difference is noted when employing the milling time longer than 15 h (Figs. 2 and 3), since an essentially monophasic $PbZrO_3$ of perovskite structure was obtained at 800 °C for 1 h or 750 °C for 6 h (or 4 h) for the milling time of 25 h (or 35 h). This was apparently a consequence of the enhancement in crystallinity of the

perovskite phase with increasing degree of mixing and dwell time, in good agreement with other works [12,18].

In the present study, an attempt was also made to calcine the powders with different milling times under various heating/cooling rates (Figs. 1-3). In this connection, it is shown that the yield of $PbZrO_3$ phase did not vary significantly with different heating/cooling rates ranging from 10 to 30 °C/min, in good agreement with the early observation for the $PbZrO_3$ powders subjected to 0.5 h of vibro-milling times [13]. The variation of calculated crystallite size of the $PbZrO_3$ powders milled for different times with the calcination conditions is given in Table 1. In general, it is seen that the calculated crystallite size of $PbZrO_3$ decreases with increasing heating/cooling rates for all different milling times. These values indicate that the particle size affects the evolution of crystallinity of the phase formed by prolong milling treatment. It should be noted that no evidences of the introduction of impurity due to wear debris from the selected milling process was observed in all calcined powders, indicating the effectiveness of the vibro-milling technique for the production of high purity $PbZrO_3$ nanopowders. Moreover, it has been observed that with increasing milling time, all diffraction lines broaden, e.g. (261) and (402) peaks, which are an indication of a continuous decrease in particle size and of the introduction of lattice strain (Fig. 4) [15].

For $PbZrO_3$ powders, the longer the milling time, the finer is the particle size (Fig. 4 and Table 1). Also the relative intensities of the Bragg peaks and the calculated crystallite size for the powders tend to decrease with the increase of milling time. However, it is well documented that, as Scherer's analysis provides only a measurement of the extension of the coherently

diffracting domains, the particle sizes estimated by this method can be significantly under estimated [15,18]. In addition to strain, factors such as dislocations, stacking faults, heterogeneities in composition and instrumental broadening can contribute to peak broadening, making it almost impossible to extract a reliable particle size solely from XRD [15,20].

In this connection, a combination between scanning electron microscopy and laser diffraction techniques was also employed for particle size measurement (Table 1). The morphological evolution and particle size distribution during various calcination conditions of $PbZrO_3$ powders milled with different times were investigated as shown in Fig. 5. At first sight, the morphological characteristic of $PbZrO_3$ powders with various milling times is similar for all cases. In general, the particles are agglomerated and basically irregular in shape, with a substantial variation in particle sizes and size distribution, particularly in powders subjected to prolong milling times. Fracture is considered to be the major mechanism at long milling times. The powders consist of primary particles of nanometers in size and the agglomerates measured ~ 0.75-6.00 μm. In addition to the primary particles, the powders have another kind of very fine particle (brighter particles) with diameter of about 30 nm. However, as unidentified by the XRD technique, a combination of SEM and EDX techniques has demonstrated that unreacted PbO phases (Fig. 6(b)) (circled in the micrographs in Fig. 5) exist in neighbouring to the parent $PbZrO_3$ phase. In general, EDX analysis using a 20 nm probe on a large number of particles of the calcined powders confirmed the parent composition to be $PbZrO_3$ (Fig. 6(a)). As listed in Table 1, the

comparison of XRD crystallite size with SEM apparent crystallite size indicates that the nanoparticles of PZ obtained in this study are indeed polycrystalline, not single-domain single crystalline as in the case of PbTiO3 nanoparticles [21]. This clearly suggests the possibility of introducing excess crystalline defects through vibro-milling.

The effect of milling time on particle size distribution was found to be significant, as shown in Fig. 5. After milling times of 15 and 25 h, the powders have a similar particle size distribution. They exhibit a single peak covering the size ranging from 35 to 2000 nm. However, upon further increase of milling time up to 35 h, a bimodal distribution curve with peak broadening between 10 and 6000 nm is observed. This behavior is believed to arise mainly from particle agglomeration, consistent with SEM result where the strong interparticle bond within each aggregate is evident by the formation of a well-established necking between neighbouring particles (Fig. 5). This observation could be attributed to the mechanism of surface energy reduction of the ultrafine powders, i.e. the smaller the powder the higher the specific surface area [22]. However, it should also be noticed in Fig. 5 that there is a possible necking is observed in long milling time, i.e. 25 h. This necking could be a result of local melting caused by vibro-milling technique. This statement is also supported by the large agglomeration at longer milling time, i.e. 35 h, detected by laser diffraction. Nonetheless, even with the possibility of thermally induced necking, the nano-sized particles could still be obtained with the vibro-milling technique, as seen in Fig. 5.

Bright field TEM images of the calcined $PbZrO_3$ powders derived from milling time of 35 and 25 h are shown in Figs. 7(a) and 8(a), respectively. By

employing a combination of both selected area electron diffraction (SAED) and crystallographic analysis, the major phase of orthorhombic $PbZrO_3$ (Figs. 7(b) and 8(b)) was identified, in good agreement with the XRD results. It is interesting to note that limited evidence for the presence of the unreacted precursor PbO (Fig. 8(c)), in good agreement with the SEM results, was also found in the TEM-SAED investigation, even though this could not be detected by XRD. It is, therefore, intriguing to note the advantage of a combination between TEM-SAED and SEM-EDX techniques, which lies in its ability to reveal microstructural features often missed by the XRD method which requires at least 5 wt% of the component [7,15].

The experimental work carried out here suggests that the optimal combination of the milling time and calcination condition for the production of the smallest nanosized high purity $PbZrO_3$ powders is 35 h and 750 °C for 4 h with heating/cooling rates of 30 °C/min, respectively. Moreover, the employed heating/cooling rates for $PbZrO_3$ powders observed in this work are also faster than those reported earlier [13,16]. This investigation indicates a strong relationship between the vibro-milling process, the calcination condition and the yield of $PbZrO_3$ nanopowders.

Furthermore, it is a well-established fact that ferroelectric nanoparticles undergo what is called a finite-size effect [21,23]. Namely, at a certain particle size called the critical size, the high-temperature paraelectric phase is stabilized at room temperature. Prior to reaching that size, the lattice parameters as well as the paraelectric-ferroelectric phase transition temperature changes. However, there has been much controversy concerning the critical size at room temperature. The critical crystallite size has been

reported to range between 25 to 200 nm [21,23-29]. In particular, earlier report has shown that the critical crystallite size in PZ is approximately 100 nm [23,24]. In view of this connection, an attempt has been made to determine the critical crystallite size for the PZ nanoparticles produced in this study. As shown in Fig. 9, the critical crystallite size for the PZ seems to be around 30-35 nm. It should also be noticed that there is an increase in lattice parameters and unit-cell volume at smaller particle size, which could be attributed to crystallite aggregation, as reported earlier in $BaTiO_3$ [25] and also in good agreement with SEM results (Fig. 5) which show aggregated clusters. It is also to be noted the critical crystallite size obtained in this study is significantly lower than previously reported values [23,24]. This is mainly due to the range of the particle size used for the critical size determination is limited to 27-60 nm, as compared to 30-250 nm in previous studies [23-29]. Therefore, more accurate value can be obtained with wider range of particle sizes.

4. Conclusions

This work demonstrated that by applying an appropriate choice of the vibro-milling time, calcination temperature and dwell time, mass quantities of a high purity lead zirconate nanopowders can be successfully produced by a simple solid-state mixed oxide synthetic route without the use of high purity starting precursors. A combination of the milling time and calcination conditions was found to have a pronounced effect on both the phase formation and particle size of the calcined $PbZrO_3$ powders. The calcination temperature for the formation of single-phase perovskite lead zirconate was

lower when longer milling times were applied. The optimal combination of the milling time and calcination condition for the production of the smallest nanosized (~28 nm) high purity $PbZrO_3$ powders is 35 h and 750 °C for 4 h with heating/cooling rates of 30 °C/min, respectively.

Acknowledgement

This work was supported by the National Nanotechnology Center (NANOTEC), the Thailand Research Fund (TRF), the Commission on Higher Education (CHE), Faculty of Science, and the Graduate School of Chiang Mai University.

References

[1] B. Jaffe, W.R. Cook, H. Jaffe, Piezoelectric Ceramics, Academic Press, New York, 1971.

[2] A.J. Moulson, J.M. Herbert, Electroceramics, 2nd ed., Wiley, Chichester, 2003.

[3] G.H. Haertling, J. Am. Ceram. Soc. 82 (1999) 797.

[4] Y.S. Rao, C.S. Sunandana, J. Mater. Sci. Lett. 11 (1992) 595.

[5] D.M. Ibrahim, H.W. Hennicke, Trans. J. Br. Ceram. Soc. 80 (1981) 18.

[6] E.E. Oren, E. Taspinar, A.C. Tas, J. Am. Ceram. Soc. 80 (1997) 2714.

[7] A. Rujiwatra, S. Tapala, S. Luachan, O. Khamman, S. Ananta, Mater. Lett. 60 (2006) 2893.

[8] M.T. Lanagan, J.H. Kim, S. Jang, R.E. Newnham, J. Am. Ceram. Soc. 71 (1988) 311.

[9] S.E. Lee, J.M. Xue, D.M. Wan, J. Wang, Acta Mater. 47 (1999) 2633.

[10] J.M. Xue, D.M. Wan, S.E. Lee, J. Wang, J. Am. Ceram. Soc. 82 (1999) 1687.

[11] A. Ngamjarurojana, O. Khamman, R. Yimnirun, S. Ananta, Mater. Lett. 60 (2006) 2867.

[12] R. Wongmaneerung, R. Yimnirun, S. Ananta, Mater. Lett. 60 (2006) 1447.

[13] W. Chaisan, O. Khamman, R. Yimnirun, S. Ananta, J. Mater. Sci. (to be published).

[14] S. Ananta, N.W. Thomas, J. Eur. Ceram. Soc. 19 (1999) 155.

[15] H. Klug, L. Alexander, X-Ray Diffraction Procedures for Polycrystalline and Amorphous Materials, 2nd ed., Wiley, New York, 1974.

[16] C. Puchmark, G. Rujijanagul, S. Jiansirisomboon, T. Tunkasiri, Ferroelectric Lett. 31 (2004) 1.

[17] Powder Diffraction File No. 35-0739. International Centre for Diffraction Data, Newtown Square, PA, 2000.

[18] R. Wongmaneerung, R. Yimnirun, S. Ananta, Mater. Lett. 60 (2006) 2666.

[19] A. Revesz, T. Ungar, A. Borbely, J. Lendvai, Nanostruct. Mater. 7 (1996) 779.

[20] J.S. Reed, Principles of Ceramic Processing, 2nd ed. Wiley, New York, 1995.

[21] S. Chattopadhyay, P. Ayyub, V.R. Palkar, M. Multani, Phys. Rev. B 52 (1995) 13177.

[22] Powder Diffraction File No. 77-1971. International Centre for Diffraction Data, Newtown Square, PA, 2000.

[23] S. Chattopadhyay, P. Ayyub, V.R. Palkar, A.V. Gurjar, R.M. Wankar, M. Multani, J. Phys.: Condens. Matter 9 (1997) 8135.

[24] S. Chattopadhyay, NanoStructured Mater. 9 (1997) 551.

[25] M.R. Leonard, A. Safari, IEEE ISAF. 2 (1996) 1003.

[26] K. Uchino, E. Sadanaga, T. Hirose, J. Amer. Ceram. Soc. 72 (1989) 1555.

[27] B.D. Begg. E.R. Vance, J. Nowotny, J. Amer. Ceram. Soc. 77 (1994) 3186.

[28] K. Saegusa, W.E. Rhine, H.K. Bowen, J. Amer. Ceram. Soc. 76 (1993) 1505.

[29] X. Li, W.H. Shih, J. Amer. Ceram. Soc. 80 (1997) 2844.

Table Caption

Table 1 Effect of calcination conditions on the variation of particle size of $PbZrO_3$ powders milled for different times.

Figure Caption

Fig. 1 XRD patterns of $PbZrO_3$ powders milled for 15 h (a) uncalcined, and calcined for 2 h with heating/cooling rates of 10 $^{\circ}$C/min at (b) 550 (c) 600 and (d) 700 $^{\circ}$C, at 800 $^{\circ}$C for (e) 1 and (f) 2 h, and at 800 $^{\circ}$C for 2 h with heating/cooling rates of (g) 20 and (h) 30 $^{\circ}$C/min.

Fig. 2 XRD patterns of $PbZrO_3$ powders milled for 25 h and calcined for 2 h with heating/cooling rates of 10 $^{\circ}$C/min at (a) 600 (b) 700 and (c) 750 $^{\circ}$C, at 750 $^{\circ}$C for (d) 5 and (e) 6 h, and at 750 $^{\circ}$C for 6 h with heating/cooling rates of (f) 20 and (g) 30 $^{\circ}$C/min, and (h) at 800 $^{\circ}$C for 1 h with heating/cooling rates of 30 $^{\circ}$C/min.

Fig. 3 XRD patterns of $PbZrO_3$ powders milled for 35 h and calcined for 2 h with heating/cooling rates of 10 $^{\circ}$C/min at (a) 600 (b) 700 and (c) 750 $^{\circ}$C, at 750 $^{\circ}$C for (d) 3 and (e) 4 h, and at 750 $^{\circ}$C for 4 h with heating/cooling rates of (f) 20 and (g) 30 $^{\circ}$C/min, and (h) at 800 $^{\circ}$C for 1 h with heating/cooling rates of 30 $^{\circ}$C/min.

Fig. 4 Enlarged zone of XRD patterns showing (261)/(402) peaks broadening of $PbZrO_3$ powders milled for (a) 15 h (Fig. 1(h)), (b) 25 h (Fig. 2(h)) and (c) 35 h (Fig. 3(g)).

Fig. 5 SEM micrographs and particle size distributions of $PbZrO_3$ powders milled for (a) 15 h (Fig. 1(h)), (b) 25 h (Fig. 2(h)) and (c) 35 h (Fig. 3(g)).

Fig. 6 EDX analysis of (a) the major phase $PbZrO_3$ and (b) the minor phase PbO (some signals of C and Cu come from coated electrodes and sample stubs, respectively).

Fig. 7 (a) TEM micrograph and (b) SAED pattern ($[13\bar{1}]$ zone axis) of $PbZrO_3$ powders milled for 35 h (Fig. 3(g)).

Fig. 8 (a) TEM micrograph of $PbZrO_3$ powders milled for 25 h (Fig. 2(h)) and SAED pattern of (b) major phase $PbZrO_3$ ($[\bar{1}02]$ zone axis) and (c) minor phase PbO ($[\bar{2}00]$ zone axis).

Fig. 9 Values of (a) a (■) and b (▲) lattice parameters, (b) c (●) lattice parameter, (c) tetragonal distortion (c/a), and (d) unit cell volume as a function of the particle size (XRD crystallite size) in single-phase $PbZrO_3$ powders.

Table
Click here to download Table: Table 1.doc

Table 1

Milling time (h)	Calcination condition *T/D/R* (°C:h:°C/min)	XRD (nm, ± 2.0)				SEM (nm, ± 10)		Laser scattering (nm, ± 200)	
		A	*a*	*b*	*c*	*D*	*P*	*D*	*P*
15	800/2/10	60.44	0.8255	1.1679	0.5873	306	65-522	720	40-2000
15	800/2/30	60.41	0.8257	1.1682	0.5875	280	53-692	700	35-2000
25	800/1/10	38.38	0.8242	1.1723	0.5877	235	36-415	190	35-800
25	800/1/30	35.11	0.8239	1.1720	0.5875	223	31-400	170	35-750
35	750/4/10	32.45	0.8227	1.1672	0.5870	160	39-420	1600	10-4500
35	750/4/20	30.94	0.8231	1.1769	0.5868	152	36-390	1580	10-5000
35	750/4/30	27.50	0.8235	1.1729	0.5854	121	31-228	1570	10-6000

A = Crystallite size
a, b, c = Lattice parameters
D = Average particle size
P = Particle size range or distribution
T/D/R = Calcination temperature, dwell time and heating/cooling rates.

New Figure 1
Click here to download Figure: Fig 1.doc

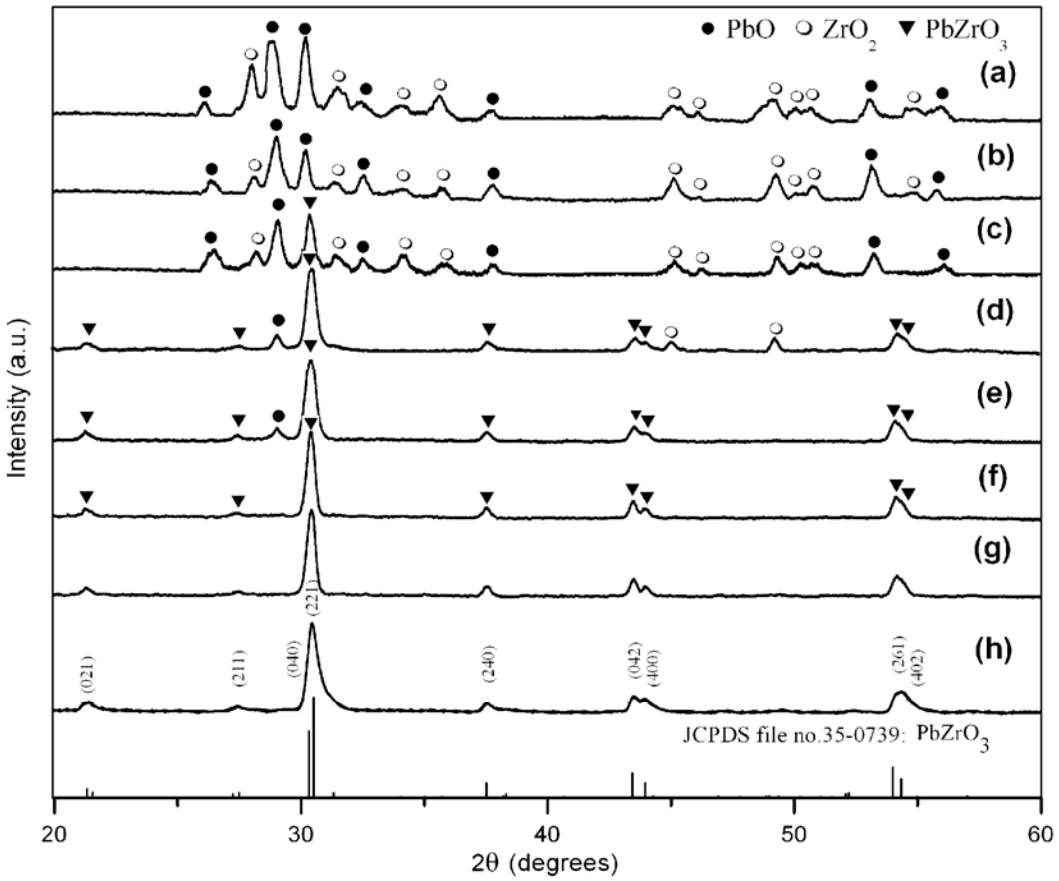

Fig. 1

New Figure 2
Click here to download Figure: Fig 2.doc

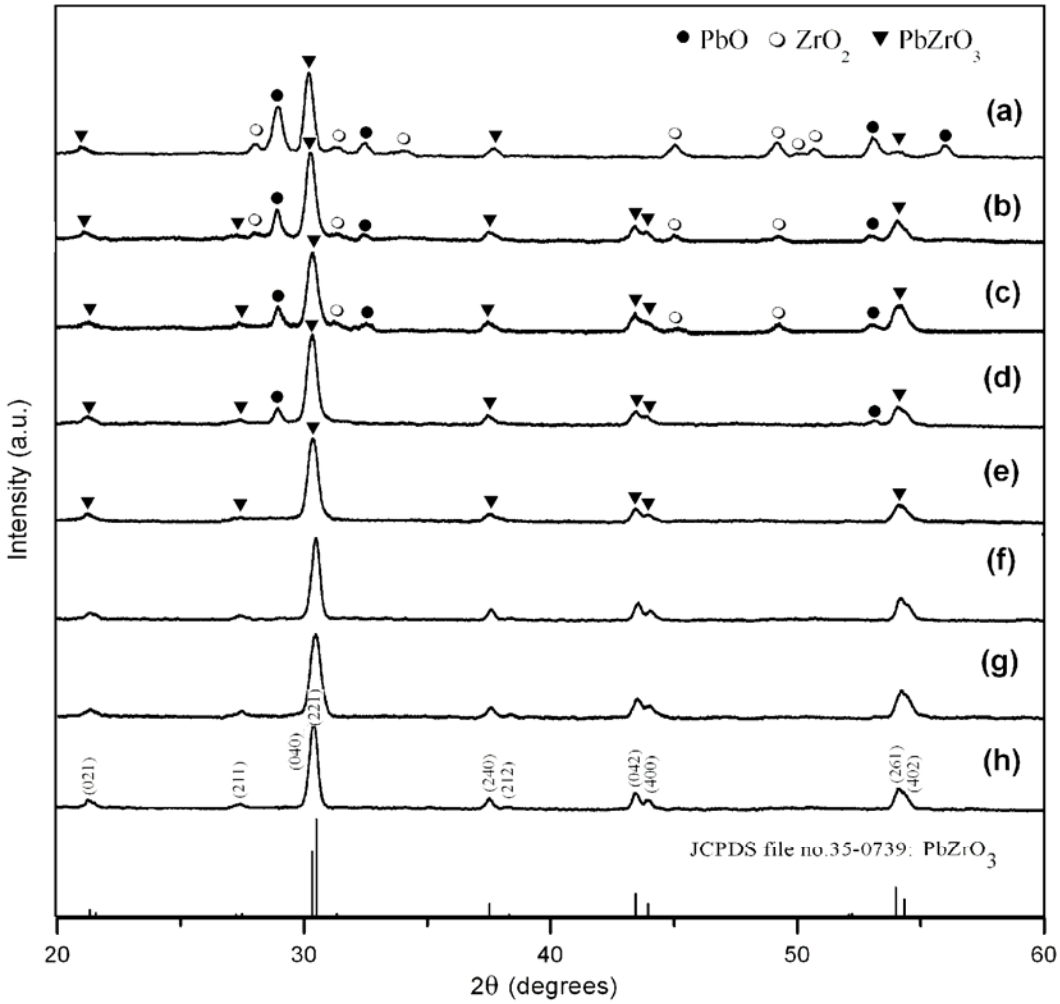

Fig. 2

New Figure 3
Click here to download Figure: Fig 3.doc

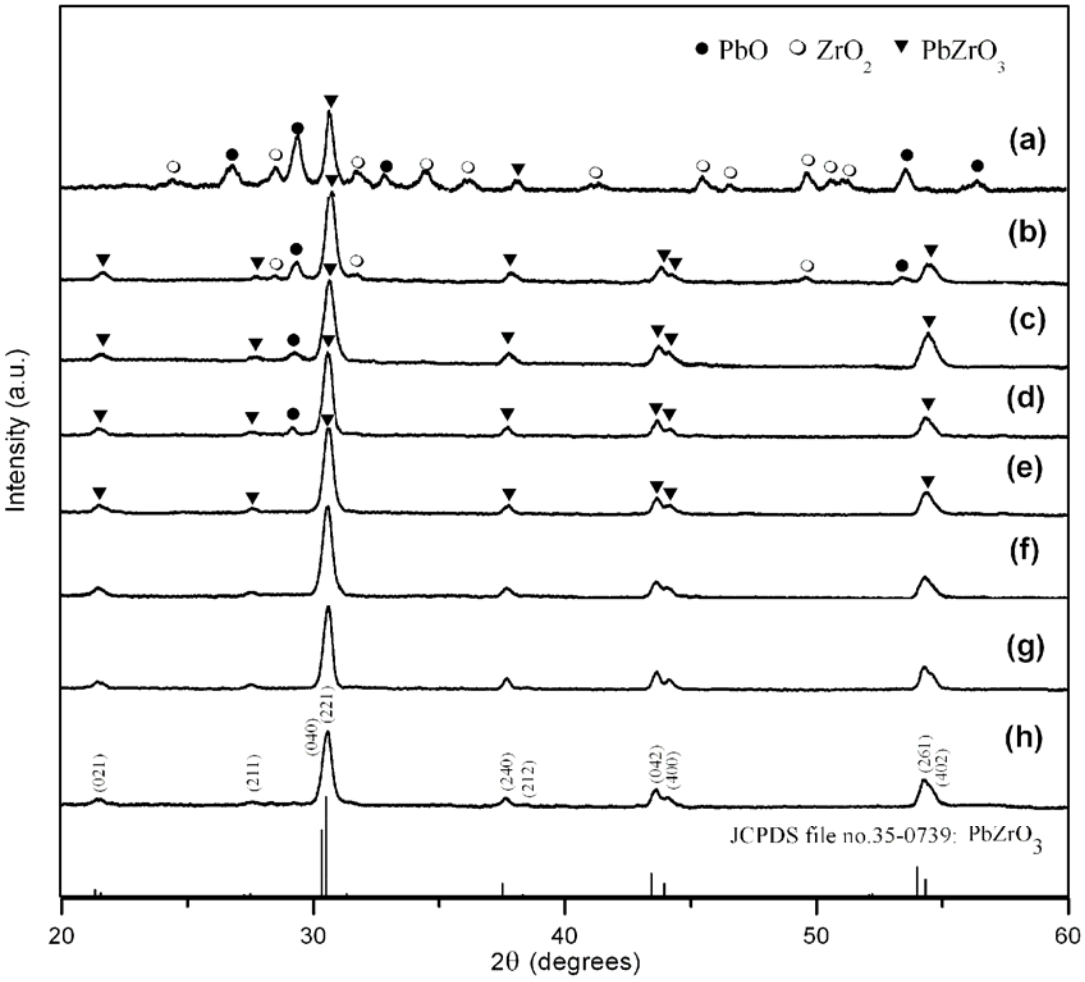

Fig. 3

Figure 4
Click here to download Figure: Fig 4.doc

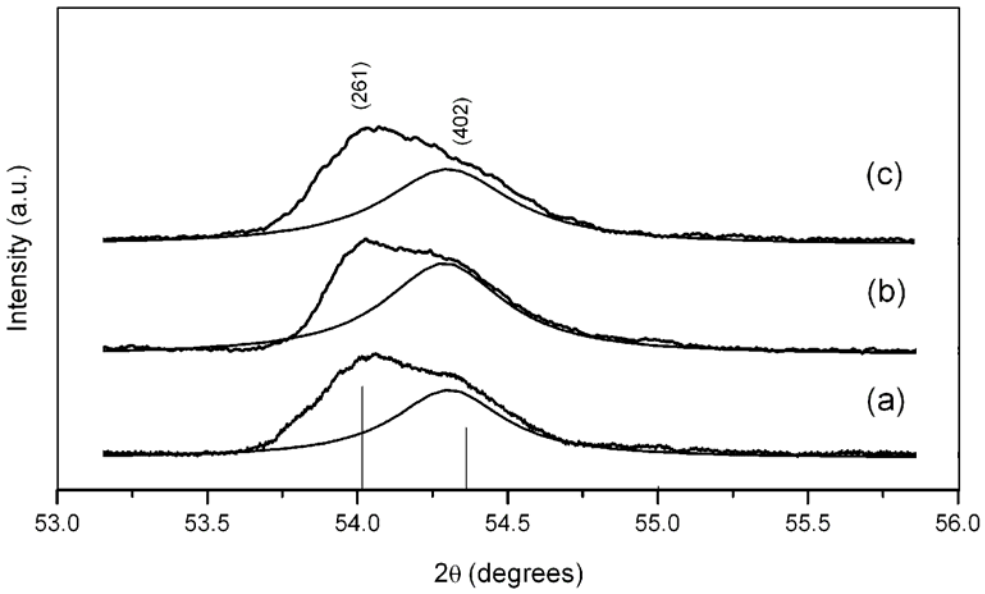

Fig. 4

Figure 5
Click here to download Figure: Fig 5.doc

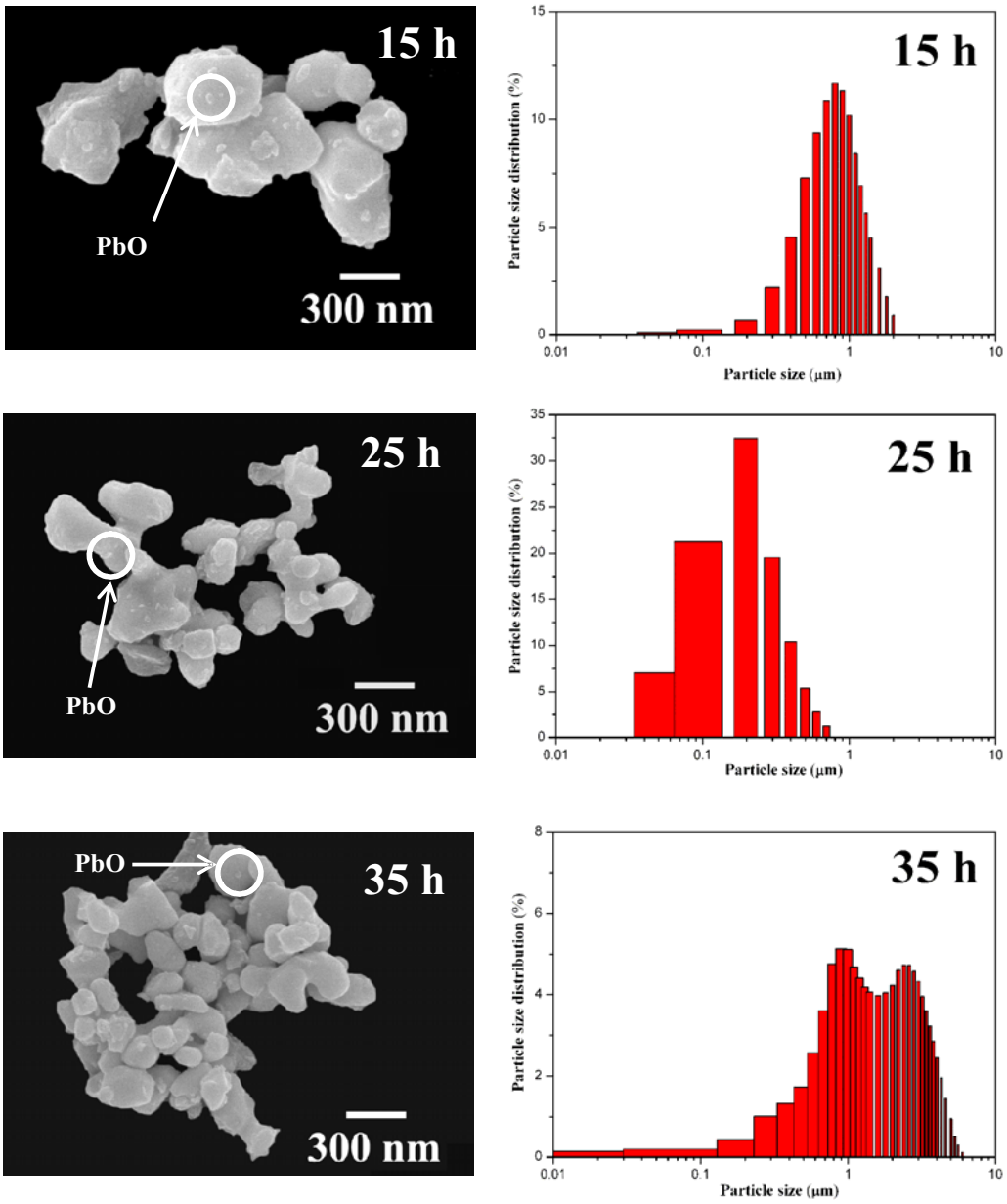

Fig. 5

Figure 6
Click here to download Figure: Fig 6.doc

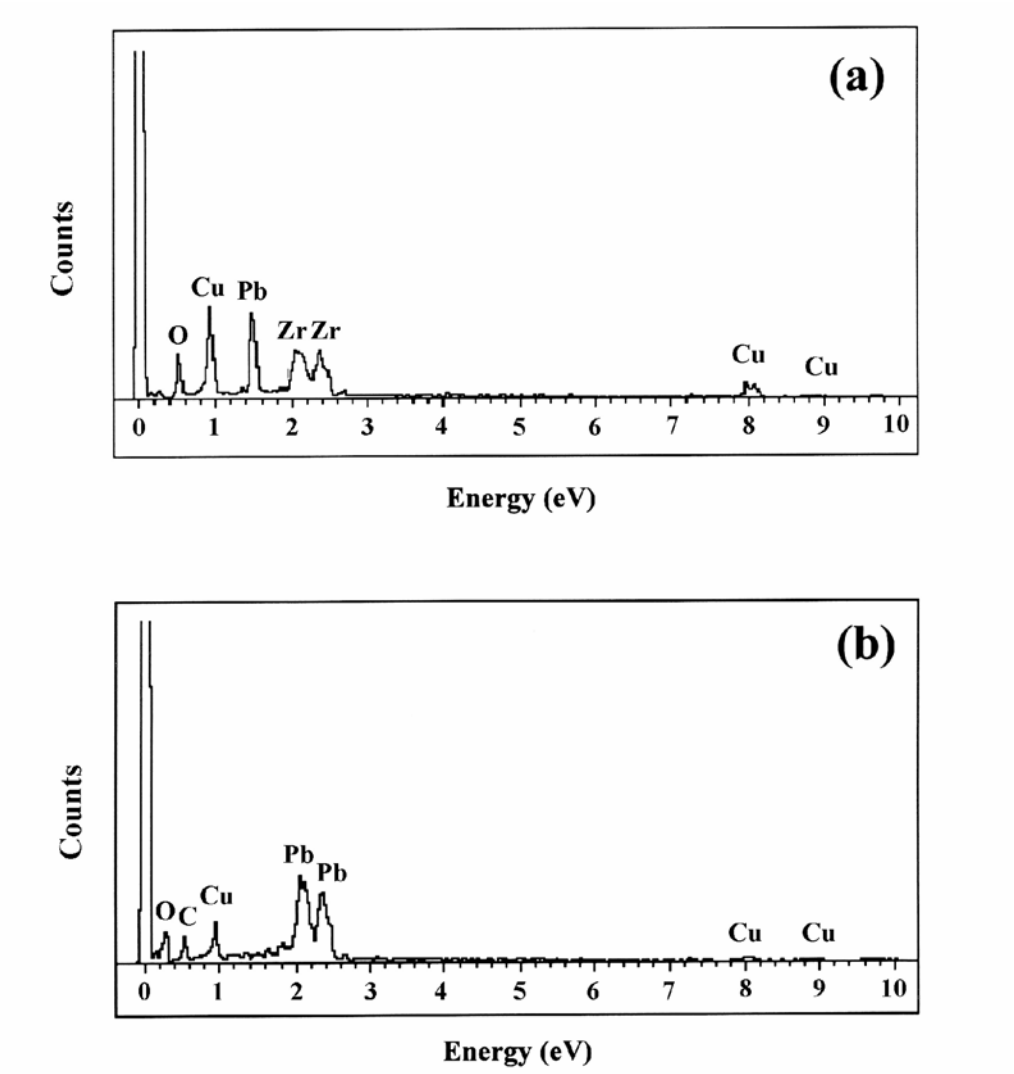

Fig. 6

Figure 7
Click here to download Figure: Fig 7.doc

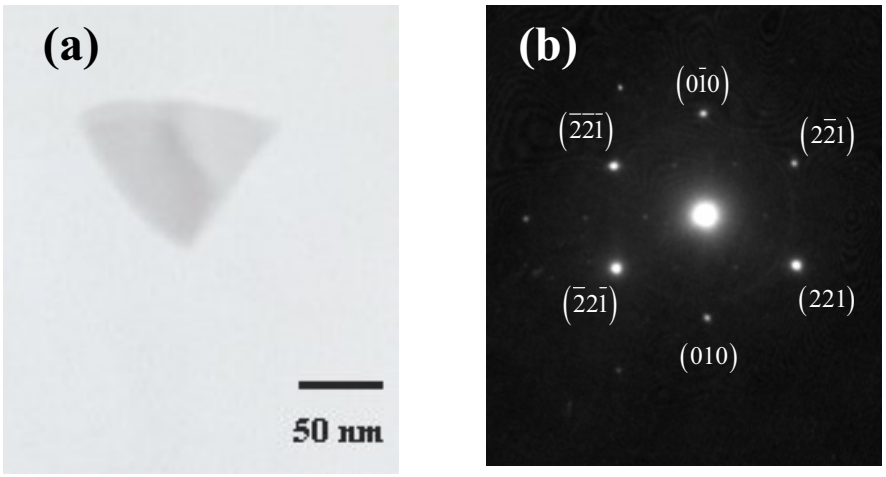

Fig. 7

Figure 8
Click here to download Figure: Fig 8.doc

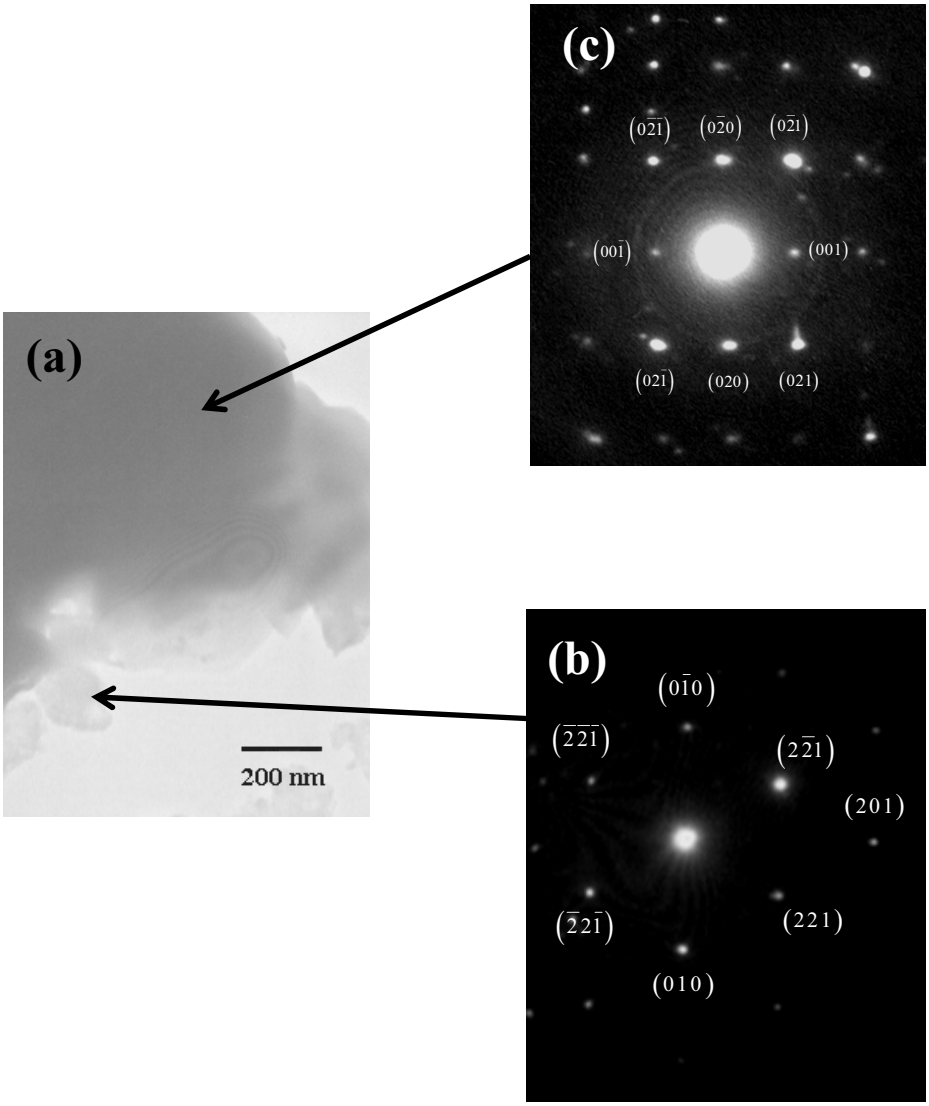

Fig. 8

Figure 9-New
Click here to download Figure: Fig 9.doc

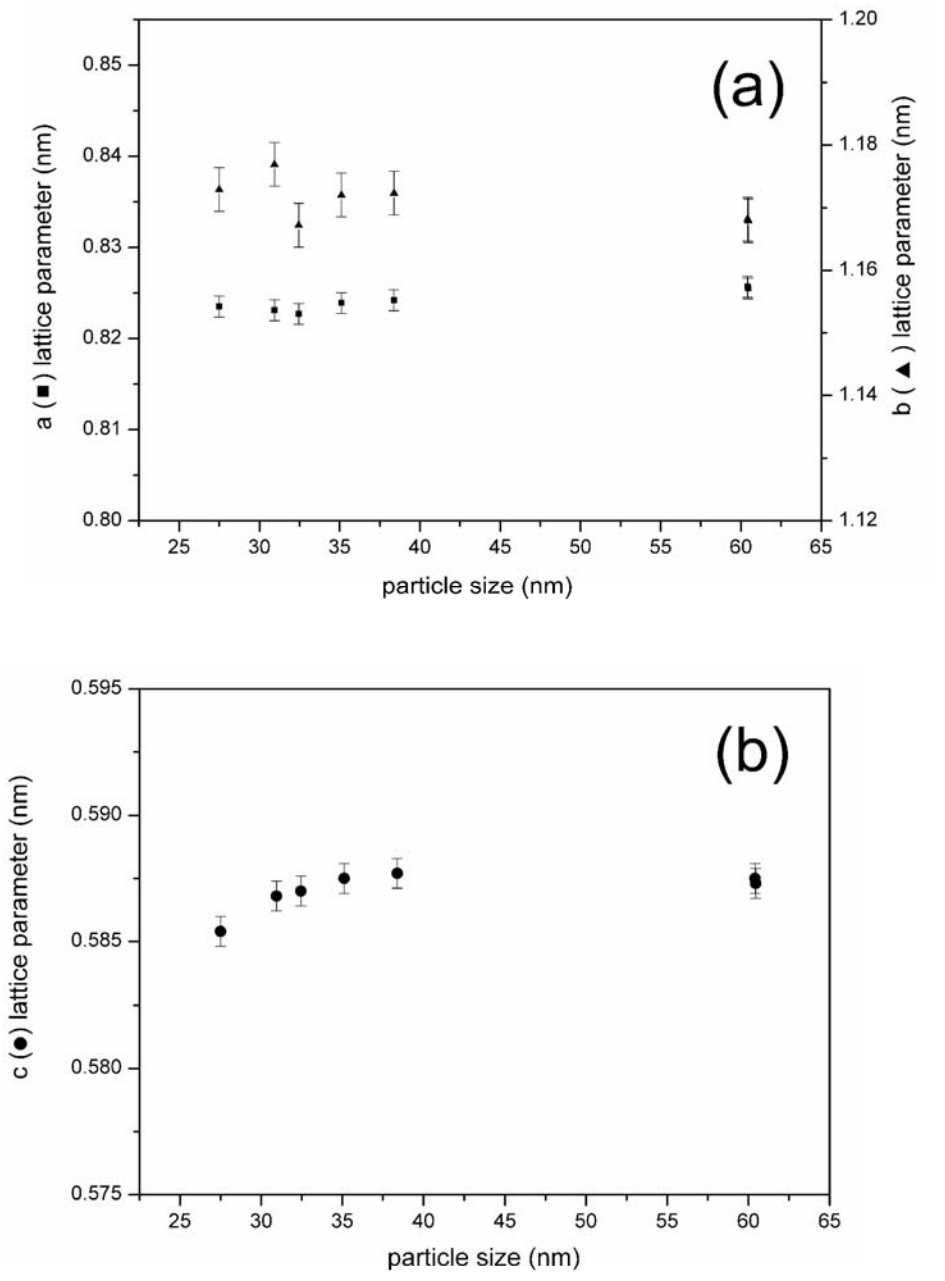

Fig. 9

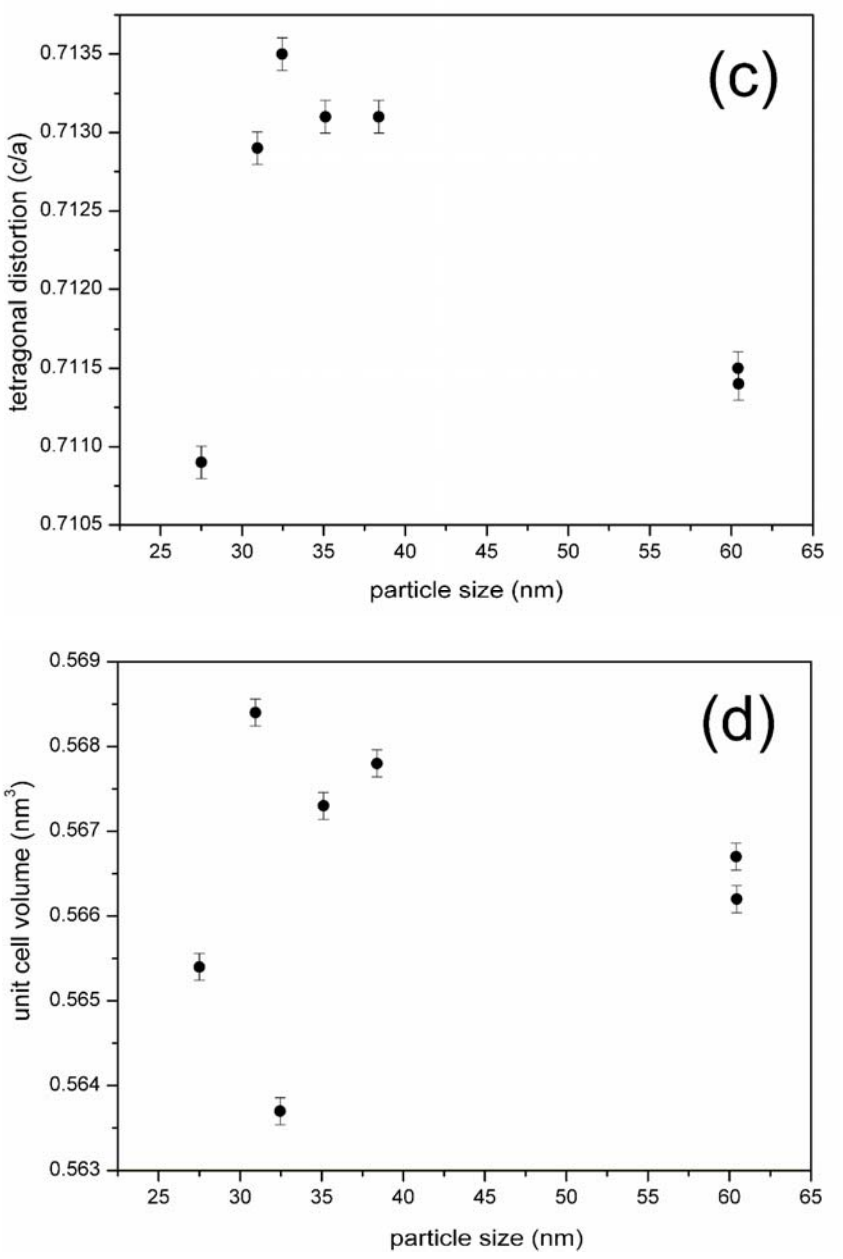
(c)
tetragonal distortion (c/a)
0.7135
0.7130
0.7125
0.7120
0.7115
0.7110
0.7105
25
30
35
40
45
50
55
60
65
particle size (nm)
(d)
unit cell volume (nm^3)
0.569
0.568
0.567
0.566
0.565
0.564
0.563
25
30
35
40
45
50
55
60
65
particle size (nm)

Fig. 9